

University of Mississippi

eGrove

Electronic Theses and Dissertations

Graduate School

1-1-2018

Novel Application of Twin Screw Extruder on Production of Diverse Formulations

Xingyou Ye

University of Mississippi

Follow this and additional works at: <https://egrove.olemiss.edu/etd>



Part of the [Pharmacy and Pharmaceutical Sciences Commons](#)

Recommended Citation

Ye, Xingyou, "Novel Application of Twin Screw Extruder on Production of Diverse Formulations" (2018). *Electronic Theses and Dissertations*. 1497.
<https://egrove.olemiss.edu/etd/1497>

This Dissertation is brought to you for free and open access by the Graduate School at eGrove. It has been accepted for inclusion in Electronic Theses and Dissertations by an authorized administrator of eGrove. For more information, please contact egrove@olemiss.edu.

NOVEL APPLICATION OF TWIN SCREW EXTRUDER ON PRODUCTION OF DIVERSE
FORMULATIONS

A Thesis
presented in partial fulfillment of requirements
for the degree of Doctor of Philosophy in Pharmaceutical Sciences
in the Department of Pharmaceutics and Drug Delivery
The University of Mississippi

by

XINGYOU YE

May 2018

Copyright © 2018 by Xingyou Ye

ALL RIGHTS RESERVED.

ABSTRACT

Twin-screw extruder has attracted considerable attention in the pharmaceutical industry as an alternative processing instrument due to its advantages compared to other conventional equipment, such as economical processing, small footprint, reduced in-process times, solvent-free and continuous processing. These superiorities have led to the application of twin-screw extruder to produce numerous dosage forms, including pellets, tablets and films. Many other formulations production can also be beneficial from the introduction of twin-screw extruder to the process.

Nanocrystal formulations are promising drug delivery systems owing to their ability to enhance the bioavailability and maintain the stability of poorly water-soluble drugs. However, conventional methods of preparing nanocrystal formulations, such as spray drying and freeze-drying, have some drawbacks, including high cost, time and energy inefficiency, traces of residual solvent. In this study, twin-screw extruder was combined with high pressure homogenizer to successfully produce nanocrystal solid dispersions (NCSDs). The process could successfully overcome the limitation of conventional methods.

Dry granulation process is necessary for some moisture sensitive APIs. However, the widely applied dry granulation technologies, slugging and roller compaction, have some limitations: single batch operation, low manufacturing throughput, high amounts of fines and dust, inferior tensile strength of final tablet and loud operation. The previously unreported study of applying twin screw extruder to the dry granulation process was successfully conducted. The

continuous processing nature, simplicity of operation and easiness of optimization made (twin-screw dry granulation) TSDG quite competitive compared to other conventional dry granulation techniques.

Kollidon[®] SR is a polyvinyl acetate (PVAc) and polyvinyl pyrrolidone (PVP) based polymer. The plastic PVAc and sticky PVP make Kollidon[®] SR an extraordinary option for direct compression of high hardness and low friability tablet. In addition, the low glass transition temperature (T_g) of about 35 °C should make Kollidon[®] SR a perfect candidate for twin screw extruder. But this application is rarely reported. This study demonstrated Kollidon[®] SR could be successfully processed by twin-screw extruder to produce tablets, which is compared to the direct compressed counterpart. The physicochemical properties of both products were analyzed. The drug release mechanism was determined.

DEDICATION

Dedicated to my parents Mr. Zhengqing Ye and Mrs. Yiqing You, and
to my lovely girlfriend Ye Luo for all their support, encouragement and affection all through
these years.

ACKNOWLEDGEMENTS

I would like to express my sincere gratitude, appreciation and thanks to my advisor Dr. Michael A. Repka, Chair and Professor, Department of Pharmaceutics and Drug Delivery for his continuous support, encouragement, patience and guidance throughout my Ph.D. studies. It is my honor to be one of his students. I have learned not only the scientific facts but also the art of thinking.

I would like to thank Dr. Soumyajit Majumdar, Dr. Chalet Tan of Department of Pharmaceutics and Drug Delivery, Dr. Ziaeddin Shariat-Madar of Department of BioMolecular Sciences, for being my committee members. Thanks for your valuable expertise, advice and suggestions for my studies. I could not complete my thesis without your help.

I would also like to acknowledge the help from Dr. Bonnie Avery, Dr. Narasimha Murthy and Dr. Seongbong Jo. I am thankful to Ms. Deborah King for her patience and assistance in handling the daily issues in the Department of Pharmaceutics. I also want to thank Dr. Vijayasankar Raman of National Center for Natural Products Research for his time and assistance in the study of scanning electron microscopy. I really appreciate for Dr. Sejal Shah, Dr. Vijay Kulkarni, Dr. Jum-Bom Park, Dr. Roshan Tiwari and Dr. Dong-Wuk Kim for their expertise and advice during their Postdoc period in the department.

In addition, I am deeply thankful to all my colleagues and friends for their support and help in all aspects, especially Dr. Xin Feng, Dr. Jiannan Lu, Dr. Hemlata Patil, Dr. Penggao Duan, Jiaxiang Zhang, Anh Q. Vo, Dr. Manjeet Pimparade, Dr. Xin Dai, Dr. Ziheng Wang, Prit

M. Lakhani, Priyanka Thipsay, Kai-wei Wu, Nan Ji and Pengchong Xu. My life is exciting and fulfilled because of you.

I also want to recall with gratitude the mentor, suggestions and help from my supervisors Dr. Steven Dale at Vertex Pharmaceuticals.

Finally, and most importantly, I am very much grateful to my parents and girlfriend, to whom this dissertation is dedicated, for their unwavering love, endless encouragement and support. I could not make the journey this far without you.

TABLE OF CONTENTS

ABSTRACT.....	ii
DEDICATION.....	iv
ACKNOWLEDGEMENTS	v
LIST OF TABLES	xii
LIST OF FIGURES	xiii
CHAPTER 1. INTRODUCTION	1
1.1. Hot Melt Extrusion.....	2
1.1.1. Twin Screw Extruder	3
1.2. Solubility Threshold.....	4
1.2.1. Dissolution Rate Improvement.....	5
1.2.2. Solid Dispersion	5
1.2.3. Nanocrystal Solid Dispersion.....	6
1.2.4. Production of Nanocrystal Solid Dispersion	7
1.3. Granulation.....	8
1.3.1. Wet Granulation	9
1.3.2. Dry Granulation.....	9
1.3.3. Twin Screw Granulation	10
1.4. Kollidon® SR.....	11
1.4.1. Processing Kollidon® SR by Twin Screw Extruder	12

CHAPTER 2. CONJUGATION OF TWIN SCREW EXTRUSION WITH HIGH PRESSURE HOMOGENIZATION: A NOVEL METHOD OF PREPARING NANOCRYSTAL SOLID DISPERSIONS	13
2.1. Objective	14
2.2. Materials.....	14
2.3. Methods.....	14
2.3.1. Preliminary Study.....	14
2.3.2. Preparation of EFZ NS	15
2.3.3. Preparation of EFZ NCSD	15
2.3.4. Characterization and Evaluation	16
2.3.4.1. Solubility of EFZ.....	16
2.3.4.2. Particle Size and Zeta Potential	16
2.3.4.3. Loss on Drying	17
2.3.4.4. Differential Scanning Calorimetry	17
2.3.4.5. Drug Content	17
2.3.4.6. Scanning Electron Microscopy.....	17
2.3.4.7. In Vitro Drug Release Study	18
2.3.4.8. UV Analysis	18
2.3.4.9. Stability Test.....	18
2.4. Results and Discussion.....	19
2.4.1. Preparation of EFZ NS	19
2.4.2. Selection of Suitable Polymers	21
2.4.3. Experimental Set Up	22

2.4.4. Crystallinity and Morphology of Extrudate	25
2.4.5. Drug Content and Residual Moisture.....	27
2.4.6. In Vitro Drug Release	29
2.4.7. Stability Testing	31
CHAPTER 3. EFFECTS OF PROCESSING ON A SUSTAINED RELEASE FORMULATION	
PREPARED BY TWIN SCREW DRY GRANULATION.....	34
3.1. Objective	35
3.2. Materials.....	35
3.3. Methods.....	35
3.3.1. Preliminary Study.....	35
3.3.2. Design of Experiment.....	36
3.3.3. Twin Screw Dry Granulation	36
3.3.4. Particle size distribution	37
3.3.5. Flow Properties	37
3.3.5.1. Angle of Repose	37
3.3.5.2. Flowability Index.....	38
3.3.6. Differential Scanning Calorimetry	38
3.3.7. Tablet Compression.....	39
3.3.8. Scanning Electron Microscopy	39
3.3.9. In Vitro Drug Release Study	39
3.4. Results and Discussion.....	40
3.4.1. Preliminary Study.....	40
3.4.1.1. Lubricant.....	40

3.4.1.2. Polymer and Excipient Ratio	41
3.4.1.3. API and Drug Loading	41
3.4.2. DoE Set up	46
3.4.3. Characterization of crystallinity	48
3.4.4. The effects of the processing parameters on the particle size distribution.....	49
3.4.4.1. Medium size granules.....	51
3.4.4.2. Fines	53
3.4.5. The effects of the processing parameters on the flow property	55
3.4.5.1. Angle of repose.....	56
3.4.5.2. Flowability Index.....	58
3.4.6. In-vitro drug release study.....	60
3.4.7. Optimization of processing parameters	65
CHAPTER 4. COMPARISON OF DRUG RELEASE FROM KOLLIDON® SR MATRICES PREPARED BY A DIRECT COMPRESSION METHOD AND TWIN SCREW EXTRUSION TECHNOLOGY	67
4.1. Objective	68
4.2. Materials.....	69
4.3. Methods.....	69
4.3.1. Twin Screw Extrusion.....	69
4.3.2. Differential Scanning Calorimetry	70
4.3.3. Tablet Compression.....	70
4.3.4. In Vitro Drug Release Study	70
4.3.5. Scanning Electron Microscopy	71

4.3.6. Dynamic Vapor Sorption	71
4.3.7. Water Sorption Pathway.....	72
4.4. Results and Discussion.....	72
4.4.1. Characterization of Crystallinity	72
4.4.2. In-vitro Drug Release	73
4.4.3. Water Sorption Ability	75
4.4.4. Water Sorption Pathway.....	78
4.4.5. Tablet Structure Test	79
CHAPTER 5. SUMMARY AND CONCLUSION	81
BIBLIOGRAPHY	84
VITA	101

LIST OF TABLES

Table 2-1. Formulation compositions of NS and extrudate.....	19
Table 2-2. LOD for NCSD and Soluplus [®] extrudates	28
Table 2-3. f2 Values of extrudates with different storage times.....	32
Table 2-4. Comparison of particle size, PDI, and zeta-potential with different storage times.....	33
Table 3-1. Candidate of APIs.....	42
Table 3-2. Morphology of 4 APIs at 3 different drug loading after TSDG.	45
Table 3-3. Experimental factors and ranges of variation.....	47
Table 3-4. Barrel Temperature Setting.	47
Table 3-5. Experimental Design.	48
Table 3-6. DoE Results.	50
Table 3-7. Statistical analysis and regression coefficients of the particle size distribution.....	51
Table 3-8. Statistical analysis and regression coefficients of the flow property.	56
Table 3-9. Dissolution time statistical analysis and coefficients of regression.	61
Table 3-10. 80% drug release time for tablet and capsule.....	64
Table 3-11. Summarization of relationship between factors and responses.....	65
Table 4-1. Maximum water sorption and time duration data.....	78

LIST OF FIGURES

Figure 1-1. Hot-melt extrusion (HME) equipment and process parameters traditionally monitored during pharmaceutical HME.....	3
Figure 1-2. Cross-section of single- and twin-screw extruders.	4
Figure 1-3. Bottom up or top down approach to preparing nanocrystals.	8
Figure 1-4. Schematic diagram of dry granulation and two different techniques.	11
Figure 1-5. Chemical structure of Kollidon SR.	12
Figure 2-1. Particle size vs. cycle curves for nanosuspension A and B.	21
Figure 2-2. Schematic representation of continuous preparation of a nanocrystal solid dispersion using HPH and TSE.	24
Figure 2-3. Screw configuration used in the preparation of nanocrystal solid dispersions by twin-screw extrusion.	25
Figure 2-4. Evaluation of crystallinity using differential scanning calorimetry.....	26
Figure 2-5. Scanning electron microscopy images.	27
Figure 2-6. Drug content for nanocrystal solid dispersion extrudate A and B.....	28
Figure 2-7. In vitro drug release profiles for pure efavirenz, extrudate A and extrudate B.	30
Figure 2-8. Appearance of milled extrudate and Soluplus®.	30
Figure 2-9. In vitro release profiles.	31
Figure 3-1. DSC thermograms of four API and products after TSDG.	43
Figure 3-2. Screw configuration utilized in TSDG.....	46

Figure 3-3. DSC thermograms.....	49
Figure 3-4. Contour plots showing the effect of screw speed on percentage of medium size granules.	52
Figure 3-5. Contour plots showing the effect of barrel temperature, screw speed and feeding rate on percentage of fines.	55
Figure 3-6. Contour plots showing the effect of barrel temperature, screw speed and feeding rate on angle of repose.....	58
Figure 3-7. Contour plots showing the effect of barrel temperature and feeding rate on percentage of medium size granules.....	60
Figure 3-8. In-vitro release profiles of a tablets from 12 runs of samples.....	62
Figure 3-9. SEM photograph of granules and tablets.....	63
Figure 3-10. Desirability plot of set goals..	66
Figure 4-1. Chemical structure of theophylline.....	68
Figure 4-2. DSC thermograms of theophylline, Kollidon [®] SR, PM and ExtM.	73
Figure 4-3. In-vitro release profiles.....	74
Figure 4-4. Macro photograph of tablets morphology before and after dissolution.	75
Figure 4-5. Dynamic vapour sorption measurements.	76
Figure 4-6. Dissolution Medium Sorption Pathway.	79
Figure 4-7. Surface structure.	80

CHAPTER 1.
INTRODUCTION

1.1. Hot Melt Extrusion

In the plastics industry, Hot melt extrusion (HME) has been utilized since the late 1930s, and still dominates the production of numerous plastic products. The technique was introduced in pharmaceutical industry after approximately four decades [1-6]. Since then, HME has attracted considerable attention in the pharmaceutical industry due to its inherent advantages, such as being a solvent-free, continuous process with no time consuming steps, ease to scale up, compared to other conventional techniques [7, 8]. Generally speaking, HME is a process that raw materials (mixture of APIs, excipients and other additives) are propelled with spinning screw(s) under high shear and temperature, and products are collected through a die block with a specific shape (Figure 1-1) [7, 9-12]. However, the application of HME is not limited to extrudates. Instead, HME has been modified, or combined with downstream processing equipment, to make a variety of dosage forms, including pellets [13], tablets [14], transdermal films [15, 16], implants [17], granules[18-21] and solid lipid nanoparticles (SLN) [22, 23].

HME, as a fusion based method to produce solid dispersions, could not avoid the intrinsic limitation of this type of techniques. Fusion based technique is simply a process to heat the raw materials to a specific high temperature and then cool the materials at a controlled rate [24-30]. Thus, the thermal stability of the material to be processed is be a prerequisite [1, 31-36]. Otherwise, the high temperature applied may cause the unacceptable thermal degradation of the materials used [37]. As a result, HME could barely utilized for processing of heat sensitive substances, such as proteins and peptides.

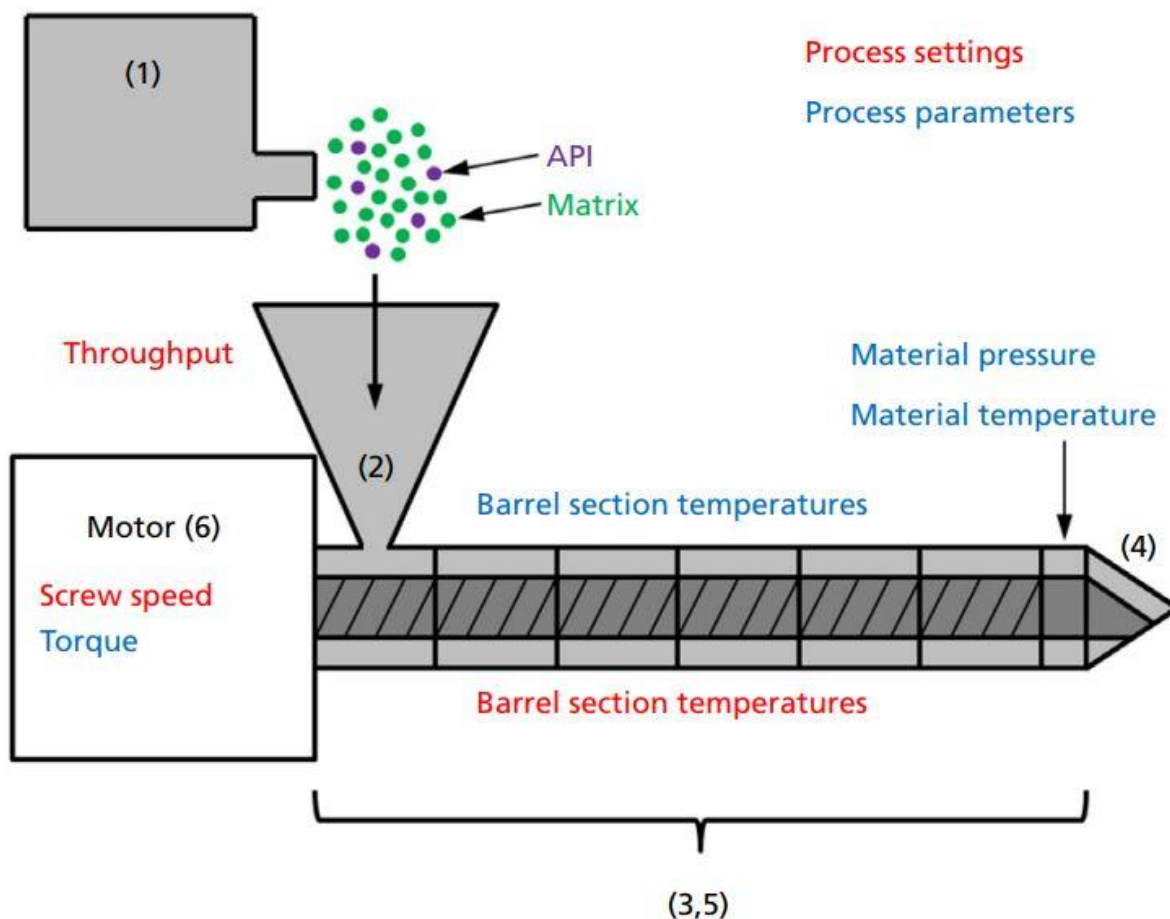


Figure 1-1. HME equipment and process parameters traditionally monitored during pharmaceutical HME. (1. Feeding system; 2. Feeding hopper; 3. Temperature controlled barrel with 1 or 2 screws; 4. Die; 5. Heating and cooling device; 6. Screw-driving unit).[10]

1.1.1. Twin Screw Extruder

Based on number of screws, hot melt extruder can be classified into two categories: single screw extruder (SSE) and twin screw extruder (TSE) (Figure 1-2) [8, 13, 38-41]. As the names straightforwardly indicate, SSE utilize one rotating screw and TSE has two screws side by side in the barrel. SSE is the most widely used extrusion extruder, especially in plastics industry, due to the advantage of mechanical simplicity and more affordable cost. However, TSE is still the more popular system in the pharmaceutical industry, owing to a series of benefits, including

high kneading/dispersing capacities, shorter transit time, less tendency to over-heat and easier material feeding. [6]

TSE can further be divided into two categories based on the direction of screw rotation (co-rotating or counter-rotating). Counter-rotating design works best for situation that very high shear force or dispersion of particles in a blend is needed. Co-rotating design is suitable for the needs of high screw speeds, high production and self-wiping.

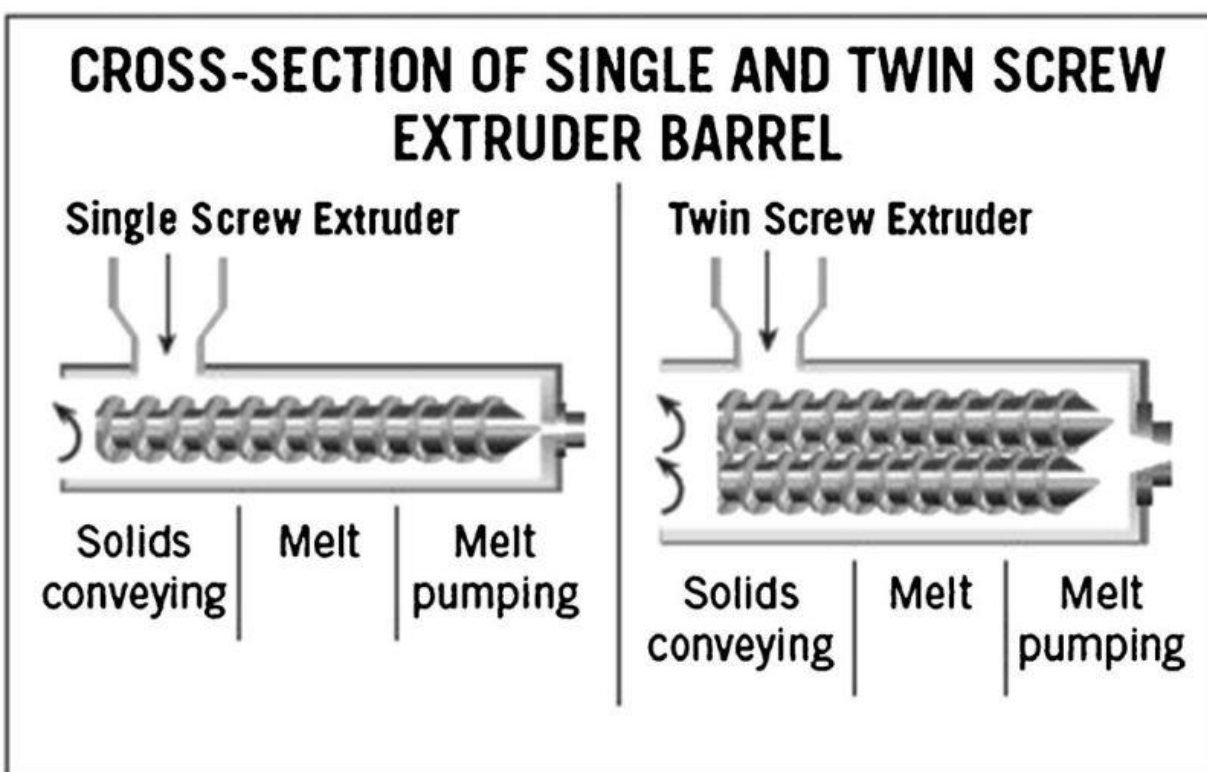


Figure 1-2. Cross-section of single- and twin-screw extruders. [8]

1.2. Solubility Threshold

More than 40 % of drugs developed by the pharmaceutical industry are poorly soluble in water [42, 43]. With the introduction of high-throughput screening (HTS) methods for the

discovery of new drugs [44], the amount of poorly water-soluble drugs is increasing rapidly. Most drugs are administrated orally, as it is the most common and convenient route for drug delivery, so poor solubility often leads to poor gastrointestinal absorption, and thus poor bioavailability [35, 45]. Solubility is also a critical parameter to be considered in parenteral formulations [46]. Thus, enhancement of the dissolution rate of poorly soluble drugs remains one of the most challenging tasks for pharmaceutical scientists.

1.2.1. Dissolution Rate Improvement

Various approaches have been employed to improve the dissolution rate of certain poorly water-soluble drugs. For example, salt formation is a chemical method used to make a drug into a prodrug to improve the dissolution rate [47]. However, this method can only be applied to weakly acidic or basic drugs, not those with neutral pH [35]. Incorporating drug molecules into cyclodextrin is also an effective way to enhance their dissolution rate, but this method requires a certain molecular size and conformation [48, 49]. The currently available dissolution rate enhancement methods are limited to drugs with certain properties, such as acid-base property, molecular size and conformation.

1.2.2. Solid Dispersion

Production of a solid dispersion (SD) is one of the most extensively studied methods of improving the dissolution rate of poorly soluble drugs [50-56]. A SD can be defined as a solid system of a poorly water soluble drug or drugs dispersed in an inert carrier, with the drug usually in the amorphous state [35, 57]. The amorphous form of drug usually has more free energy than

the crystalline counterpart, which leads to an increased dissolution rate [58]. However, this high free energy also tends to create thermodynamic instability, which is a major drawback of amorphous SDs. Recrystallization is usually observed during the storage of SDs [58-60].

1.2.3. Nanocrystal Solid Dispersion

In order to solve the recrystallization problem, initially formulating drugs into a crystalline state in a smaller size is a feasible method. It has been reported that the micronization of drug powders to particle sizes of between 1 and 10 μm is not sufficient to overcome bioavailability problems of very poorly soluble drugs [61], so the natural progression is to move from micronization to nanonization, the production of nanocrystals [62-75]. Nanocrystals are crystals with a particle size below 1000 nm. The reduction in particle size increases the surface area, which directly affects the dissolution rate. Thus, by decreasing the particle size, a higher dissolution rate can be achieved. This can be explained with the help of the Noyes–Whitney equation:

$$\frac{dW}{dt} = \frac{DA(C_s - C)}{L} \quad [76]$$

where dW/dt is the rate of dissolution, A is the surface area of the solid, C is the concentration of the solid in the bulk dissolution medium, C_s is the concentration of the solid in the diffusion layer surrounding the solid, D is the diffusion coefficient, and L is the diffusion layer thickness.

However, it has been reported that decreasing the particle size below a critical value of 1–2 μm increases the saturation solubility [61]. This can be derived from the Kelvin equation, below, which is usually used to describe the vapor pressure of a curved droplet but can also be

used to describe the dissolution process, in which P and P_0 represent the actual and saturated dissolution pressure:

$$\ln \frac{p}{p_0} = \frac{2\gamma V_m}{rRT} \quad [77]$$

where γ is the surface tension, V_m is the molar volume of the liquid, R is the universal gas constant, r is the radius of the particle, and T is the temperature. As can be seen from the equation, P directly depends on r . A decrease in r means a decrease in the particle size, which will increase the saturated dissolution pressure and thus increase the saturated solubility.

1.2.4. Production of Nanocrystal Solid Dispersion

The methods for production of nanocrystals can be divided into two basic types: bottom-up technologies (controlled precipitation/crystallization) and top-down technologies (media milling/high pressure homogenization [HPH]) (Figure 1-3) [70, 72]. Currently, five nanocrystal products have been approved by the US FDA, all of which are based on top-down technologies (four of these products are prepared by wet-ball milling and one is prepared by high-pressure homogenization) [73], which indicates that the top-down process is more industrially feasible [65]. After completion of these processes, the drugs are present in a suspended state as a nanosuspension (NS). However, it is usually important for the NS to be transformed into a solid product, both for physical stability and patient convenience [66, 73]. The most widely used processes for transformation include freeze-drying and spray-drying [78]. However, these two methods have several disadvantages, such as high cost, time and energy inefficiency, and residual solvent trace [1]. There is therefore a need for a new technology to complete the transformation process. HME is considered as a promising technique for this objective based on

the advantage mentioned in section 1.1. In addition, the preparation of nanocrystal solid dispersions (NCSDs) by combining HPH and HME is not yet explored much [79].

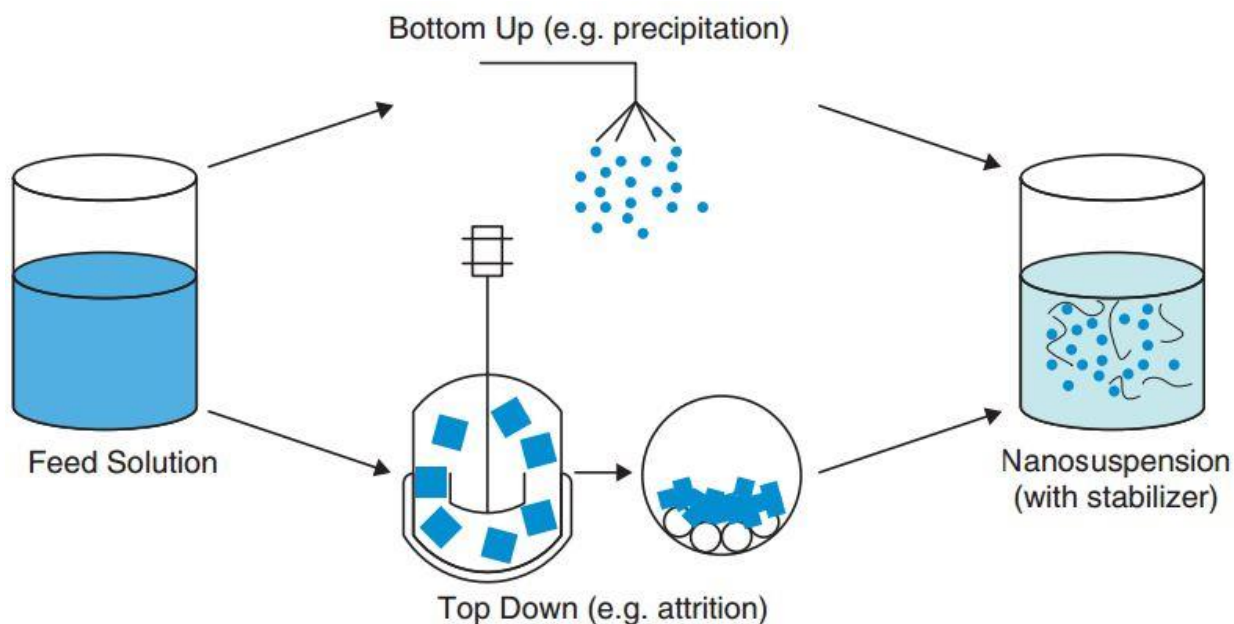


Figure 1-3. Bottom up or top down approach to preparing nanocrystals.[70]

1.3. Granulation

Based on Perry's *Chemical Engineer's Handbook*, granulation process was defined as "any process whereby small particles are gathered into larger, permanent masses in which the original particles can still be identified" [80]. Granulation is widely utilized in numerous industries, such as agriculture, mining, chemical, pharmaceutical and food industry [81]. The application of granulation process in pharmaceutical industry was triggered by the invention of tablet press in 1843 [82]. Nowadays, granule has become a very important intermediary before tablet compression and capsule filling [83-85]. The main purpose of granulation in pharmaceutical industry is to convert small API and excipient particles into larger agglomerates,

which have some beneficial physicochemical properties, such as better flow properties, more uniform drug distribution, reduced dust, prevention of segregation, increased compactability and enhanced appearance of product [86-89].

1.3.1. Wet Granulation

Wet granulation, which is employed to produce 70% of the worldwide industry's granules [86], is the most popular granulation technique in pharmaceutical industry, owing to lots of available knowledge and equipment. In general, wet granulation comprises of several steps: liquid binder addition, agglomeration, drying and screening [90-93]. The aggregation of primary particulates is achieved by the liquid binder [90]. Melt granulation is considered as a particular form of wet granulation as the mechanism of these two methods are similar [83, 94]. However, the limitation of wet granulation is also obvious, such as multiple unit feature, time inefficiency, high cost, large space requirement and especially unsuitability for moisture sensitive APIs [90-92]. Thus an alternative technology of dry granulation is necessary [95].

1.3.2. Dry Granulation

Unlike wet granulation, dry granulation employs dry binders and high mechanical force to enable the agglomeration process [83, 90, 96]. Slugging and roller compaction are two widely used dry granulation techniques in the pharmaceutical industry (Figure 1-4) [86, 90, 95-98]. Slugging was the favorable dry granulation technique in the 1950s-1970s in the pharmaceutical industry [96]. In this process, the primary powders are compressed into large tablets or slugs, followed by the milling and sieving process. The quality of granules highly depends on the flow

ability of raw materials, which may cause the inhomogeneity problem [86]. Other disadvantages of slugging include: single batch processing, low manufacturing throughput, frequent maintenance and so on. Compared to slugging, an auger-feed system is utilized in roller compaction to constantly deliver raw material, which can ensure the good content uniformity of granules. In addition, roller compaction is a highly efficient and continuous process, which has a much higher output than slugging. Thus, roller compaction is considered as a more competitive dry granulation technique in pharmaceutical plants. Although roller compaction shows many advantage over slugging, it is not perfect. It has been reported that this method also comprises some disadvantages, including relative high amount of fines and dust [86, 99-101], inferior tensile strength of final tablet [88, 89, 98, 100] and loud operation environment [86]. Therefore, there is an increasing need for an alternative dry granulation technique that can solve the problem mentioned above.

1.3.3. Twin Screw Granulation

The benefits of TSE have led to innumerable application in the pharmaceutical industry, including wet granulation [18, 21] and melt granulation [20, 102]. The only difference between twin screw granulation (TSG) and TSE is that the die is removed during the process to prevent the extreme densification of material inside the barrel. The successful application of twin screw extruder on wet and melt granulation can be a positive indication that dry granulation could also be efficaciously accomplished utilizing this technique.

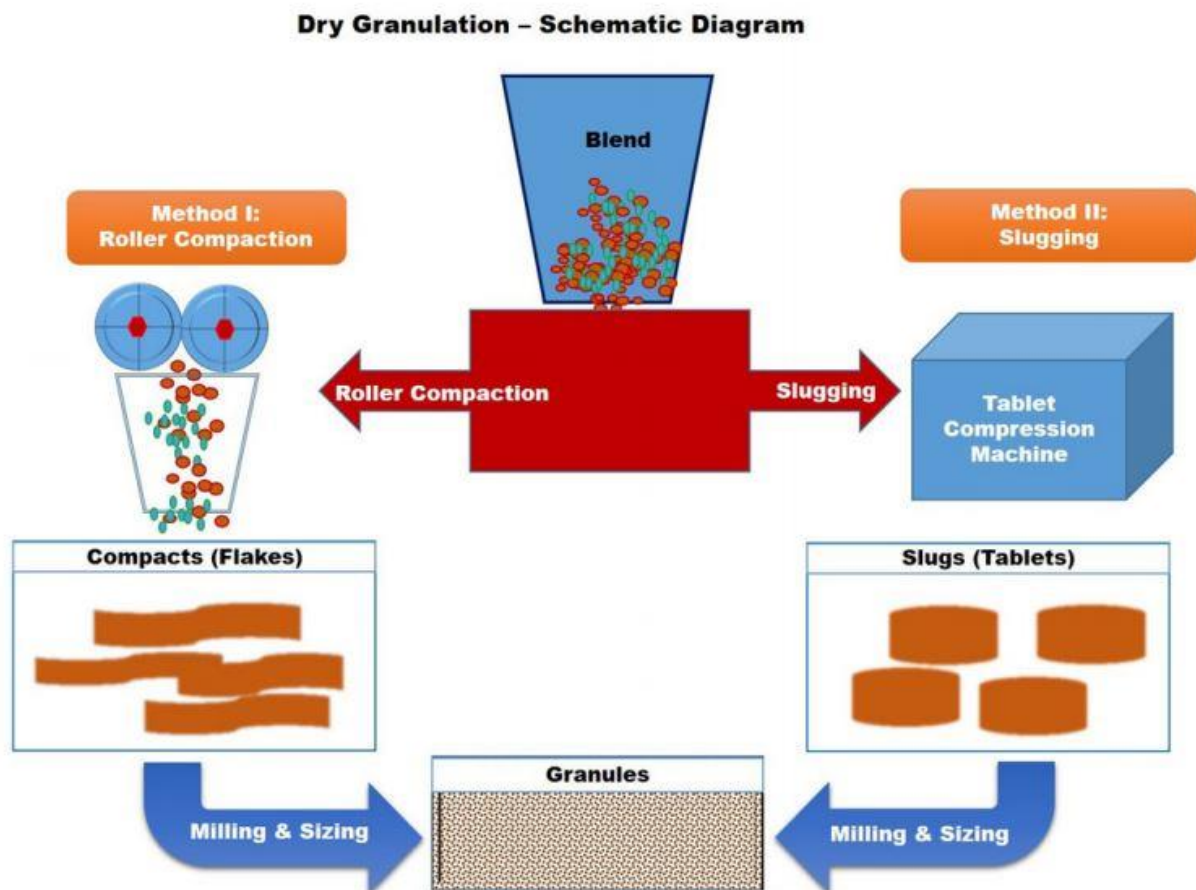


Figure 1-4. Schematic diagram of dry granulation and two different techniques. [90]

1.4. Kollidon® SR

Kollidon® SR (Figure 1-5) is one type of polyvinyl acetate (PVAc) and polyvinyl pyrrolidone (PVP) based polymer, which is especially appropriate for the production of pH-independent sustained release formulations [62]. The two major compositions of Kollidon® SR are 80 % of PVAc and 19 % of PVP (Kollidon® 30). Other than that, about 0.8 % of sodium lauryl sulfate (SLS) and 0.2 % of silica serve as stabilizers for the whole physical mixture [103]. The plastic nature of PVAc guarantees the production of coherent tablet even under low compression forces. In addition, the sticky PVP can tightly bind materials together. Combining

these properties together, Kollidon® SR shows the outstanding property of compression and production of high hardness and low friability tablet. Moreover, the excellent flowability of Kollidon® SR itself, as well as the potential to improve the flowability of other material added to the formulation, make Kollidon® SR a competitive candidate for direct compression. Therefore, numerous sustained release tablets have been produced using Kollidon® SR by direct compression method [104-107].

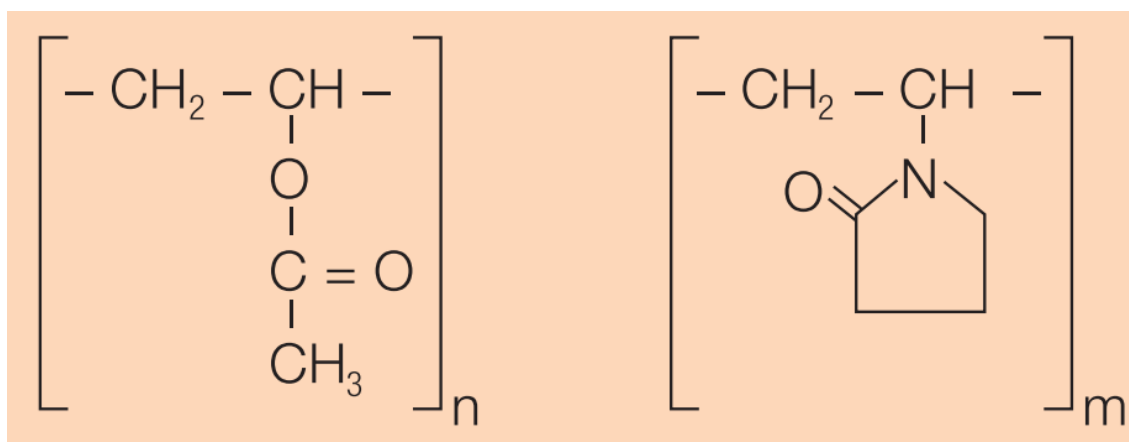


Figure 1-5. Chemical structure of Kollidon SR.

1.4.1. Processing Kollidon® SR by Twin Screw Extruder

The application of Kollidon® SR on HME was rarely reported. This phenomenon is quite eccentric, because the low glass transition temperature (T_g) of about 35 °C should make this polymer a perfect contender for HME. To the author's knowledge, only two manuscripts, whose topic was on utilization of Kollidon® SR for HME, were published [108, 109].

CHAPTER 2.

CONJUGATION OF TWIN SCREW EXTRUSION WITH HIGH PRESSURE HOMOGENIZATION: A NOVEL METHOD OF PREPARING NANOCRYSTAL SOLID DISPERSIONS

2.1. Objective

The primary objective of this study was to develop a new method of preparing a NCSD by applying TSE after HPH. The first step was to prepare a NS using HPH. The resulting suspension was extruded utilizing TSE with the help of a selected polymer (Soluplus[®]) to obtain a NCSD. In addition, various physical and chemical properties were evaluated within the NCSD. Finally, the stability of the NCSD was studied.

2.2. Materials

Efavirenz (EFZ) was purchased from Ria International LLC (East Hanover, NJ, US). SLS was purchased from Fisher Scientific (Hanover Park, IL, US). Kollidon[®] 30 and Soluplus[®] were kindly donated by BASF SE (Ludwigshafen, Germany). All other reagents used in this study were of analytical grade.

2.3. Methods

2.3.1. Preliminary Study

A preliminary study was carried out to evaluate the formulation and process parameters to be used in the preparation of the NCSD. The three most critical parameters in the HPH process were found to be drug concentration, homogenization pressure, and time, while in the TSE process, the parameters taken into consideration were the ratio of NS to polymer, feeding rate, barrel temperature, screw configuration, screw speed, and zone for NS addition. All of these parameters were optimized to successfully prepare a NCSD by HPH-TSE technique.

2.3.2. Preparation of EFZ NS

EFZ NS was prepared by HPH technique. Briefly, different concentrations of EFZ powder (2 % and 4 %, w/v) were poured into an aqueous surfactant solution (Kollidon[®] 30, 1.0 % w/v and SLS 0.5 % w/v) [110], and further mixed on a magnetic stirrer at 500 rpm for 12 h in order to achieve complete dispersion of EFZ in the solution. After dispersion, the mixtures were homogenized using a T25 digital ULTRA-TURRAX[®] basic homogenizer (IKA-Werke, Staufen, Germany) at 15000 rpm for 5 min. The resulting suspension was further homogenized using an EmulsiFlex-05 high-pressure homogenizer (Avestin Inc., Ottawa, Canada) at 1500 bar for selected cycles.

2.3.3. Preparation of EFZ NCSD

NCSD was prepared by mixing aqueous phases of NS and polymer (Soluplus[®]) using an 11-mm co-rotating twin-screw extruder (Thermo Fisher Scientific, Waltham, MA, US). The extruder consists of eight zones, the individual temperature of which, excluding zone 1, can be precisely controlled. The barrel was maintained within a temperature range of 100–140 °C. Soluplus[®] was fed into the extruder via an 11-mm single screw feeder (Thermo Electron, Karlsruhe, Germany) at a feeding rate of 1 % (approximately 1.2 g/min). NS was injected into zone 5 using a 520S pump (Watson Marlow, Golden, Colorado, US) at 0.3 rpm (approximately 0.6 g/min). The screw speed was set at 50 rpm.

2.3.4. Characterization and Evaluation

2.3.4.1. Solubility of EFZ

The solubility of EFZ was assessed at room temperature. EFZ (20 mg) was added to glass vessels containing 20 mL of ultra-purified water. The glass vessels were then placed on an MTS 2/4 microtiter shaker (IKA, Wilmington, NC, US), which was operated at a speed of 200 min⁻¹ for 24 h. The samples were then withdrawn and centrifuged at 6000 rpm for 5 min. The supernatant was analyzed using a GENESYS 6 UV-Vis spectrophotometer (Thermo Scientific, Madison, WI, US). The experiment was then repeated at least three times for all the samples. The means and standard deviations were then calculated.

2.3.4.2. Particle Size and Zeta Potential

As stated above, particle size can significantly affect the dissolution velocity and saturation solubility. Zeta potential is one of the critical parameters affecting the stability of NS [111]. These two parameters were measured using a Zetasizer Nano ZS (Malvern Instruments, Worcestershire, UK). The NS sample was first diluted with sufficient ultra-purified water, then the diluted sample was transferred to a cuvette for measurement. Dynamic light scattering was used to measure the Z-average (particle size) and polydispersity index (PDI). Laser doppler micro-electrophoresis was used to measure the zeta potential. The parameters used for measurement were scattering angle of 173°, refractive index of 1.33, viscosity of 0.89 cP, and temperature of 25 °C.

2.3.4.3. Loss on Drying

Soluplus[®] was extruded using identical processing conditions to those used for NCSD, then NCSD and Soluplus[®] were subjected to a loss on drying (LOD) test using a MB45 Moisture Analyzer (Ohaus, Switzerland) by heating at 110 °C for 10 min.

2.3.4.4. Differential Scanning Calorimetry

A Diamond DSC (PerkinElmer, Shelton, CT, US) was used to measure the degree of crystallinity of the samples. The instrument's Pyris manager software was utilized to analyze the data. About 2–5 mg of sample was weighed and hermetically sealed in an aluminum pan. The heating rate was set at 20 °C/min from 20 to 200 °C under an inert atmosphere of nitrogen at a flow rate of 20 mL/min.

2.3.4.5. Drug Content

The extrudate was first milled to a fine powder. Accurately weighed powder (10 mg) was dissolved in 10 mL of methanol, and then diluted 10 times with methanol. The sample was analyzed by UV-Vis spectrophotometry.

2.3.4.6. Scanning Electron Microscopy

Scanning electron microscopy (SEM) was used to determine the morphology of pure EFZ and EFZ NCSD. Adhesive carbon tape was used to mount the sample onto an aluminum stage, then the samples were sputter coated with gold under an argon atmosphere using a Hummer 6.2 Sputter Coater (Ladd Research Industries, Williston, VT, US). The coater was kept in a high-

vacuum evaporator equipped with an omni-rotary stage tray to guarantee a uniform coating. Finally, images were captured using a JSM-5600 scanning electron microscope (JEOL USA, Inc., Waterford, VA, US) at an accelerating voltage of 5 kV.

2.3.4.7. *In Vitro* Drug Release Study

The dissolution media used was 900 mL of 0.2 % SLS in 0.1 M HCl (pH 1.2, simulated gastric medium) [112]. SR8-plus™ dissolution apparatus (Hanson, Chatsworth, CA, US) was maintained at 37 ± 0.5 °C and the paddle speed was set at 50 rpm. Milled extrudates equivalent to 10 mg of EFZ were filled into capsules (size 0) for dissolution. Samples were collected at intervals of 5, 15, 30, 60, and 120 min through a stainless steel cannula with a 0.2-μm nylon filter tip attached to a 2.5-mL syringe. The samples were analyzed directly using a UV-Vis spectrophotometer.

2.3.4.8. UV Analysis

Samples were analyzed using a GENESYS 6 UV-Vis Spectrophotometer (Thermo Scientific, Madison, WI, US) at a wavelength of 247 nm. The standard curve was linear over the range of 1–50 μg/mL with an R^2 equal to 0.9998.

2.3.4.9. Stability Test

Stability studies were conducted to determine the effect of storage on the physical and chemical properties of the drug in two formulations (see Table 2-1 for formulation compositions). Milled extrudates were stored in screw-capped glass vials at real-time storage

conditions (25 °C/60 % relative humidity [RH]). Samples were taken at 1, 2, 3, and 6 month intervals and characterized by dissolution and micromeritics studies. For the micromeritics studies, the extrudates were dispersed in ultra-purified water and then vortexed for 30 sec. The resulting dispersions were then analyzed using a Zetasizer Nano ZS (Malvern Instruments, Worcestershire, UK).

Table 2-1. Formulation compositions of NS and extrudate.

Formulation		Soluplus [®]	Kollidon [®] 30	SLS	EFZ
		% (w/w)	% (w/v) for NS, % (w/w) for extrudate	% (w/v) for NS, % (w/w) for extrudate	% (w/v) for NS, % (w/w) for extrudate
NS	A	N/A	1.0	0.5	2.0
	B	N/A	1.0	0.5	4.0
Extrudate	A	98.25	0.5	0.25	1.0
	B	97.25	0.5	0.25	2.0

EFZ: efavirenz; NS: nanosuspension; SLS: sodium lauryl sulfate.

2.4. Results and Discussion

2.4.1. Preparation of EFZ NS

Three different drug loadings (2%, 4%, and 8% w/v) were assessed to determine the highest drug content that can be used for NS. Before the HPH process, a regular homogenizing process (using a ULTRA-TURRAX[®] basic homogenizer) was carried out to pre-treat the EFZ dispersion. This method significantly reduced the processing time for HPH as the size reduction

was partially completed. The 2% formulation did not block HPH during processing. However, HPH blockage was observed during the first few cycles of 4% formulation processing. This issue was easily fixed by pre-treating the formulation using a regular homogenizer. However, this was not true in the case of the 8% formulation as it blocked the HPH during processing, even after pretreatment, indicating that 8% drug loading was too high for the HPH used in this study. Thus, the highest drug loading that was used was 4%.

Different cycles of homogenization were carried out to determine the optimum homogenization parameters (Figure 2-1). The particle size of NS A (2% drug loading) was stable at around 320 nm after 20 homogenization cycles. Even after a few more homogenization cycles, there was no significant decrease in the particle size. Apart from particle size, polydispersity index (PDI) is also a very important parameter for NSs. A small PDI value indicates a narrow size distribution, whereas a high PDI value indicates a broad size distribution. Usually, a PDI value below 0.5 is acceptable [113]. The HPH process was optimized and after 25 homogenization cycles for NS A the PDI value decreased to below 0.5. Similarly, the HPH process was optimized for NS B (4% drug loading), and after 45 homogenization cycles the particle size was stable at around 350 nm and the PDI value was below 0.5. It has been previously reported that a zeta potential of ± 20 mV is sufficient to make a dispersion physically stable [114]. In this study, the zeta potentials for all resulting homogeneous materials were in the range of -20 to -30 mV, indicating that Kollidon[®] 30 and SLS were able to maintain the zeta potential within the desired range.

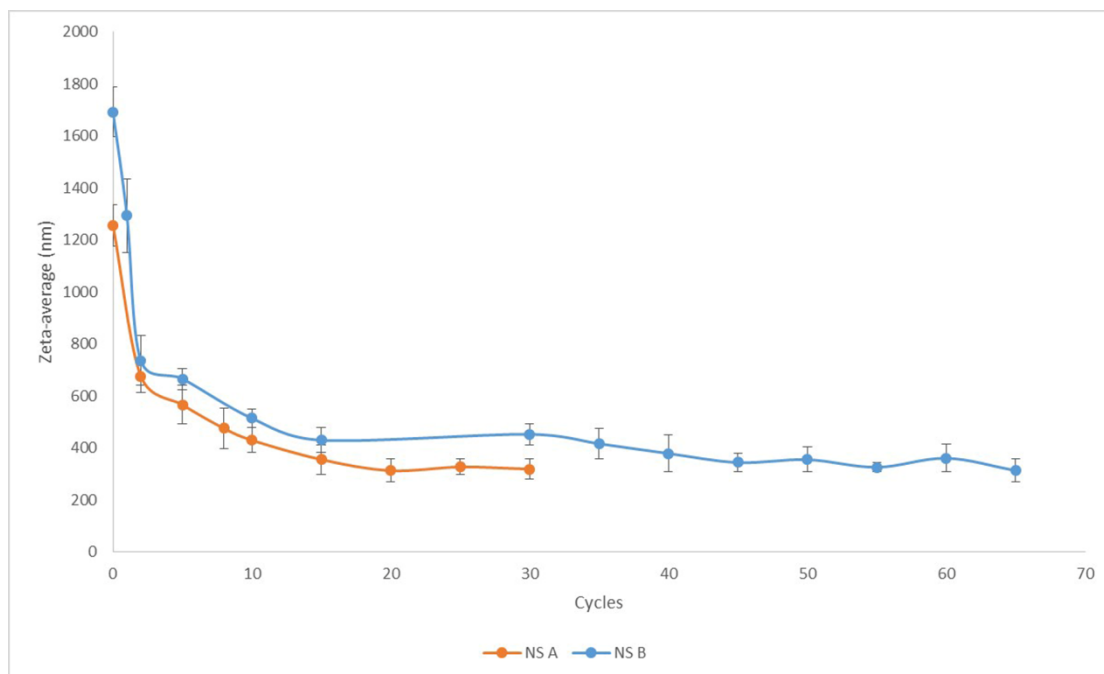


Figure 2-1. Particle size vs. cycle curves for nanosuspension A and B.

2.4.2. Selection of Suitable Polymers

The first step of the TSE process was to choose an appropriate polymer. It is critical that the selected polymer is stable at the extrusion temperature and has the appropriate thermoplastic behavior to make extrusion possible (extrudable) [115]. The glass transition temperature (T_g) is an important parameter affecting the extrudability of polymers because a high T_g will require a high temperature for processing, and in such situations the API may degrade [116]. As per the literature, the suitable T_g range for the TSE process is considered to be between 50 – 180 °C [117].

However, in this study, the T_g requirement is even more stringent. EFZ is a poorly water-soluble (9.2 µg/mL, pH 8.7, 25 °C) lipophilic (log P = 5.4) drug with a crystalline state. The melting temperature (T_m) of EFZ is around 140 °C [118]. To maintain the crystalline state of EFZ, the TSE operating temperature must be kept below 140 °C. Generally, the extrusion

process is carried out at least 20–40 °C above the T_g [119], thus there is a need to choose a polymer with a T_g below 100 °C. It is also important that the polymer is soluble in water in order to produce a homogeneous NCSD. Finally, there is a period when only the polymer is present in the barrel, so the operation temperature for the pure polymer is another important parameter.

Only a few polymers satisfy the above-mentioned requirements, including Soluplus[®], a graft copolymer composed of polyvinyl caprolactam–polyvinyl acetate–polyethylene glycol. It is polymeric solubilizer with an amphiphilic chemical structure, making it an excellent solubilizer for poorly water-soluble drugs in aqueous media. Furthermore it has a low T_g of about 70°C, which also makes it a suitable choice for this study [120]. The approximate temperature range for pure Soluplus[®] for use in TSE was reported to be in the range of 120–200 °C [121].

2.4.3. Experimental Set Up

A schematic illustration of NCSD production by HPH-TSE technique is shown in Figure 2-2. Two parts were included in this system, a high-pressure homogenizer and a twin-screw extruder. For this study, we used a modified screw configuration, as shown in Figure 2-3.

The first zone of the extruder was used for feeding the polymer (Soluplus[®]) into the extruder barrel using a feeding hopper. The elements used in this section were 2.0 L/D feed screws (conveying elements), which had sufficient free volume to take in the purging material for cleaning after processing. The 1.0 L/D feed screws in zone 2 were used to compact the polymer and transport it forward. The temperature of 140 °C applied to this section assisted in the melting of the polymer, thus decreasing the torque in the next mixing zone. The temperature of zone 3 was set at the same value as that of zone 2. Three kinds of mixing elements with 30°, 60°, and 90° offset angles were successfully assembled and installed in the barrel. This setting

provided enough energy for the melting of the polymer and avoided any rapid increase in the torque. Zones 4 and 5 were both formed of conveying elements, and the NS can be injected in any one of these zones. The temperatures were set at 120 and 110 °C for zones 4 and 5, respectively, to avoid transformation of EFZ from the crystalline to the amorphous state. The water of the NS was expected to evaporate rapidly when the NS came into contact with the hot barrel and the molten polymer, and the EFZ nanocrystals would remain on the molten polymer. However, instant and complete evaporation of water was difficult to achieve, and a back-flow phenomenon was observed after NS injection. Therefore, zone 5 was selected for the injection of the NS in order to provide more time and space for contact with the molten polymer, and to reduce the back-flow of the NS. The 90° mixing elements in zone 2 also assisted in this function. This screw configuration forced unevaporated NS to move back and forth between zone 4 and zone 5 until complete evaporation of water was achieved. Furthermore, this process would increase the contact between NS and the polymer, thus providing better distribution. Mixing elements with offset angles of 30° and 60° were used in zone 6. The kneading of these elements contributed to the homogeneous distribution of the matrix material. A 90° offset angle was not used in these mixing elements in order to avoid the generation and use of too much mechanical energy with the EFZ nanocrystals, which may result in the transformation of the crystalline state. The temperature for zone 6 and the remaining subsequent zones was set at 130 °C, which would further eliminate the remaining water in the matrix material. In zones 7 and 8, 1.0 L/D feed screws were used to convey the matrix material to the die. Solidified extrudates coming out of the die were milled and processed for further analysis.

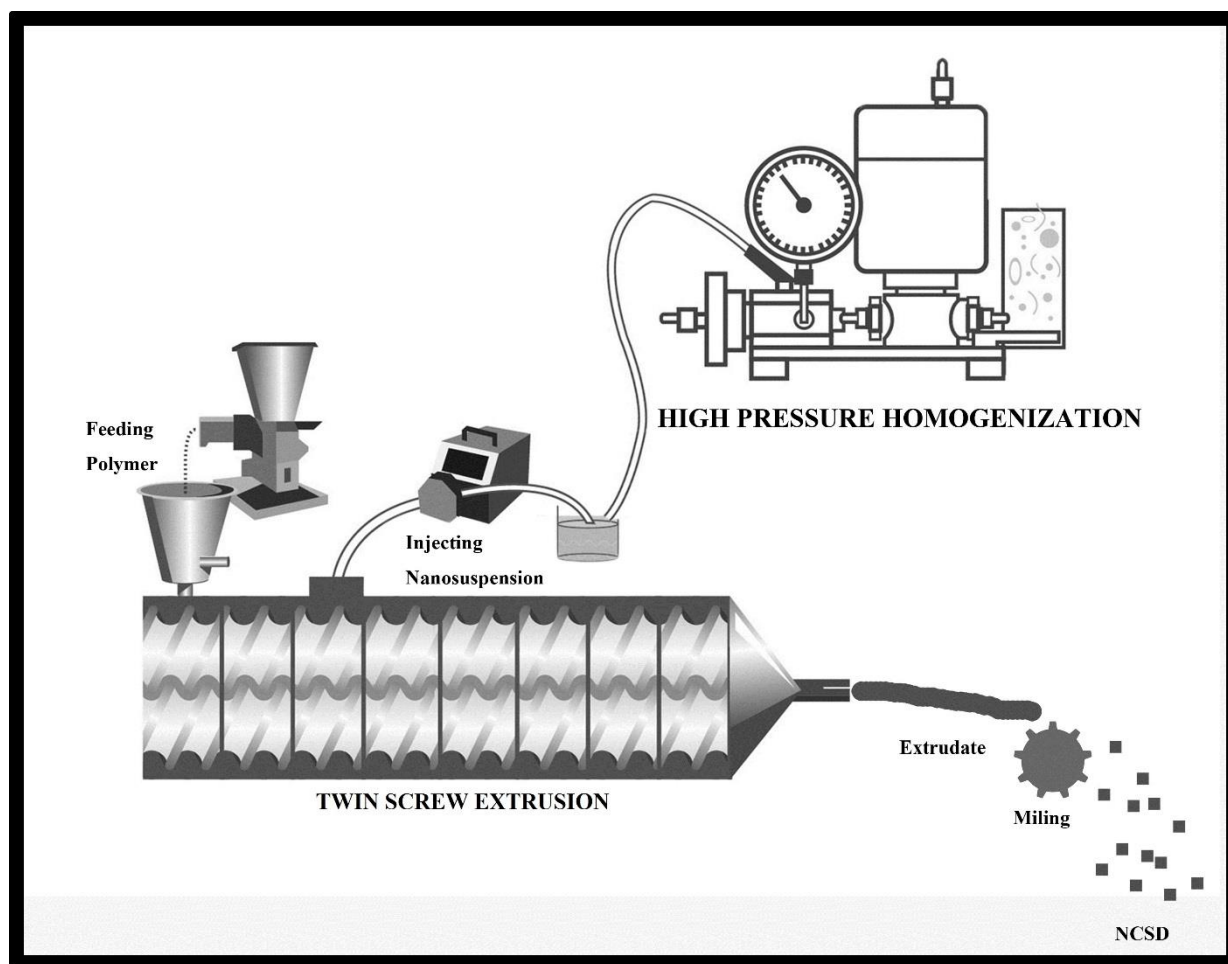


Figure 2-2. Schematic representation of continuous preparation of a nanocrystal solid dispersion using HPH and TSE.

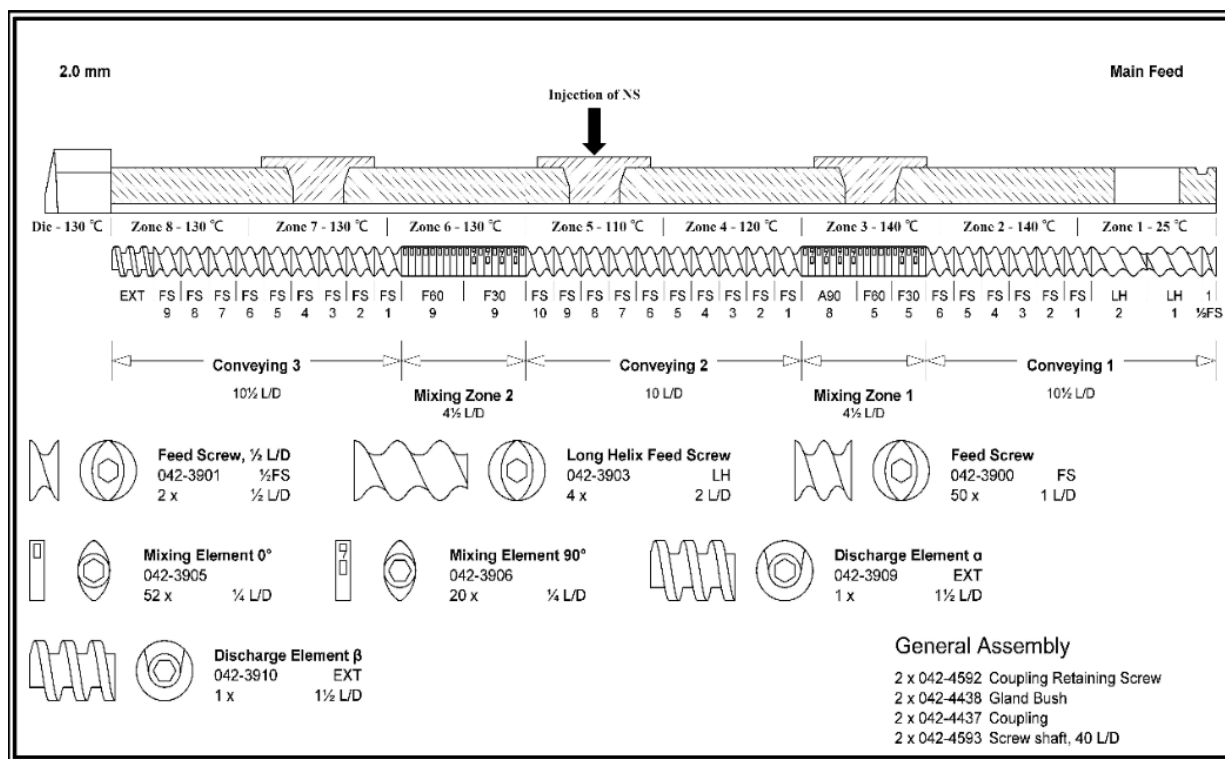


Figure 2-3. Screw configuration used in the preparation of nanocrystal solid dispersions by twin-screw extrusion.

2.4.4. Crystallinity and Morphology of Extrudate

Differential scanning calorimetry was used to confirm the crystallinity of EFZ after extrusion (Figure 2-4). A single sharp endotherm peak was observed for pure EFZ at about 140 °C (Figure 2-4a), which was identical to that of EFZ form I [118]. Since the drug loading in the extrudate was low, the thermograph was magnified, as shown in Figure 2-4b. The endotherm peak around 140 °C reappeared in both extrudate A and B. This indicated the EFZ maintained crystallinity after the extrusion.

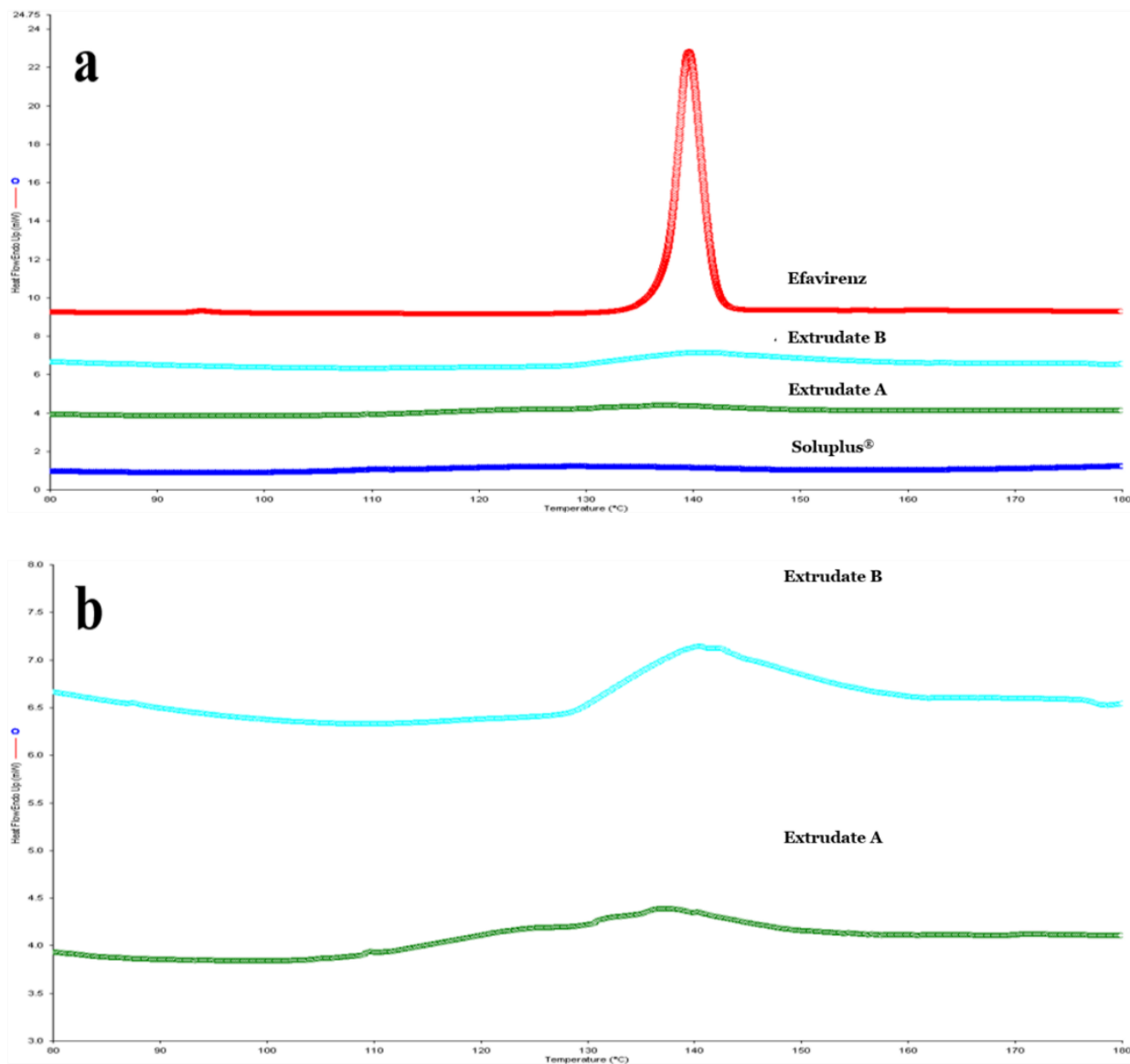


Figure 2-4. Evaluation of crystallinity using differential scanning calorimetry. (a) Comparison of pure efavirenz, extrudate A (1.02 % drug loading), extrudate B (2.06 % drug loading), and Soluplus®. (b) Magnified differential scanning calorimetry thermograph for comparison of extrudates A and B.

SEM was used to determine the morphology and distribution of the EFZ particles (Figure 2-5). Pure EFZ existed as sharp and long needles (Figure 2-5a). The particle size of EFZ was around 20 μm . After HPH and HME, the particle size of EFZ was further decreased to less than 1000 nm. The distribution of EFZ nanocrystals on Soluplus® is quite uniform (Figure 2-5b). The

distance between different EFZ nanocrystals prevents them from coming into contact with each other and the size consistency will prevent the occurrence of Oswald ripening [122]. These features thus establish the conjugated HPH-TSE technique as a novel process to decrease the size of EFZ crystals that also aids in the uniform distribution of EFZ nanocrystals.

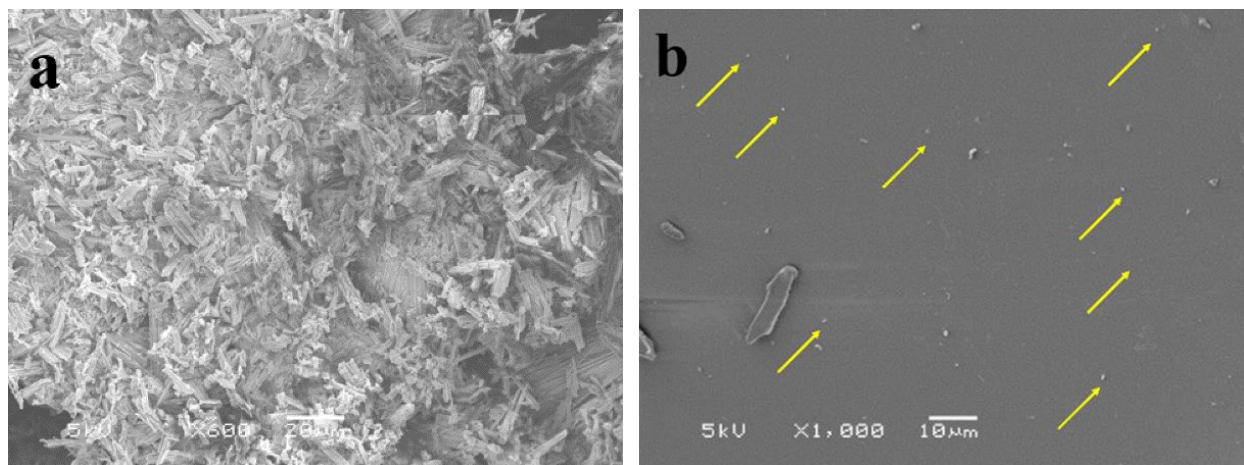


Figure 2-5. Scanning electron microscopy images of (a) pure efavirenz and (b) efavirenz nanocrystal solid dispersion (nanocrystals are marked by arrows).

2.4.5. Drug Content and Residual Moisture

After extrusion, both extrudates were analyzed for drug content. The drug loadings of extrudate A and B were around 1.02% and 2.06%, respectively. The drug contents of extrudate A and B were $102.47 \pm 1.87\%$ and $102.78 \pm 4.69\%$, respectively (Figure 2-6). This indicated that all the EFZ in the NS was enveloped in Soluplus[®]. Considering the low drug loading in the extrudates, EFZ nanocrystals were regarded as homogeneously distributed in the extrudates.

The mean LOD values for the Soluplus[®] extrudate A, and extrudate B were 2.10, 2.24, and 2.26, respectively (Table 2-2), which indicates that there were no significant differences in

residual moisture between these three samples (p value > 0.05). Thus, it can be concluded that all the water that was added during the process was evaporated.

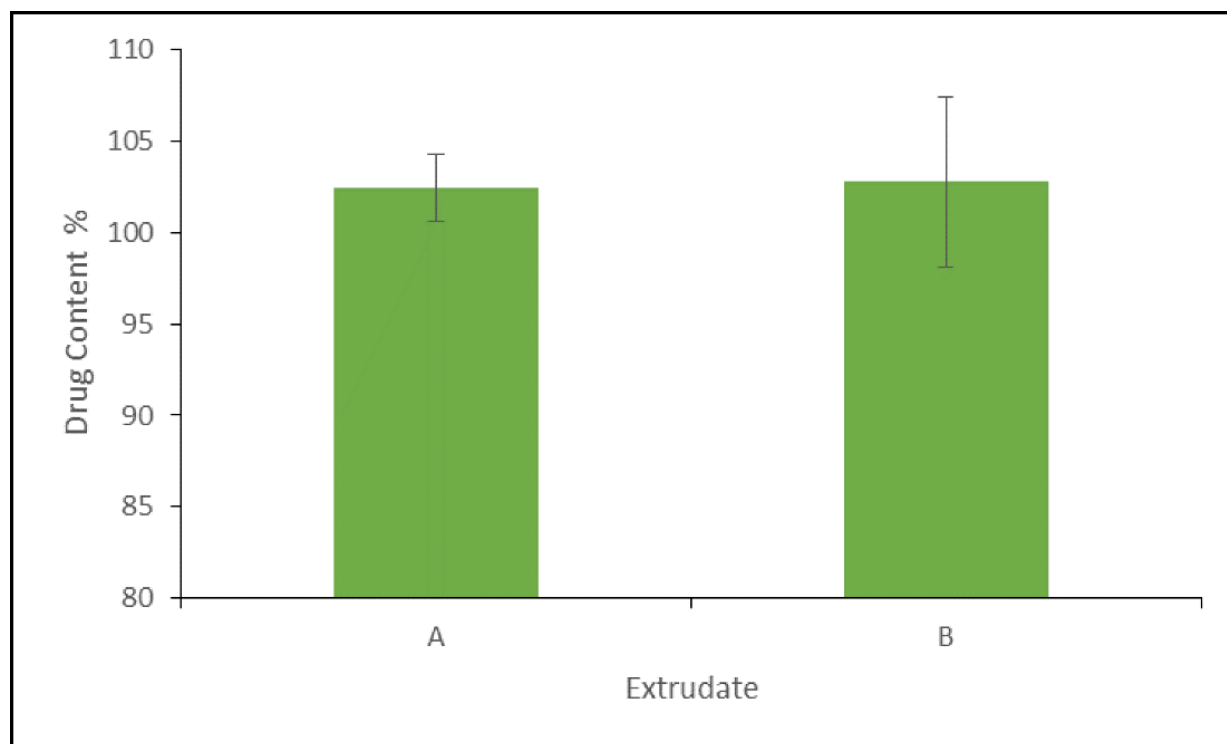


Figure 2-6. Drug content for nanocrystal solid dispersion extrudate A and B.

Table 2-2. LOD for NCSD and Soluplus[®] extrudates

Extrudate	LOD (%)
Soluplus [®]	2.10 ± 0.16
A	2.24 ± 0.07
B	2.26 ± 0.12

LOD: loss on drying

2.4.6. *In Vitro* Drug Release

In vitro drug release was assessed for pure EFZ and both the extrudates (Figure 2-7). As the aqueous solubility of EFZ is very low (recorded as $5.26 \pm 2.3 \mu\text{g/mL}$), 0.2% SLS was added to the dissolution media in order to increase the saturation solubility of EFZ, as well as to maintain the sink condition.

Owing to the poor solubility and wettability, only $14.04 \pm 0.80\%$ of pure EFZ was released after 120 min of dissolution. Both extrudate A and B showed markedly enhanced dissolution rates with $96.86 \pm 0.99\%$ and $96.20 \pm 1.26\%$ drug release observed for extrudate A and B, respectively. It is evident that HPH-TSE successfully increased the dissolution rate. This effect could have partially resulted from decreasing the particle size, or from the increase in the wettability of EFZ caused by Soluplus®.

Although the same percentage drug release was reached at 120 min, it was observed that the release from extrudate B was slower than that from extrudate A. The difference in the dissolution velocity may be because of the different ratios of Soluplus® and EFZ. In extrudate B, EFZ was surrounded by a relatively smaller amount of Soluplus® compared to that in extrudate A. The different appearances of milled extrudates A and B supported this assumption (Figure 2-8). In extrudate A, EFZ nanocrystals were completely covered by Soluplus®. Therefore, the milled extrudate A was the same yellowish color as the pure Soluplus®. However, the appearance of extrudate B was white, which may be because of the uncovered EFZ. This difference will result in slower wetting of EFZ, thus decreasing the dissolution velocity of extrudate B.

However, the differences between these two formulations were not significant. The similarity factor (f_2) was calculated to determine the similarity between the two formulations. The equation used to calculate f_2 is:

$$f_2 = 50 \times \log \left\{ \left[1 + (1/n) \sum_{t=1}^n (R_t - T_t)^2 \right]^{-0.5} \times 100 \right\}$$

Where R_t and T_t are the dissolution value at time point t of the reference and test product, respectively. According to US FDA guidance for industry, two dissolution profiles are considered similar when the f_2 value is greater than 50 [123]. The calculated f_2 value was 55.0, which indicated that the two formulations were similar.

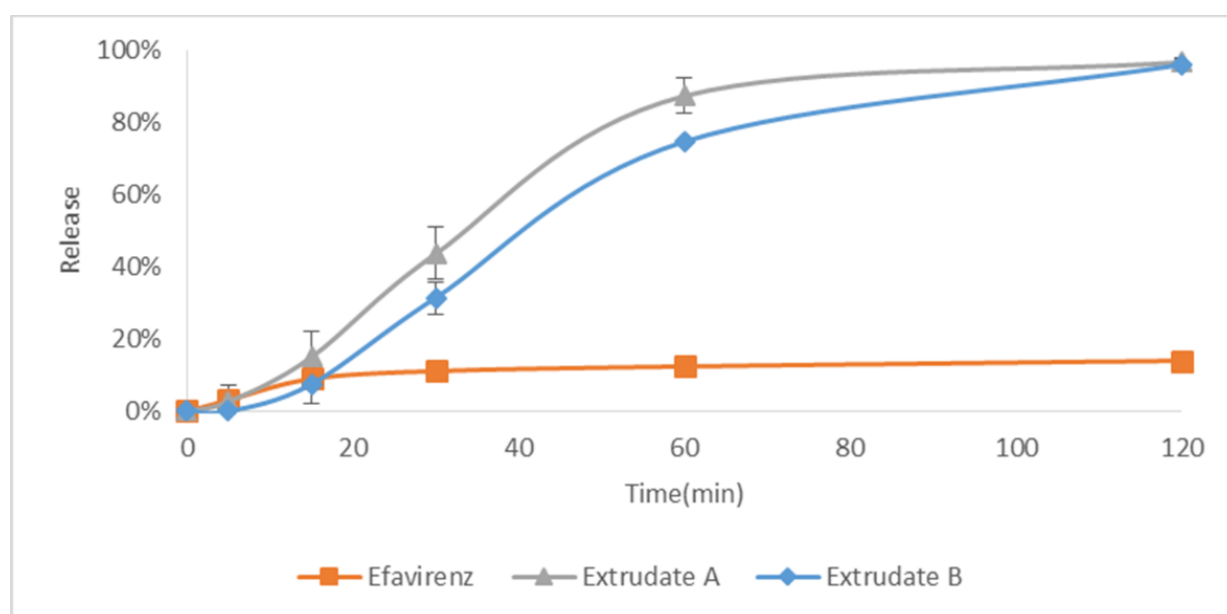


Figure 2-7. *In vitro* drug release profiles for pure efavirenz, extrudate A and extrudate B.



Figure 2-8. Appearance of milled (a) extrudate A, (b) extrudate B, and (c) Soluplus®.

2.4.7. Stability Testing

Stability testing was conducted for both formulations by storing at 25 °C/60% RH for a period of 6 months. At various time points, samples were removed from storage and tested for *in vitro* drug release and micromeritics.

The release profiles for both the extrudates (A and B) were unchanged over the storage period of 6 months (Figure 2-9). The f_2 values were calculated versus the initial samples for both the extrudates (Table 2-3). All the f_2 values were greater than 50, which indicated that the release profiles obtained for both the extrudates at each time point were similar to the initial release profiles.

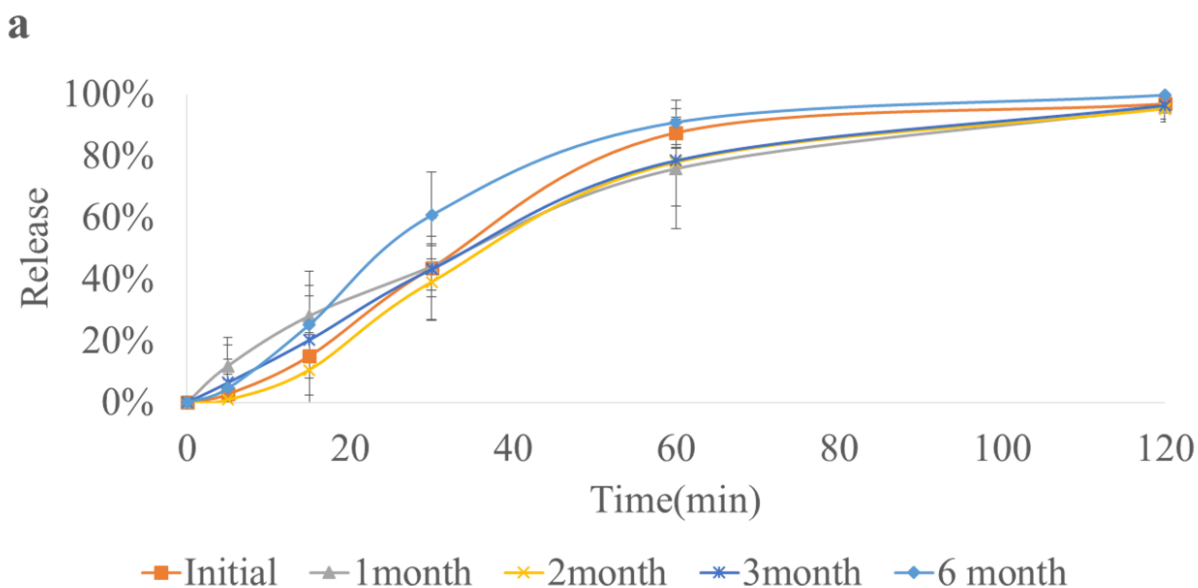


Figure 2-9. *In vitro* release profiles of (a) extrudate A stored at 25 °C/60% relative humidity.

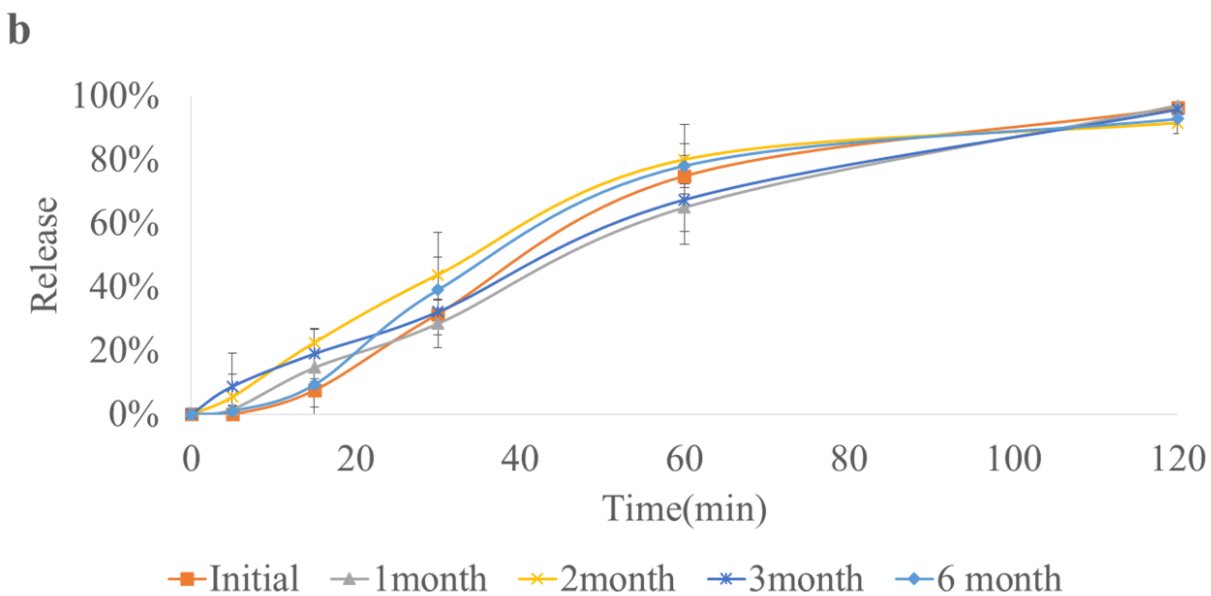


Figure 2-9. *In vitro* release profiles of (b) extrudate B stored at 25 °C/60% relative humidity.

Table 2-3. f_2 Values of extrudates with different storage times

	f_2			
	1 month	2 months	3 months	6 months
Extrudate A	54.5	65.5	66.7	53.8
Extrudate B	63.9	52.9	58.7	70.7

Comparison of particle size, PDI, and zeta-potential was conducted for the extrudates at each time point (Table 2-4). There was no significant change observed at any time point. (P value > 0.05). All the above data indicates that the EFZ NCSD prepared by HPH-HME technique possesses good stability for a period of 6 months at 25 °C/60% RH.

Table 2-4. Comparison of particle size, PDI, and zeta-potential with different storage times.

Item	Time	Particle Size (nm)	PDI	Zeta-Potential (mV)
Extrudate A	Initial	28.04 ± 1.35	0.184 ± 0.03	-16.82 ± 1.21
	1 Month	28.04 ± 0.17	0.183 ± 0.03	-17.86 ± 1.73
	2 Months	29.78 ± 6.81	0.190 ± 0.04	-17.13 ± 1.32
	3 Months	29.60 ± 4.33	0.179 ± 0.02	-17.26 ± 1.51
	6 Months	29.05 ± 0.26	0.186 ± 0.01	-18.13 ± 5.92
Extrudate B	Initial	34.11 ± 5.03	0.193 ± 0.04	-14.38 ± 2.10
	1 Month	30.82 ± 2.78	0.189 ± 0.02	-15.07 ± 1.68
	2 Months	30.67 ± 2.93	0.186 ± 0.03	-14.68 ± 1.52
	3 Months	39.66 ± 5.75	0.185 ± 0.03	-13.75 ± 1.87
	6 Months	32.94 ± 0.88	0.189 ± 0.01	-13.93 ± 0.76

PDI: polydispersity index.

CHAPTER 3.
EFFECTS OF PROCESSING ON A SUSTAINED RELEASE FORMULATION
PREPARED BY TWIN SCREW DRY GRANULATION

3.1. Objective

The objective of this study was to apply twin-screw dry granulation (TSDG) technology to produce a sustained-release dry granule formulation, and subsequently compress the sustained release tablets. Theophylline was used as a model drug in this research. Design of experiment (DoE) was applied in the process to understand the effect of different processing parameters on the dry granule properties and optimize these factors.

3.2. Materials

Theophylline was purchased from Ria International LLC (Saint Louis, MO, US). Caffeine citrate was supplied by Fisher Scientific (Pittsburgh, PA, USA). Acetaminophen was kindly contributed by Mallinckrodt Inc. (Raleigh, NC, USA). Chlorpheniramine maleate was obtained from Medchemexpress LLC (Princeton, NJ, USA). Hydroxypropyl cellulose (Klucel™ EF) was generously gifted by Ashland Specialty Ingredients (Wilmington, DE). Ethyl cellulose (Ethocel Standard 10) was kindly donated by Dow chemical company. Magnesium stearate was purchased from Spectrum Laboratory Products Inc. (Gardena, CA, US). All the other reagents used in this study were of the analytical grade.

3.3. Methods

3.3.1. Preliminary Study

Four different APIs (Theophylline, Caffeine citrate, Acetaminophen and Chlorpheniramine maleate) at three levels of drug loading (30, 40 and 50 %, respectively) were

tested for the feasibility of being applied in TSDG. Different formulation parameters, such as polymer ratio, lubricant concentration was pretested for their influence on the quality of granules.

3.3.2. Design of Experiment

A Resolution V Irregular Fraction Design was created using Design-Expert® 8.0.6 (Stat-Ease, Inc., Minneapolis, MN, USA), with three numeric factors (screw speed, feeding rate and barrel temperature) and one categorical factor (screw configuration), which all varied over only two levels. Flow properties (angle of repose and flowability index), particle size distribution, and dissolution time were selected as response variables to optimize the process.

3.3.3. Twin Screw Dry Granulation

Theophylline was selected as a model drug for this study based on the result of preliminary study. All the ingredients were passed through US # 35 mesh screen in order to remove any aggregates that might be formed. Theophylline (50% w/w) was premixed with Klucel™ EF (25% w/w) and Ethocel (25% w/w) using a Maxiblend™ V-shell blender (GlobePharma, New Brunswick, NJ) at 25 rpm for 20 min. Magnesium stearate (0.2% w/w) was then added and mixed for 4 min. Dry granulation was prepared using an 11-mm co-rotating twin-screw extruder (Thermo Fisher Scientific, Waltham, MA, USA) without a die. The extruder consists of eight zones, the individual temperature of which, excluding zone 1, can be precisely controlled. The barrel was maintained within a temperature range of 70–110 °C. The physical mixture was fed into the extruder using an 11-mm single-screw feeder (Thermo Electron,

Karlsruhe, Germany) at a selected feeding rate of 3 or 10% (approximately 1.42 or 5.09 g/min). The screw speed was set at either 50 or 100 rpm. The materials were collected at the end of the extruder after the steady state of was achieved. The collected samples were stored in polyethylene bags for further processing and analysis.

3.3.4. Particle size distribution

The particle size distribution was determined by utilizing the sieve analysis method. The granules were divided into three portions by two USA standard test sieve, # 35 (500 μm) and # 12 (1.68 mm). The large size granules (over 1.68 mm) were retained at the upper sieve (# 12), the medium size granules (between 500 μm and 1.68 mm) were retained at the lower sieve (# 35), the fines (under 500 μm) which were not retained by either sieve were collected by the wax paper under the sieves. Each portion of granules were weighed, and the percentile weight distribution was calculated accordingly.

3.3.5. Flow Properties

3.3.5.1. Angle of Repose

The fixed funnel method was applied to measure Angle of repose. The material was poured through a funnel to form a cone. In order to minimize the impact falling particles, the height of funnel was gradually elevated to ensure the tip of funnel was held close to the rising cone with no touch. Stop pouring the material when the predetermined width of the pile was reached. The height and the radius of the base of the cone was measured. The equation to calculate the Angle of repose (θ) is as follows:

$$\tan (\theta) = \frac{h}{r}$$

Where, h is the height of the formed cone and r is the radius of the base of the cone, respectively.

3.3.5.2. Flowability Index

The flowability index was measured using a Flodex powder flowability index test instrument (Hanson Research, Chatsworth, CA, USA). The height of funnel was adjusted in the way that the funnel bottom was close to but not touching the material surface. 10 g of material was poured into the central of the cylinder through the funnel. 30 sec was allowed after loading was completed for the possible flocculation of individual material or whole load. 16 mm flow disk was used for previously untested material. Slowly turn on the release lever to open the hole in the disk without vibration. The test was considered positive when the open hole on the disk was observable from the top of cylinder. Repeat tests with disk possessing smaller holes for positive results until negative result was achieved. Repeat tests with disk possessing larger holes for negative results until positive result was achieved. The smallest hole that the sample could fall freely for three successive tests was considered the flowability index [124].

3.3.6. Differential Scanning Calorimetry

Approximately 2-5 mg samples of interest were weighed and hermetically sealed in an aluminum pan. A Diamond DSC (PerkinElmer, Shelton, CT, USA) was used to measure the degree of crystallinity of the samples. The instrument's Pyris manager software (Shelton, CT,

USA) was utilized to analyze the data. The heating rate was set at 20 °C/min from 20 to 300 °C under an inert atmosphere of nitrogen at a flow rate of 20 mL/min.

3.3.7. Tablet Compression

200 mg obtained granules were mixed with 0.3% magnesium stearate just prior to manual direct compression on a MCTMI single punch tablet press (GlobePharma Inc., New Brunswick, NJ, USA). A 0.375 inch flat round punch was used, and a compression force of 150 kg/cm was applied.

3.3.8. Scanning Electron Microscopy

The morphology of all samples (granules, tablets and raw material) was determined by utilizing scanning electron microscopy (SEM). Samples was mounted onto an aluminum stage by an adhesive carbon tape, and then sputter coated with gold under an argon atmosphere using a Hummer 6.2 Sputter Coater (Ladd Research Industries, Williston, VT, US). The coater was kept in a high-vacuum evaporator equipped to guarantee a uniform coating. Finally, images were captured using a JSM-5600 scanning electron microscope (JEOL USA, Inc., Waterford, VA, US) at an accelerating voltage of 5 kV.

3.3.9. In Vitro Drug Release Study

Both tablets and granules equivalent to 100 mg of theophylline were checked for *in-vitro* drug release. The dissolution media used was 900 mL 0.1 N HCl (pH 1.2, simulated gastric medium). SR8-plus™ dissolution apparatus (Hanson, Chatsworth, CA, US) was maintained at

37 ± 0.5 °C and the paddle speed was set at 50 rpm. Granules were filled into capsules (size 0) for dissolution. The UV spectra were collected by an in-site Rainbow UV-Vis probes (Pion Inc., Billerica, MA, USA) at λ_{max} 270 nm every 5 min for first 1 h, then every 15 min until 2 h. Tablets were directly dropped into dissolution vessel for test. The UV spectra were collected at λ_{max} 270 nm using the same instrument every 15 min for first 1 h and then for every 30 min until 24 h.

3.4. Results and Discussion

3.4.1. Preliminary Study

3.4.1.1. Lubricant

While conducting the preliminary study, a grinding noise, which was never found during the Hot-Melt Extrusion (HME) process, was heard. This noise indicated the existence of some friction in the twin screw extruder. In HME, the flexible nature of melt will not cause any rubbing at powder-instrument interfaces (wall friction) [125]. The lubrication effect of the melt itself will also prevent the abrasion between the screw and barrel. However, in the TSDG process, all materials were kept in solid state, friction could occur universally where the contact of equipment and material occurred. Thus, addition of dry lubricant was necessary to both protect the instrument and prevent the contamination of products. Magnesium stearate, which was widely used dry lubricants in the pharmaceutical industry, was applied to the formulation. It was found that magnesium stearate was able to eliminate the noise mentioned above. Nevertheless, too much amount of magnesium stearate may significantly decrease the yield of granule, even results in entire fines. This phenomenon was resulted from the nature of lubrication

effect. The lubricant molecules will form some oriented monolayer or multilayer boundary, which will prevent the additional contact between instruments and powder particles. However, too much lubricant or long time mixing with API and excipients will result in the boundary formed between particles, thus prevention of agglomeration of powder particles. In this case, a moderate quantity of 0.2% magnesium was selected and added to the formulation at the final stage of mixing.

3.4.1.2. Polymer and Excipient Ratio

Hydroxypropyl cellulose (HPC), which is a thermoplastic polymer, has been previously studied as dry binders for both tablet compression [126-128] and roller compaction [129]. Ethylcellulose (EC), which is a water-insoluble polymer has applied to prepare lots of sustained release formulation [130-132]. Thus, the combination of HPC (dry binder) and EC (release controller) was selected for the excipients for preparation of sustained release dry granulation. Two ratios of EC and HPC (1:1 and 3:1) were studied to optimize the blend of polymers. The 1:1 combination exhibited a better probability to produce medium size granule. Therefore, 1:1 ratio of EC and HPC was used as excipients for this study.

3.4.1.3. API and Drug Loading

Four different APIs (Chlorpheniramine maleate, Acetaminophen, Caffeine citrate and Theophylline) with a broad melting point range from 140 °C to 270 °C were selected as candidates for TSDG process. Physical mixture with each API at three drug loadings (30, 40 and 50%, respectively) was prepared for the test of feasibility to be applied in TSDG (Table 3-1). All

the tests were conducted at same feeding rate, screw speed, screw configuration and barrel temperature.

Table 3-1. Candidate of APIs.

No.	Drug name	BCS	MP Literature /Measurement
1	Chlorpheniramine maleate	I	142/139.26 °C
2	Acetaminophen	I	169/172.7 °C
3	Caffeine Citrate	I	235.6 - 236.2/168.69 °C
4	Theophylline	I	273/276.77 °C

Each product after TSDG was tested with DSC to detect the crystallinity of API (Figure 3-1). All the DSC thermograms showed a single sharp endotherm peak, which demonstrated the preservation of the crystallinity after TSDG.

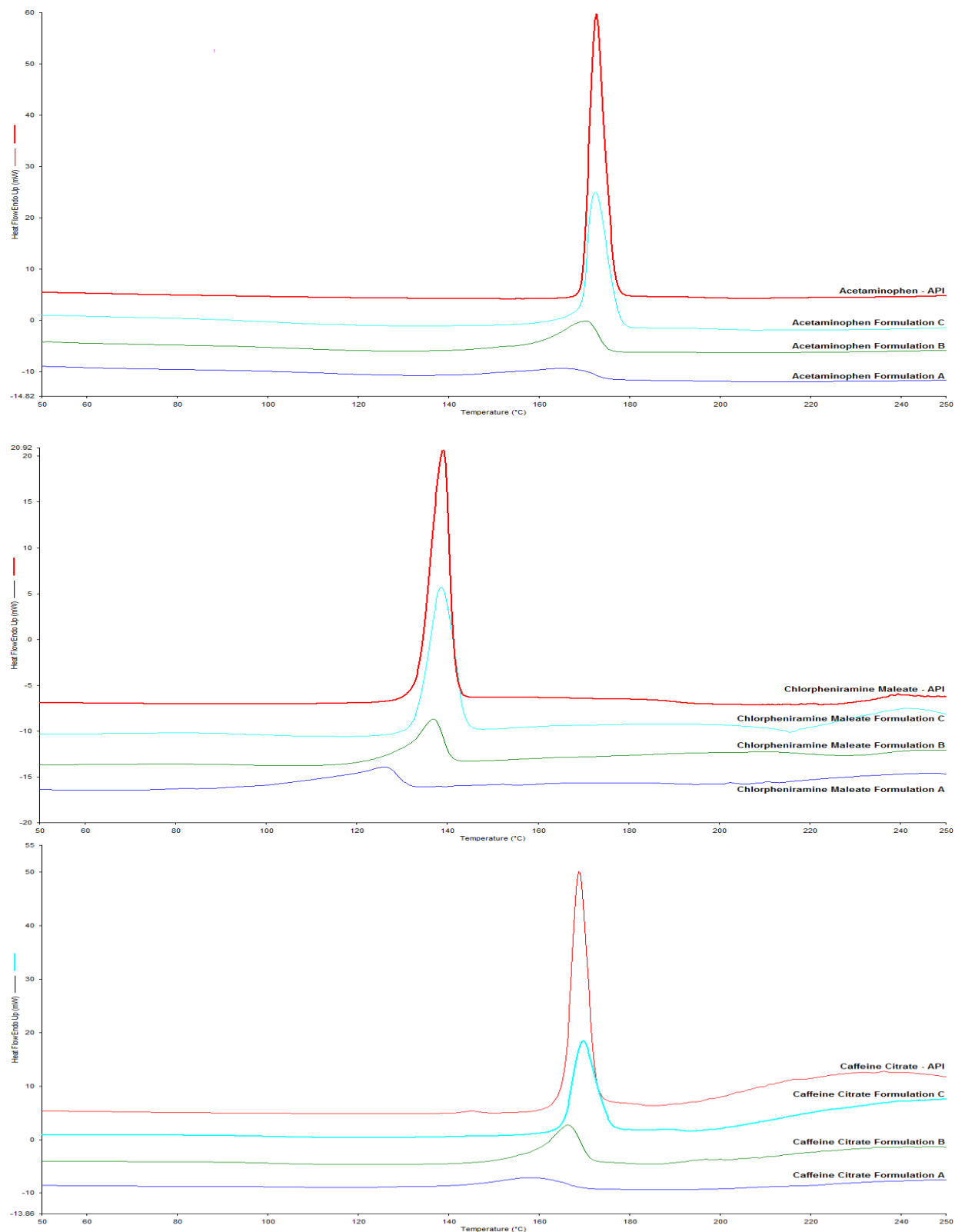


Figure 3-1. DSC thermograms of four API and products after TSDG. Formulation A: 30 % drug loading, formulation B: 40% drug loading, C: 50% drug loading.

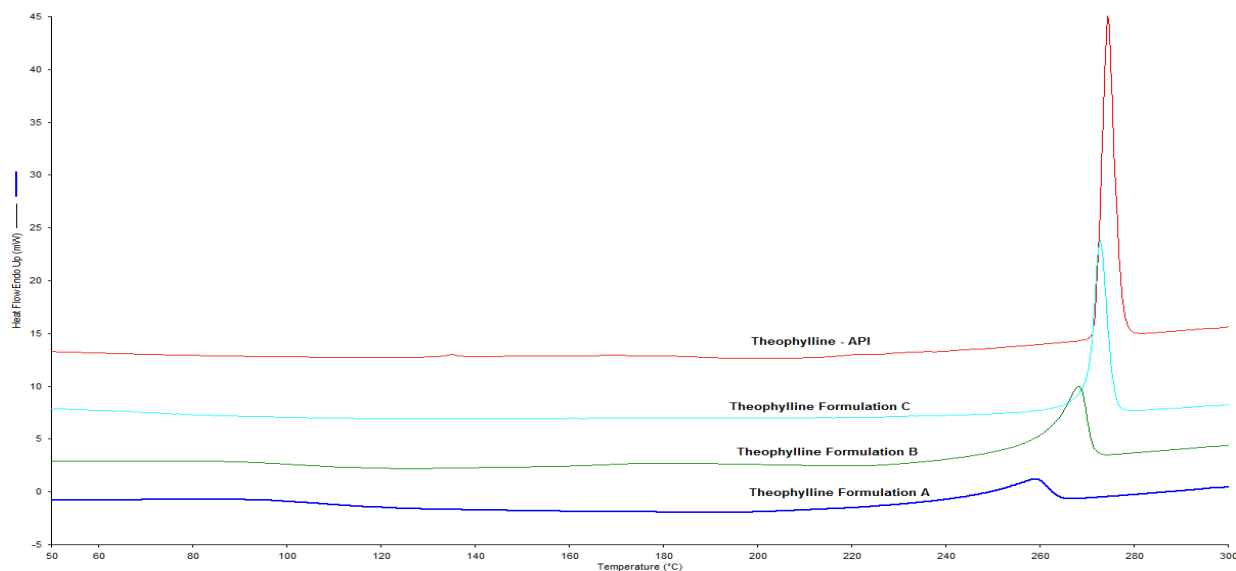














Figure 3-1. DSC thermograms of four API and products after TSDG. Formulation A: 30 % drug loading, formulation B: 40 % drug loading, C: 50 % drug loading.

The morphology of products obtained was summarized in Table 3-2. It was obvious that the low drug loading PM tended to achieve more robust and greater size granule after TSDG. However, none of these four APIs could form granule at high drug loading of 50%. That's because more binder was presented in the low drug loading formulation. The higher binder ratio could more effectively assisted the agglomeration of raw materials, thus granulation. Due to the low ratio of binder in the 50% formulation, the raw material could not accumulate together to form granules, hence presented as fine powders. From the API aspect, Acetaminophen and Caffeine citrate showed the best ability to be granulated. More sturdy and bigger size granules were attained at 30% drug loading. On the contrary, 30% of chlorpheniramine maleate and theophylline could only achieve smaller and long strip shape granule. The theophylline granule is even weaker than the chlorpheniramine maleate granule. For the 40% drug loading, Acetaminophen and Caffeine citrate still can form some long striped shape granule. However, barely any granule could be seen from the chlorpheniramine maleate and theophylline

formulation. In summary, higher drug loading will hinder the formation of granulation. And theophylline was the most difficult one to be granulated among these four APIs. If dry granulation could be accomplished for the most difficult formulation combination, it could be much easier for another recipe. Therefore 50% drug loading of theophylline was designated for the DoE study of processing parameters optimization.

Table 3-2. Morphology of 4 APIs at 3 different drug loading after TSDG.

	30%	40%	50%
Chlorpheniramine maleate			
Acetaminophen			
Caffeine Citrate			
Theophylline			

3.4.2. DoE Set up

Other than the formulation parameters, processing parameters are also critical to the final product quality. To determine the appropriate ranges of experimental design, a series of processing parameters were tested. From these initial results, four processing parameters (screw configuration, screw speed, barrel temperature and feeding rate) were selected and the operation ranges were shown in Table 3-3. Two screw configurations utilized in the experimental design were shown in Figure 3-2. For screw configuration 1, only one mixing zone, which was comprised of 7 mixing elements with 60° offset angles, was presented at zone 5. For screw configuration 2, another small mixing zone, which was comprised of 5 mixing elements with 30° offset angles, was added at zone 7. The barrel temperature profile was shown in Table 3-4. The highest temperature was set at zone 5 to assist the granulation process.

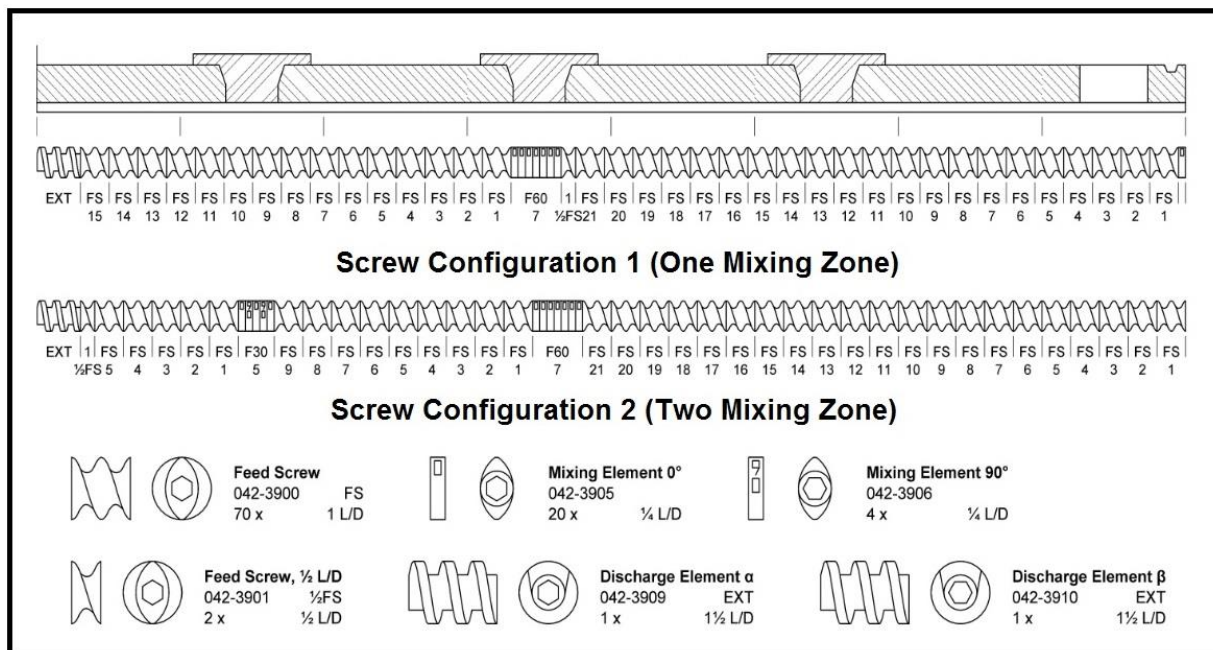


Figure 3-2. Screw configuration utilized in TSDG.

Table 3-3. Experimental factors and ranges of variation.

Type	Independent Variable (Factor)	Symbol	Unit	Upper Level (+1)	Lower Level (-1)
Categorical	Screw Configuration	A	N/A	Two Mixing Zone	One Mixing Zone
Numeric	Barrel Temperature (Zone 5)	B	°C	110	90
	Screw Speed	C	Rpm	100	50
	Feeding Rate	D	%	10	3

Table 3-4. Barrel Temperature Setting.

	Zone 8	Zone 7	Zone 6	Zone 5	Zone 4	Zone 3	Zone 2
	°C						
Temperature (-1)	70	70	80	90	80	70	70
Temperature (+1)	90	90	100	110	100	90	90

Twelve runs of experimental design were proposed using a Resolution V Irregular Fraction Design (Table 3-5). This experimental design was selected because it would allow of estimation of all main effects. The two-factor interactions will be aliased only by three-factor or higher interactions [133]. This design was considered as an excellent design, which was a worthwhile alternative to the full factorial design, to reduce the number of runs and still obtain clean results.

Table 3-5. Experimental Design.

Std	Run	A	B	C	D
2	1	+1	110.00	50.00	3.00
4	2	+1	90.00	100.00	3.00
12	3	-1	110.00	100.00	10.00
5	4	-1	110.00	100.00	3.00
1	5	-1	90.00	50.00	3.00
8	6	+1	90.00	50.00	10.00
7	7	-1	90.00	50.00	10.00
9	8	-1	110.00	50.00	10.00
11	9	+1	90.00	100.00	10.00
6	10	+1	110.00	100.00	3.00
10	11	+1	110.00	50.00	10.00
3	12	-1	90.00	100.00	3.00

3.4.3. Characterization of crystallinity

Theophylline was categorized as a Biopharmaceutics Classification System (BCS) I drug. Thus the crystallinity of theophylline was expected to be maintained in order to prevent the potential thermal stability problem [134]. The crystallinity of theophylline as pure drug and in all twelve runs was confirmed by utilizing DSC (Figure 3-3). A single sharp endotherm peak at around 275 °C, as well as a small endotherm peak at about 288 °C, was observed for pure theophylline. This demonstrated the API we used was belong to the theophylline anhydrous form I [59, 135]. After TSDG, the big endotherm peaks of all runs were preserved, however it was

compressed to around 270 °C. In the meantime, the small endotherm peak also shifted a little bit to lower temperature. These results confirmed that the crystallinity of theophylline was preserved after TSDG. Nevertheless, some interaction between theophylline and polymers was likely to occur [136].

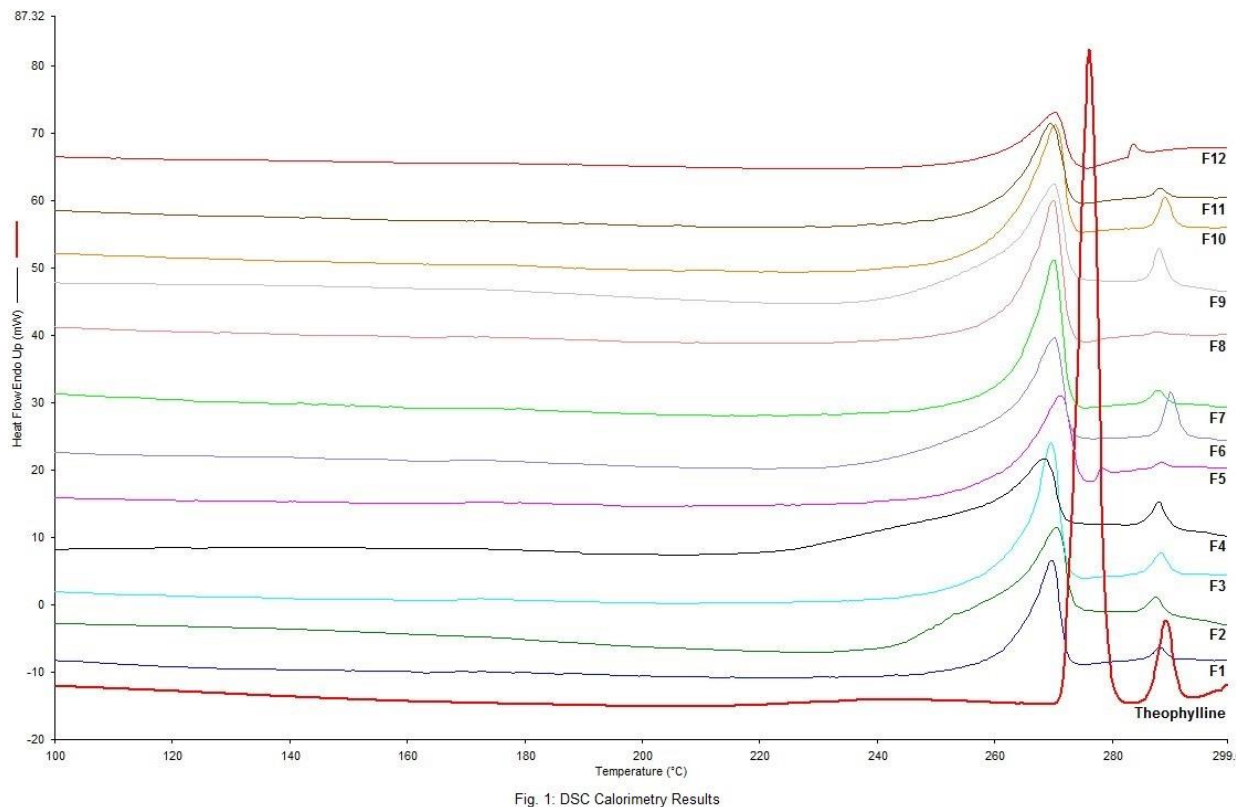


Figure 3-3. DSC thermograms.

3.4.4. The effects of the processing parameters on the particle size distribution

Each run of samples was separated into three portions: the large size granules (over 1.68 mm), the medium size granules (between 500 μ m and 1.68 mm) and the fines (under 500 μ m). The granule size distribution results for all runs were shown in Table 3-6. The medium size granules are the most important part for the tableting process. In addition, fines are also very

important to the compression and compaction features, since the vacant space between granules could be occupied by them. However, the amount of fines should not be over 10% [137]. It was also mentioned that a small amount of fines could improve the appearance of tablet [87]. Thus, both the medium size granule and fines were selected as dependent variable (response) in the Resolution V Irregular Fraction Design. The regression equations for both medium size granules and fines fraction were calculated from the experimental results. The coefficients and the statistical significance were summarized in Table 3-7. It should be mentioned that only the parameters related to independent variables (factors) and models were given. The full regression equation was shown under each section.

Table 3-6. DoE Results.

Run	Fines (< 500 μ m)/%	Medium Size Granule (500 μ m - 1.68 mm)/%	Large Size Granule (> 1.68 mm)/%	Angle of Repose/ $^{\circ}$	Flowability Index/mm	Dissolution Time for Maximum Drug Release/h
1	2.69	32.29	65.02	28.92	20	13
2	74.63	25.37	0	31.23	22	23
3	6.88	70.42	22.7	27.6	14	16
4	13.74	59.23	27.03	30.65	24	12
5	25.24	56.15	18.61	27.02	20	23
6	12.41	51.49	36.1	26.67	22	16
7	12.46	64.76	22.78	25.49	9	15
8	4.98	53.84	41.18	26.93	14	10
9	29.39	57.93	12.68	29.18	20	18
10	23.71	66.98	9.31	28.48	22	20
11	0.61	11.45	87.94	30.14	34	16
12	30.36	59.43	10.21	29.24	20	21

Table 3-7. Statistical analysis and regression coefficients of the particle size distribution.

Variables	Angle of repose		$1/\sqrt{\text{Flowability index}}$	
	Coefficient	P	Coefficient	P
Model		0.0332		0.0007
Intercept	28.01		0.23	
A	0.42	0.1032	-0.027	0.0003
B	0.50	0.0697	-0.016	0.0006
C	0.75	0.0248	0.000	1.0000
D	-0.54	0.0567	0.016	0.0007
	$R^2 = 0.9694$		$R^2 = 0.9998$	
	Pred $R^2 = 0.5107$		Pred $R^2 = 0.9936$	

3.4.4.1. Medium size granules

The percentage of medium size granules in all 12 runs varied in a wide range of 11.45 – 70.42%, where run 1, 2 and 11 showed the least medium size granule yield (less than 35%), and run 3,7 and 10 could achieve the highest amount of medium size granule (Over 60%). The regression equation for the percentage of medium size granules was created as follows:

% Medium size granule

$$= +56.07 - 10.25 * A - 0.69 * B + 6.83 * C + 3.15 * D + 3.16 * A * C \\ + 5.19 * B * C - 6.35 * B * D + 7.00 * C * D + 8.87 * A * B * C$$

Based on the ANOVA analysis, the p value of the model was 0.0347, which indicated the model was reliable. The most significant factors for the percentage of medium size granule was

found to be screw configuration and screw speed. The relationship between the response and these two factors could be better understood by the contour plot shown in Figure 4. Figure 3-4a and 3-4b were both obtained at the feeding rate of 10%. The only difference was the screw configuration: one mixing zone for Figure 4a and two mixing zones for Figure 3-4b.

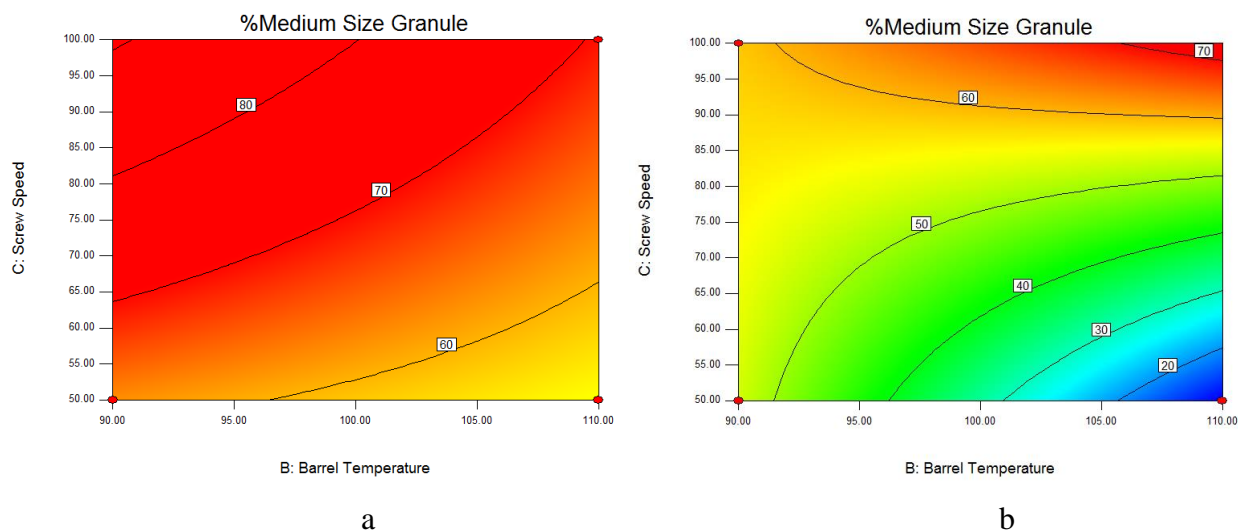


Figure 3-4. Contour plots showing the effect of screw speed on percentage of medium size granules (a) one mixing zone configuration, (b) two mixing zone configuration.

It was obvious that the Figure 3-4a showed more medium size granule than Figure 3-4b, which meant the one mixing zone configuration is beneficial for the generation of this mid-size portion particles. This result was in accordance with the negative coefficient (-10.25) in front of A. This phenomenon could be explained by the effect of the second mixing zone. It was reported by Dhenge et al. that the second mixing zone could either decrease or increase the size of agglomerated granule by the first mixing zone. This size alteration was owing to several functions of the second mixing zone: shearing, deformation, breaking, mixing, re-granulation and consolidation [138]. In our circumstances, if the granule generated by the first mixing zone was not strong enough, it could be broken down into smaller granule or fines. On the contrary, if

the previously obtained granule had adequate strength, it would be further combined to form bigger granule. In either situation, the amount of medium size granule would decrease. Hence the second mixing zone was considered as a hindrance of the medium size granule.

Both Figure 3-4a and 3-4b showed the same tendency that the increased screw speed would lead to higher percentage of medium size granule. At first glance, it seemed to conflict with the data of Tu et al., who claimed the increasing screw speed would decrease the granule size[139]. However, it was same when the large size granule was taken into consideration as well. From the regression equation of large size granule (data not shown), the negative correlation was found between large size granule amount and screw speed. Hence it could be roughly equivalent to the condition, which the increased screw speed would cause the decrease of large size granule and increase of medium size granule, i.e., decrease the whole granule size. The possible mechanism should be the mean residence time decreases with increasing screw speed, resulting in less kneading effect on powder particles, thus generating smaller granules.

3.4.4.2. Fines

The fines amount also varied largely among 12 experimental design (0.61 – 74.63%). Similar to medium size granules quantity, the regression equation was also given for percentage of fines. However, based on the Box-Cox Plot, it was recommended by the software to do the square root transformation for the response, which was presented as $y' = \sqrt{y + k}$, $k = 0$ in this case. Hence the new regression equation was shown as follows:

$$\sqrt{\% \text{ Fines}} = +3.96 + 0.19 * A - 1.11 * B + 0.75 * C - 0.83 * D - 0.43 * A * B + 0.62 * A * C$$

The p value of 0.0018 was a visible sign that the model was dependable. Based on the significant effect (Table 3-7), barrel temperature, screw speed and feeding rate all had significant effect on fines amount ($p < 0.05$). The regression results could be visually assessed by the contour plot as shown in Figure. 5.

Figure 3-5a and 3-5b was gained under screw speed of 100 rpm with two different screw configuration. Negative correlation could be found for percentage of fines with barrel temperature and feeding rate. The decrease of fines could also be thought as the increase of granulated particles. Therefore, this phenomenon was transformed to the situation that higher feeding rate and barrel temperature would lead to more granules. Osborne et al. [140] and Palzer et al. [141] both stated the contact points between powder particles might sinter together to form solid bridges when the temperature was increased to close the the glass transition temperature. The solid bridge would bond the particles together to form strong agglomerates, i.e. granules. In this case, the increased temperature would support the formation of granules. The same relationship between granule and feeding rate was also observed by a lot of authors [19, 142, 143]. Higher feeding rate would cause more powder in the barrel, thus easier for them to be condensed and compacted into granules.

Unlike the two factors mentioned above, screw speed positively affect the percentage of fines (Figure 3-5c and 3-5d). This effect could be easily explained by the mechanism mentioned in the medium size granule part. The increased screw speed would decrease the particle size, thus generating more fine particles.

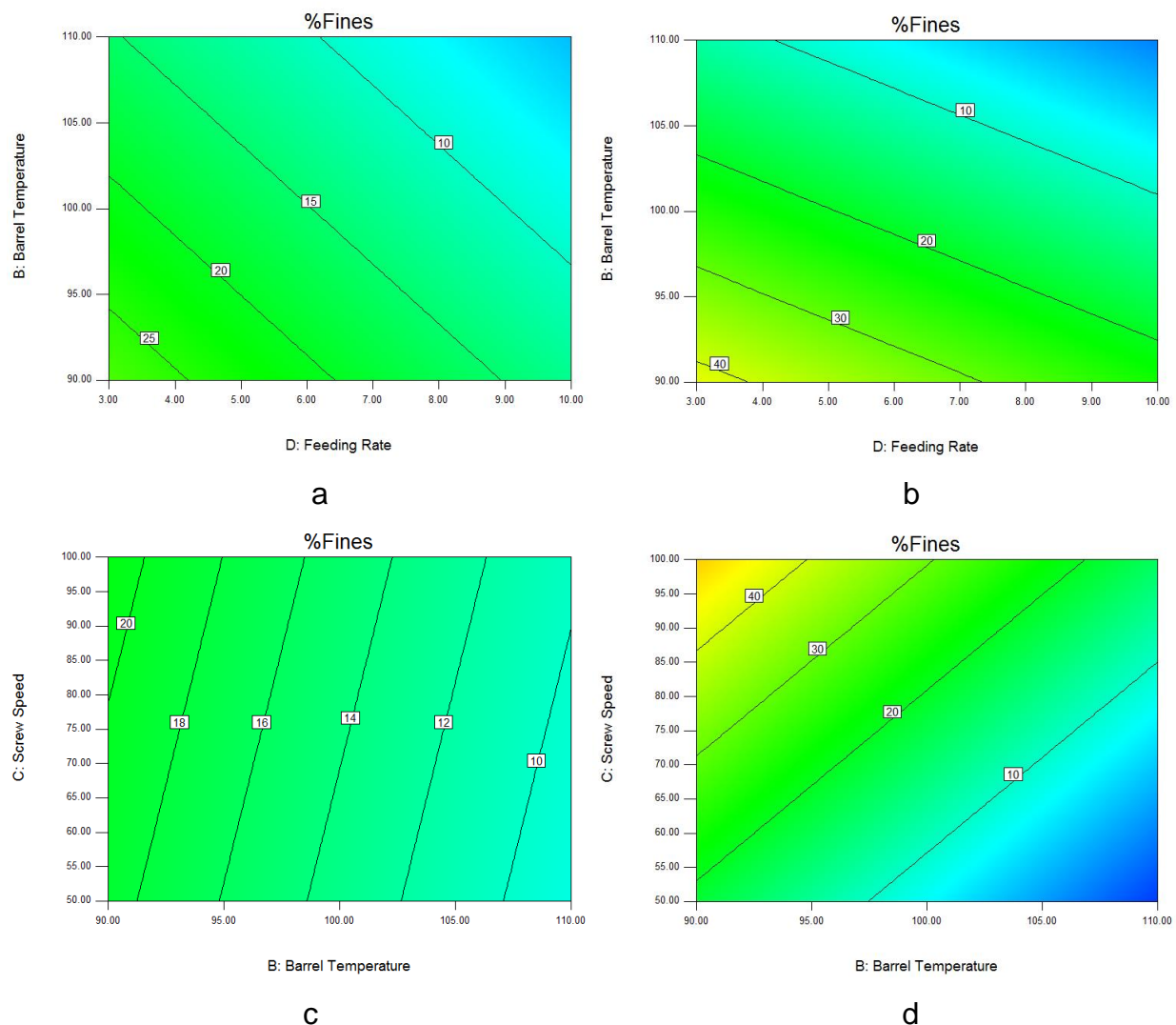


Figure 3-5. Contour plots showing the effect of barrel temperature, screw speed and feeding rate on percentage of fines: (a) & (c) one mixing zone configuration, (b) & (d) two mixing zone configuration.

3.4.5. The effects of the processing parameters on the flow property

One of the most important objectives of granulation was to improve the flow property of raw materials. This increased flow property could have numerous advantages, such as consistent tablet properties, more uniformed formulation and high production speed. Therefore, the assessment of flow property of granule became a very important step to examine the effect of granulation operation. Angle of repose was the most widely used method to determine the flow

property. However, it was also mentioned the data obtained from angle of repose was not a dependable because this method did not mimic the powder's behavior in the instrument [124]. To solve this problem, another technique called flowability index was developed to characterize the flow property. In this study, both methods were utilized to test the flow property of samples. The data gained was further apply to experimental design to obtain the regression equation. The coefficients and the statistical significance were summarized in Table 3-8.

Table 3-8. Statistical analysis and regression coefficients of the flow property.

Variables	Angle of repose		$1/\sqrt{\text{Flowability index}}$	
	Coefficient	P	Coefficient	P
Model	N/A	0.0332	N/A	0.0007
Intercept	28.01	N/A	0.23	N/A
A	0.42	0.1032	-0.027	0.0003
B	0.50	0.0697	-0.016	0.0006
C	0.75	0.0248	0.000	1.0000
D	-0.54	0.0567	0.016	0.0007
	$R^2 = 0.9694$		$R^2 = 0.9998$	
	Pred $R^2 = 0.5107$		Pred $R^2 = 0.9936$	

3.4.5.1. Angle of repose

The angle of repose for samples of 12 runs dispersed in a very narrow range. Other than run 2, 4 and 11, all runs shows excellent flow property ($25^\circ < \text{angle of repose} < 30^\circ$). The resultant regression equation was created as follows:

Angle of repose

$$\begin{aligned} &= +28.01 + 0.42 * A + 0.50 * B + 0.75 * C - 0.54 * D + 0.52 * A * D \\ &- 0.67 * B * C - 0.60 * C * D - 0.77 * A * B * C \end{aligned}$$

The p-value was given as 0.0332, which demonstrated the model was reliable. Screw speed showed the most significant effect on angle repose ($p < 0.05$). However, the effect of barrel temperature and feeding rate were also not negligible ($p < 0.10$).

The positive coefficient for screw speed implied the increase of screw speed would cause the high angle of repose, which represented the low flow property. While the feeding rate exhibited a negative coefficient, which meant the higher feeding rate would lead to lower angle of repose and better flow property. Both of these parameters corresponded with the fines amount very well. Increasing screw speed or decreasing feeding rate would result in more fines, leading to poorer flow property and higher angle of repose. Nevertheless, the positive constant in front of barrel temperature, which represented higher temperature would increase angle of repose and decrease flow property of granules, seemed to be conflict with data achieved from the percentage of fines. This could be explained by the granule shape. In spite of particle size, particle shape was also quite a critical parameter to affect the flow property. It was observed the granule produced in higher temperature would be more tend to be in a long stripe shape, which was definitely had poor flow property. The effect of aforementioned parameters on angle of repose was plotted into contour as showing in Figure 3-6.

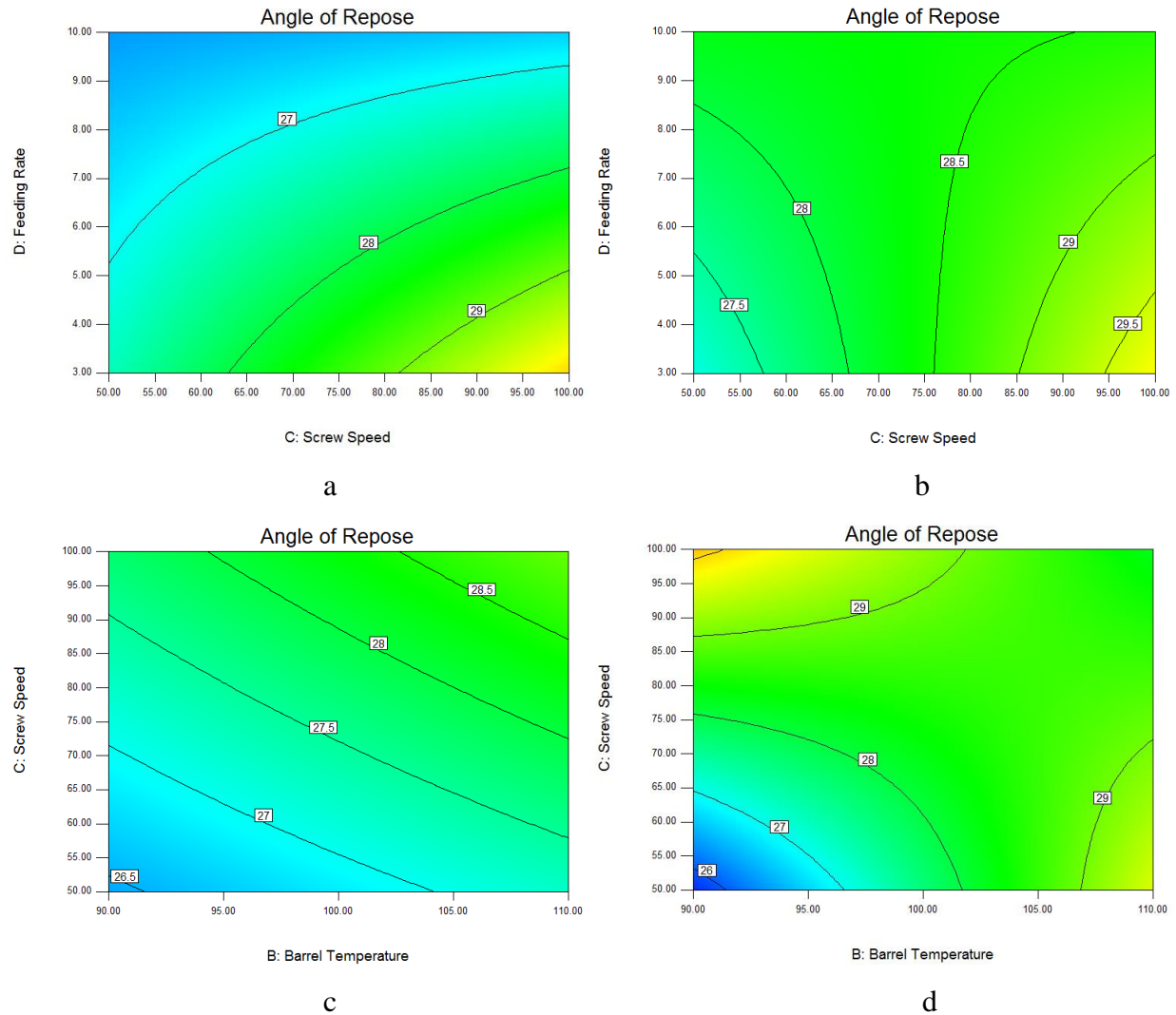


Figure 3-6. Contour plots showing the effect of barrel temperature, screw speed and feeding rate on angle of repose: (a) & (c) one mixing zone configuration, (b) & (d) two mixing zone configuration.

3.4.5.2. Flowability Index

The flowability index was defined as the smallest hole through which the core cylinder of powder could overcome the side internal friction and pass. Based on this definition, flowability index was similar to angle of repose: higher number presented lower flow property. It was mentioned a good range of flowability index was 10–24 mm [124]. For this parameter, an inverse square root transformation was suggested by the software, resulting in the regression equation as:

$$\frac{1}{\sqrt{\text{Flowability index}}}$$

$$= +0.23 - 0.027 * A - 0.016 * B + 0.016 * D + 5.482e - 003 * A * B \\ - 0.027 * A * D - 2.602e - 003 * B * C - 0.014 * B * D + 2.296e - 003 \\ * C * D$$

This model accompanied with a p-value of 0.007 implied its high confidence level. Screw configuration, barrel temperature and feeding rate were found to have significant effect on flowability index. However, the complicated transformation did make the relationship between different factors unclear. Hence it is best to look into the contour plot to better understand the effect of different factors (Figure 3-7).

When looking into Figure 3-7a (one mixing zone), it was found higher temperature and lower feeding rate would result in higher flowability index, thus poorer flow property. This result was the same with the angle of repose. In Figure 7b, the effect of barrel temperature was still the same. Interestingly, the effect feeding rate showed different effect at different conditions. When barrel temperature was below 95 °C, feeding rate barely had any effect on flowability index. This was because the ability of higher feeding rate to decrease fines was offset by the second mixing zone. However, when the temperature was over 95 °C, higher feeding rate was more tend to increase the portion of large size granule, thus lead to higher flowability index. When comparing Figure 3-7a and 3-7b, it was found the granules produced with two mixing zone configuration would have less flow property, which correlate with the fact the second mixing zone will create more fines or large size granules.

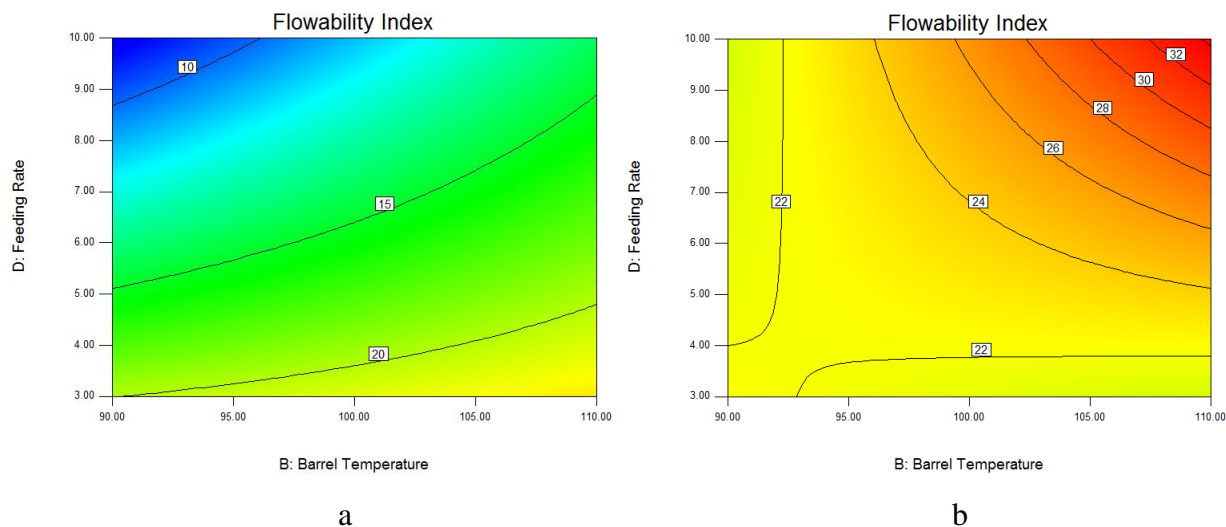


Figure 3-7. Contour plots showing the effect of barrel temperature and feeding rate on percentage of medium size granules (a) one mixing zone configuration, (b) two mixing zone configuration.

3.4.6. In-vitro drug release study

The simulated gastric solution (0.1 N HCl, pH = 1.2) was utilized in the dissolution study as dissolution medium. Ten runs of samples released more than 95% drug in 23 hours (Run 2 and Run 5 > 94%). The maximum drug release time for tablets varied from 10 to 23 hours (Figure 3-8 and Table 3-6). The regression equation suggested by Design Expert software was shown as follows:

Dissolution Time

$$= +16.92 + 2.13 * A - 2.42 * B + 1.62 * C - 0.75 * D + 1.37 * A * B \\ + 1.63 * B * C + 2.50 * B * D$$

The p-value provided for this model was 0.0056 (Table 3-9), Three factors (screw configuration, barrel temperature and screw speed) were discovered to have significant effect on dissolution time. The positive coefficient of screw configuration and screw speed implied that when two mixing zone configuration and high screw speed were applied, the dissolution time of

tablet would increase, that was slower release. However, when the higher temperature was utilized, the release would be faster. Actually, this result was totally opposite to what have been expected, which was based on the granule properties mentioned above. The only explanation could be the tableting process had done some change to the granule property.

Table 3-9. Dissolution time statistical analysis and coefficients of regression.

Variables	Dissolution time for maximum drug release (h)	
	Coefficient	P
Model		0.0056
Intercept	16.92	
A	2.12	0.0065
B	-2.42	0.0019
C	1.62	0.0164
D	-0.75	0.1401
	$R^2 = 0.9726$ $\text{Pred } R^2 = 0.7537$	

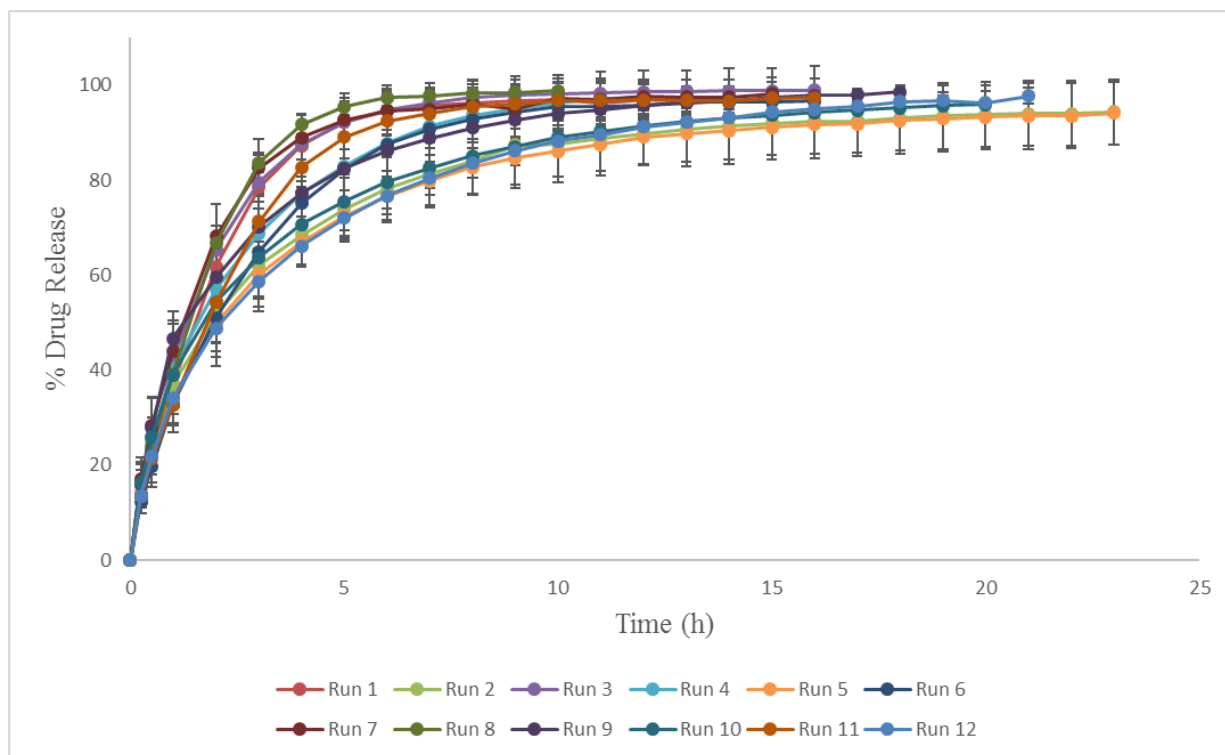


Figure 3-8. *In-vitro* release profiles of a tablets from 12 runs of samples.

To confirm the aforementioned assumption, the dissolution of primary granules was conducted as well. The time for 80% drug release of both tablets and granules were compared. 80% percent drug release was selected because the release time for different runs of samples at this level showed enough distinction degree. The result was summarized in Table 3-10. It was quite noticeable that the dissolution time could be divided into two groups. In addition, the release time for tablet and granule from same run of experiment was opposite. In detail, counterpart (capsule) of fast release tablet will release slow, vice versa.

This negative correlation of tablet and capsule release time was quite interesting. The principle under this phenomenon could be explained by the effect of binder. When the big size or strong granule was formed (these two parameters usually have positive correlation based on our observation), which release relatively slow, more binder in the formulation would be occupied in

the granule. The binder outside of granule would be in small amount. In this case, when the tablet was compressed, the binder to connect granules together would not be enough, which meant the adhesion of granules would be weak. The tablet would be more easily to disintegrated into granules, and release faster because of the enhanced surface area. This hypothesis was supported by the SEM photograph taken for granules and tablets (Figure 3-9). All the images were taken at 25 times magnification. As can be seen from the picture, from run 11 to run 2, the granule size decreased gradually, simultaneously, the diminution of cleavage on the counterpart tablet was apparent. The cleavage was a very clear sign of the weak adhesion among granules. Thus, the hypothesis should be reasonable.

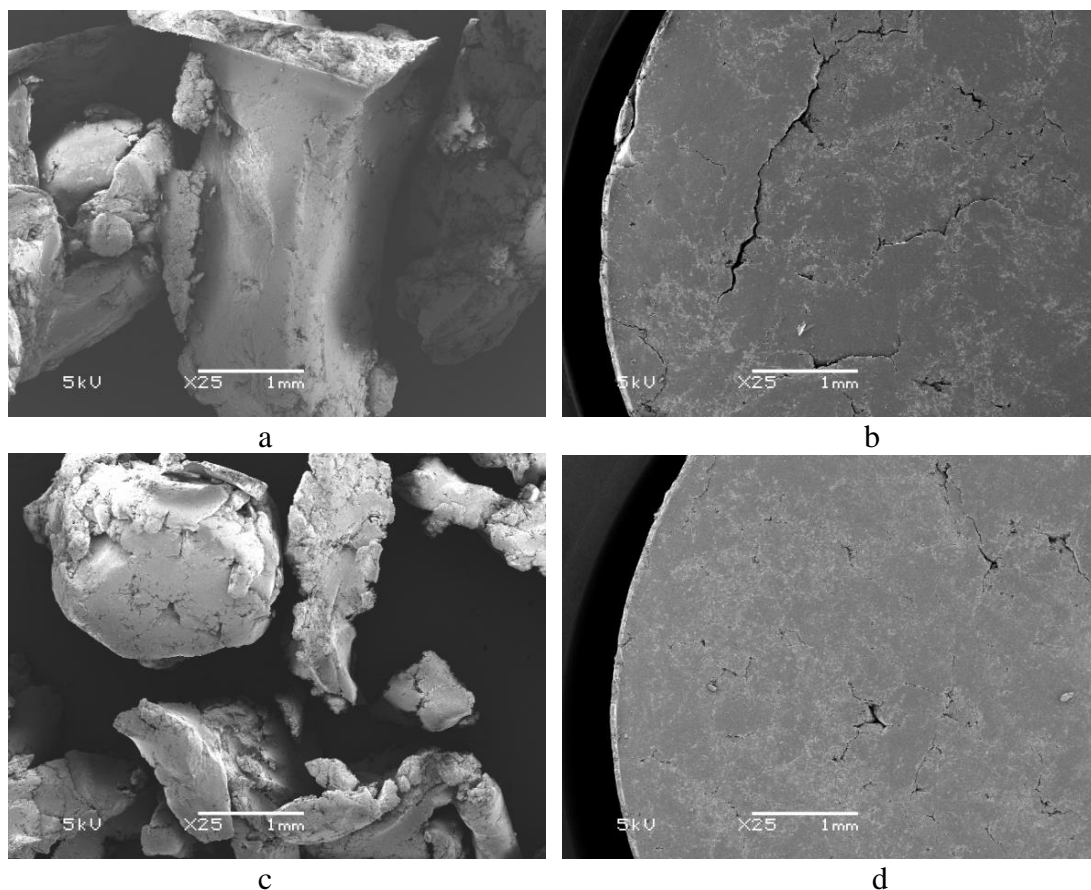


Figure 3-9. SEM photograph of granules and tablets: (a) & (b) Run 11, (c) & (d) Run 3

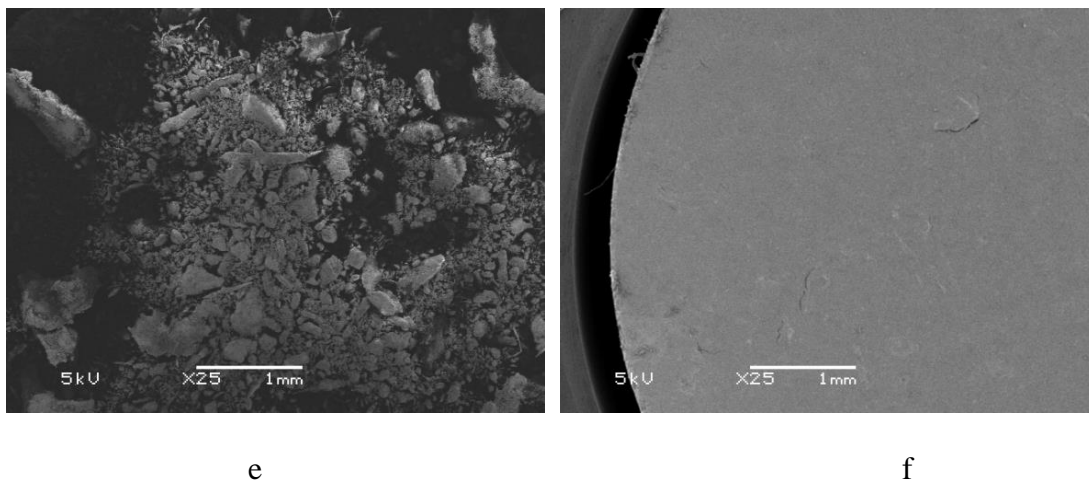


Figure 3-9. SEM photograph of granules and tablets: (e) & (f) Run 2.

Table 3-10. 80% drug release time for tablet and capsule.

	Tablet (h)		Capsule (min)	
F1	3.2	Release Time < 4 h	25	Release Time > 15 min
F3	3.1		15	
F7	2.5		25	
F8	2.9		17.5	
F11	3.8		29	
F2	6.9	Release Time > 4 h	7	Release Time < 15 min
F4	4.5		14	
F5	6		7	
F6	4.7		13	
F9	4.5		9	
F10	6.3		10	
F12	7		14	

3.4.7. Optimization of processing parameters

From a serial of experiments, the relationship between different factors and responses was quite clear. However, it was too complicated to analyze them together (Table 3-11). What's worse, some of the parameters required by different responses conflict with each other. For example, less amounts of fines and larger quantity of medium size granules were both preferred, but screw speed have opposite effect on these two responses. Therefore, a sophisticated model to optimize the factors was necessary. Luckily enough, all the models we obtained from the software had high R^2 and pred R^2 , which guaranteed the possibility of utilizing these models to do the optimization. Based on the previous description and experiment data, the goal was set as, fines (5-10%), Medium size granules (60-80%), Angle of repose (25-30°), Flowability index (10-24 mm), Dissolution time (12-16 h). The desirability plot was given in Figure 3-10. The conclusion could be drawn was high feeding rate and screw speed should be utilized. Relatively low barrel temperature was beneficial for the goal. Only one mixing zone configuration should be applied.

Table 3-11. Summarization of relationship between factors and responses.

	% Fines	% Medium size granules	Angle of repose	Flowability index	Release time
Screw configuration	N/A	-	N/A	+	+
Barrel temperature	-	N/A	+	+	-
Screw speed	+	+	+	N/A	+
Feeding rate	-	N/A	-	-	N/A

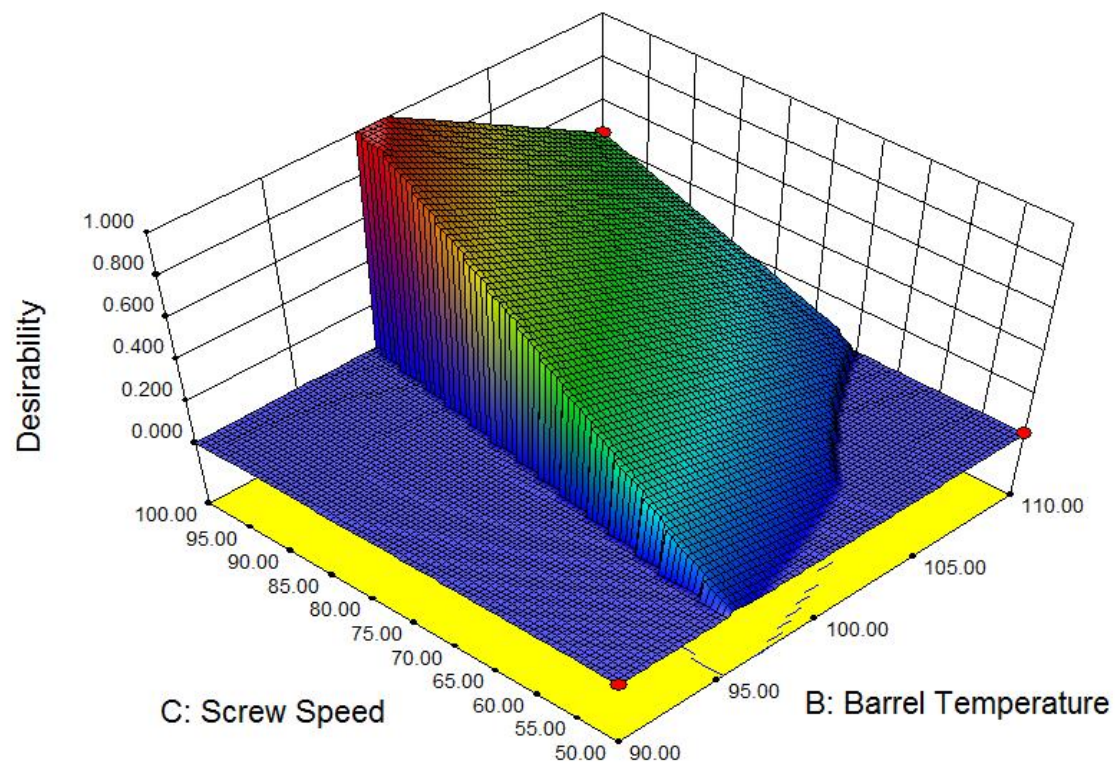


Figure 3-10. Desirability plot of set goals.

CHAPTER 4.

**COMPARISON OF DRUG RELEASE FROM KOLLIDON® SR MATRICES
PREPARED BY A DIRECT COMPRESSION METHOD AND TWIN SCREW
EXTRUSION TECHNOLOGY**

4.1. Objective

The major objective of the present project was to produce sustained-release tablets by both direct compression and HME technique. The physicochemical properties of both products were analyzed to determine the drug release mechanism. Theophylline (Figure 4-1) was chosen for this study for two reasons. Firstly, theophylline was a Biopharmaceutics Classification System (BCS) class I drug, which means it has high solubility and permeability. This property will make the observation of the sustained release effect easier. Secondly, the melting of theophylline is over 270 °C, which can effectively prevent the unexpected API transformation from crystalline to amorphous state in HME. Because this conversion may interrupt the analysis about effects of two techniques.

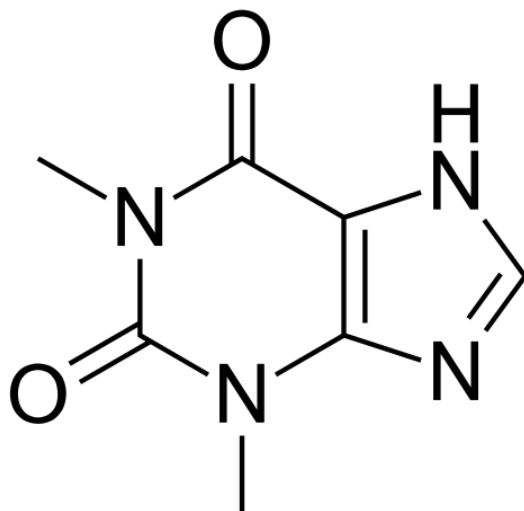


Figure 4-1. Chemical structure of theophylline.

4.2. Materials

Theophylline was purchased from Ria International LLC (Saint Louis, MO, US). Kollidon[®] SR was generously gifted by BASF SE (Ludwigshafen, Germany). Magnesium stearate was purchased from Spectrum Laboratory Products Inc. (Gardena, CA, US). Food Color, Blue (Liquid) was purchased from PCCA[™] (Houston, TX, US). All the other reagents used in this study were of the analytical grade.

4.3. Methods

4.3.1. Twin Screw Extrusion

All the ingredients were passed through US # 35 (500 μ m) mesh screen, in order to remove any aggregates that might be formed. Theophylline (30% w/w) was premixed with Kollidon[®] SR (70% w/w) using a Maxiblend[™] V-shell blender (GlobePharma, New Brunswick, NJ) at 25 rpm for 20 min. These binary physical mixtures (PM) were extruded using a HAAKE MiniLab II counter-rotating twin screw extruder (Thermo Fisher Scientific, Waltham, MA, USA) at a screw speed of 100 rpm and barrel temperature of 100 °C to obtain resultant extrudates (Ext). The Ext were collected at the end of the extruder after the steady state of was achieved. Half of the Ext were milled and passed through USA standard sieve # 35 to achieve Milled Extrudates (ExtM). Either Ext or ExtM were stored separately in polyethylene bags for further processing and analysis.

4.3.2. Differential Scanning Calorimetry

Approximately 2-5 mg samples of interest were weighed and hermetically sealed in an aluminum pan. A Diamond DSC (PerkinElmer, Shelton, CT, USA) was used to measure the degree of crystallinity of the samples. The instrument's Pyris manager software (Shelton, CT, USA) was utilized to analyze the data. The heating rate was set at 20 °C/min from 20 to 300 °C under an inert atmosphere of nitrogen at a flow rate of 20 mL/min.

4.3.3. Tablet Compression

100 mg obtained PM or ExtM were mixed with 0.3% magnesium stearate just prior to manual direct compression on a MCTMI single punch tablet press (GlobePharma Inc., New Brunswick, NJ, USA). An 8 mm flat round punch was used, and a compression force of 120 kg/cm was applied.

4.3.4. In Vitro Drug Release Study

The compressed ExtM tablets (ExtT), direct compressed tablets (DCT), theophylline, Ext, PM, ExtM equivalent to 30 mg of theophylline were evaluated for *in-vitro* drug release. The dissolution media used was 900 mL 0.1 N HCl (pH 1.2, simulated gastric medium). SR8-plus™ dissolution apparatus (Hanson, Chatsworth, CA, US) was maintained at 37 ± 0.5 °C and the paddle speed was set at 50 rpm. PM and ExtM were filled into capsules (size 0) for dissolution. Tablets and Ext were directly dropped into dissolution vessel for test. Samples were collected at intervals of 1/6, 1/2, 1, 2, 4, 8, 12 and 24 h through a stainless-steel cannula with a 0.2-μm nylon filter tip attached to a 2.5-mL syringe. The samples were analyzed directly using a GENESYS 6

UV–vis spectrophotometer (Thermo Scientific, Madison, WI, US) at a wavelength of 270 nm. The standard curve was linear over the range of 1–50 µg/mL with an R^2 equal to 0.9996.

4.3.5. Scanning Electron Microscopy

The surface morphology of all samples (theophylline, Kollidon® SR, Ext, ExtT, DCT) and interior structure of tablets (ExtT and DCT) were determined by utilizing scanning electron microscopy (SEM). Samples were mounted onto an aluminum stage by an adhesive carbon tape, and then sputter coated with gold under an argon atmosphere using a Hummer 6.2 Sputter Coater (Ladd Research Industries, Williston, VT, US). The coater was kept in a high-vacuum evaporator equipped to guarantee a uniform coating. Finally, images were captured using a JSM-5600 scanning electron microscope (JEOL USA, Inc., Waterford, VA, US) at an accelerating voltage of 5 kV.

4.3.6. Dynamic Vapor Sorption

The water sorption behavior of API, polymer, tablets, milled and primary extrudates were determined by Intrinsic DVS (Surface measurement systems, London, UK). 20 ± 0.5 mg samples were exposed to the controlled relative humidity profile (0-100-0%) at a constant temperature (37 °C), and the weight changes were measured by a CahnD200 ultra-microbalance (± 0.01 mg mass resolution). The dm/dt mode was used in all the steps, and the limitation was set at 0.01 %/min to detect the equilibrium (the instrument would start next step when the samples dm/dt value equal or less than 0.001%/min). At first step, sample was dried at 0% RH, and the

equilibrated mass at 0% RH was used as reference mass. The water sorption isotherms were calculated using the equilibrated sample mass from each step [144].

4.3.7. Water Sorption Pathway

2 mL of food color was uniformly mixed with the 898 mL above mentioned dissolution media in the *in vitro* drug release study section. All dissolution apparatus and parameters were set identically as the *in vitro* drug release study. Tablets were directly dropped into dissolution vessel for test. Soaked tablets were removed from the dissolution media at intervals of 1, 2, 4, 8, 12 and 24 h. The outside surface of tablets was dried quickly utilizing paper towels. The tablets were then evenly split into two parts. The cross sections of each tablets were photographed for comparison.

4.4. Results and Discussion

4.4.1. Characterization of Crystallinity

The crystallinity of theophylline as pure drug and in ExtM and PM was confirmed by utilizing DSC (Figure 4-2). A single sharp endotherm peak at around 275 °C was observed for pure theophylline. This demonstrated the API we used was belong to the theophylline anhydrous form I [135]. After HME, the endotherm peak could still be seen from the DSC thermogram, however it was compressed to around 255 °C. These results confirmed that the crystallinity of theophylline was preserved after HME. Nevertheless, some interaction between theophylline and Kollidon[®] SR was likely to occur [136].

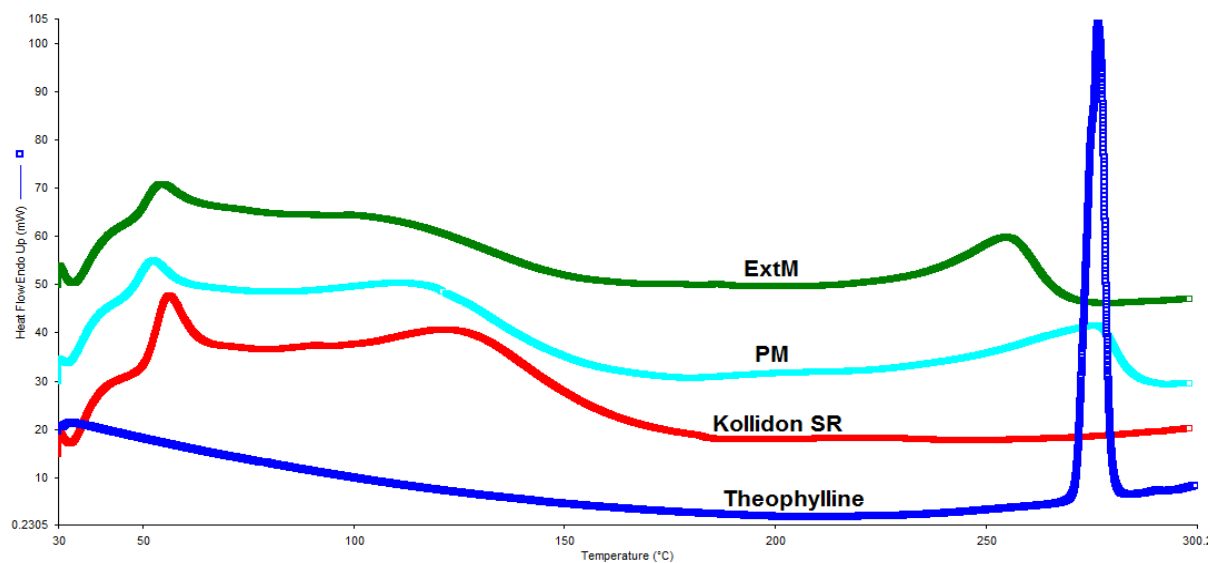


Figure 4-2. DSC thermograms of theophylline, Kollidon[®] SR, PM and ExtM.

4.4.2. In-vitro Drug Release

The release profile of all samples was summarized in Figure 4-3. Obviously, the pure theophylline achieved the fastest release rate, owing to its high solubility. More than 95% of drug was released in just 30 min, and full drug release was attained in the dissolution period. The release of PM was quite similar to that of theophylline, while a little bit slower. 95% drug release was achieved at 1 h time point, and about 97% of drug was released at 24 h. This could be the result of release-retardation effect of Kollidon[®] SR. The release rate of ExtM was faster than the ExtT in first 8 h, because the higher surface area of ExtM could have more contact with dissolution medium. Interestingly, the dissolution curve of ExtM and ExtT overlapped completely after 8 h, which indicated all materials of ExtT were exposed to dissolution medium, just like what happened in ExtM. This should be because ExtT expanded enough to make room for dissolution medium to get inside the tablets (disintegration was not observed during whole dissolution process). Ext exhibited the slowest release profile. Less than 15% of theophylline

release was observed after 24 h dissolution. This was because of the highly condensed nature of Ext. When materials were pushed out of the die, the high pressure existing at this area would compact the material a lot, which resulted in increased density and less cavity [145]. These properties would prevent the diffusion of dissolution medium into the center of Ext, thus decrease the release.

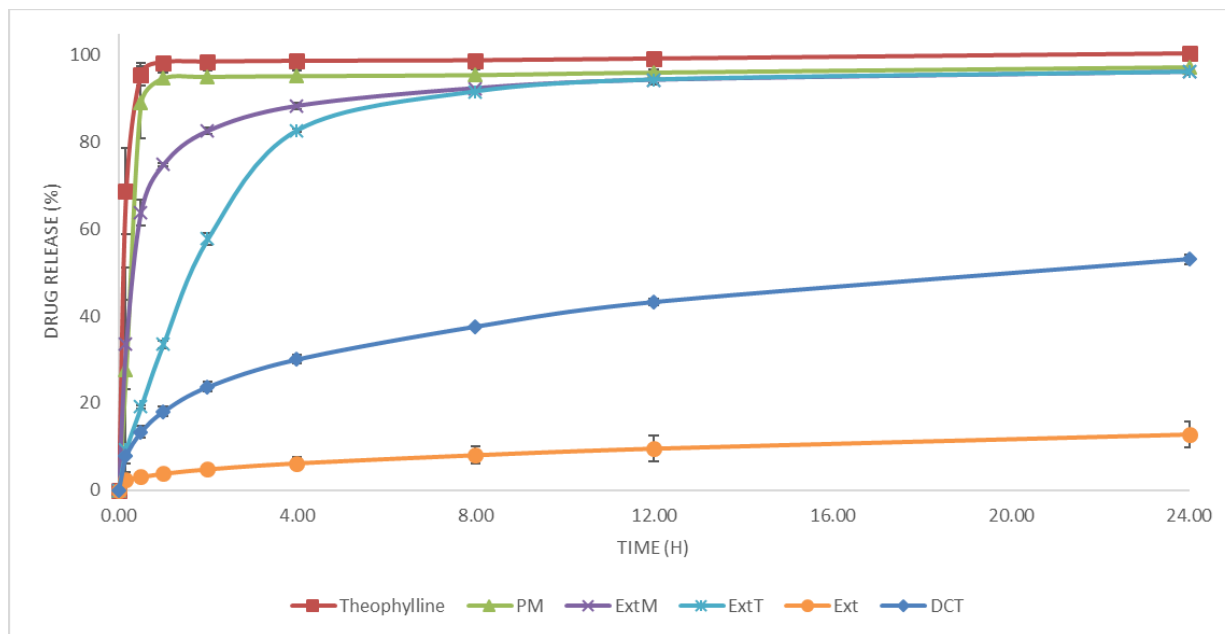


Figure 4-3. *In-vitro* release profiles.

Slower release of theophylline in ExtT, compared to that of DCT, was anticipated in the beginning. Because theophylline was expected to be better covered by Kollidon[®] SR after HME process, which would slow down the release of API. Actually, this was true when the release of PM and ExtM was compared. However, the ExtT and DCT dissolution result was totally reversed. This may be owing to the water sorption ability of these two tablets. The morphology of tablets before and after dissolution were compared (Figure 4-4). ExtT swelled much more than the DCT did, which indicated the ExtT could absorb more water into itself, hence increased release.

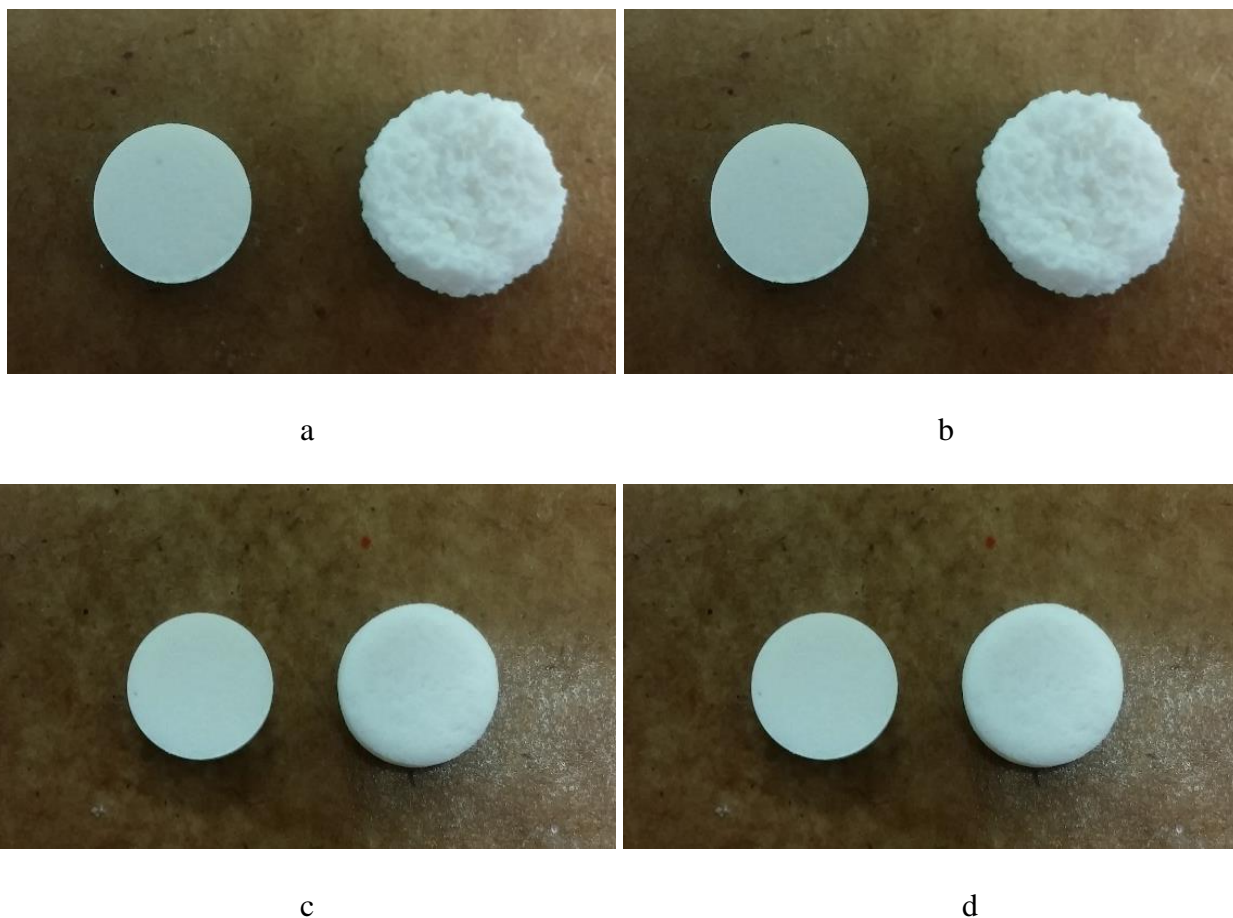
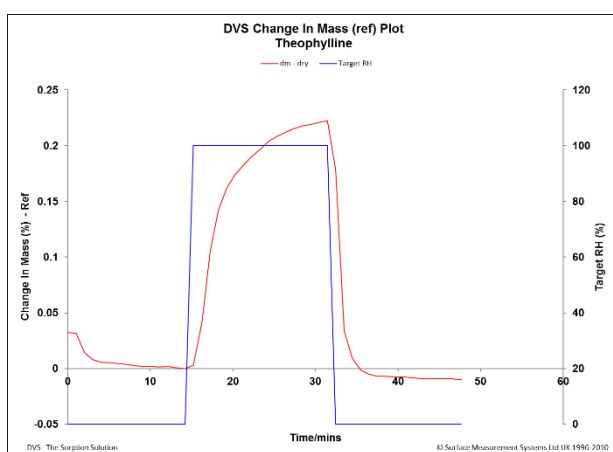


Figure 4-4. Macro photograph of tablets morphology before and after dissolution of: (a) & (b) ExtT, (c) & (d) DCT.

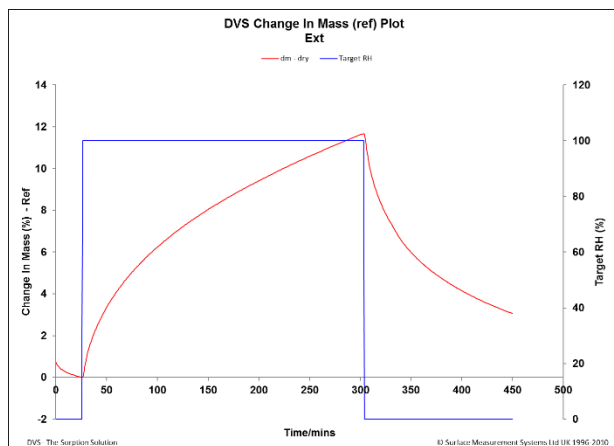
4.4.3. Water Sorption Ability

Macro image of tablets was just a subsidiary characterization method of water sorption behavior. Thus, the DVS was utilized to directly detect this property. The study condition was set at 37 °C and 100% RH to mimic the dissolution condition. It is necessary to point out that the RH achieved at stable state was only 98%, which may due to the instrument limit. This condition might have some effect on the results at some point. The water sorption behavior of each samples was summarized in Figure 4-5 and Table 4-1. Theophylline barely absorbed any water during the process. Only 0.22% gain in weight was recorded by the instrument. Kollidon[®] SR, on

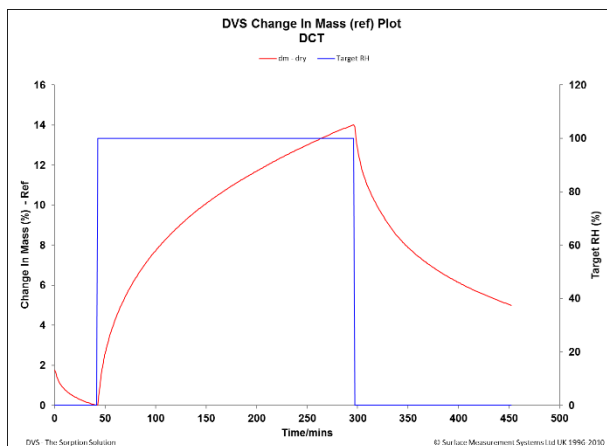
the contrary, absorbed moisture equal to around 33% of its own weight. The moisture sorption data correlated very well with the dissolution data. More water sorption would lead to faster and higher drug release. The only exception would be ExtT and ExtM. Both of them achieved 96% of drug release, but the water sorption amount was different. This could be explained by the different time range of two experiments. These two materials obtained the same drug release at 8 h in dissolution study. But the water sorption study lasted less than 5 h.



a

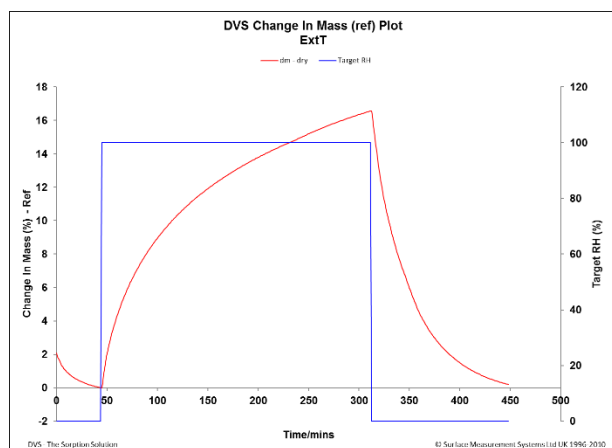


b

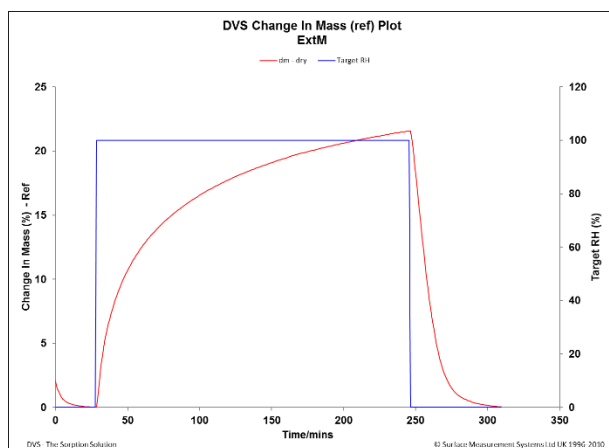


c

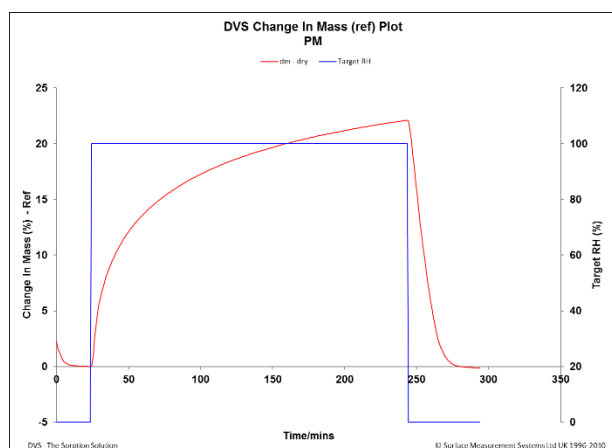
Figure 4-5. Dynamic vapour sorption measurements of: (a) theophylline, (b) Ext, (c) DCT



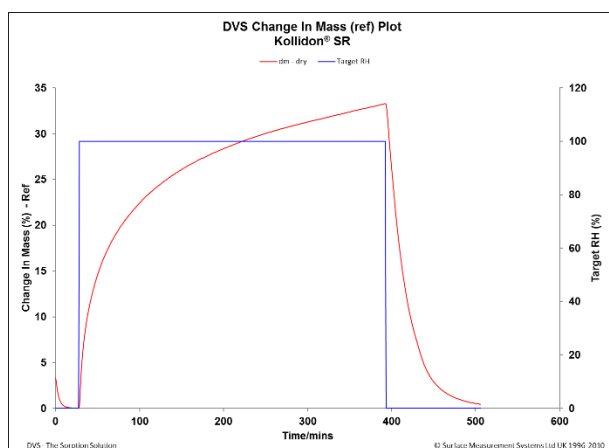
d



e



f



g

Figure 4-5. Dynamic vapour sorption measurements of: (d) ExtT, (e) ExtM, (f) PM, (g) Kollidon® SR.

Table 4-1. Maximum water sorption and time duration data.

	Maximum water sorption	Time of water sorption
	%	min
Theophylline	0.22	17.24
Ext	11.68	277.89
DCT	14.02	254.56
ExtT	16.58	267.77
ExtM	21.57	218.01
PM	22.10	220.03
Kollidon [®] SR	33.29	365.15

4.4.4. Water Sorption Pathway

The DVS study had clearly revealed the correlation of sample water sorption ability with API release speed as well as extent, i.e., theophylline in ExtT released more and faster than that of DCT. To better understand the process of drug release at real time, the water sorption pathway study was also conducted. In short, the original dissolution medium was dyed to blue color so that the pathway that the dissolution medium was absorbed by both tablets could be easily recorded and compared. The cross-section comparison of both tablets at different time points was shown as in Figure 4-6. The picture was adjusted by photoshop to provide better contrast between wetted and unwetted part. From the picture, it was clear that the water entered both tablets from the out layer to inner layer. However, at the endpoint of 24 h, ExtT was fully soaked by the water, which make the whole tablet blue. However, DCT still showed some of the original color of material at the same time point. This result conformed with the DVS study result very

well, which was ExtT absorbed more water than DCT. At each time point, more area of ExtT, compared to that of DCT, was wetted by the water at the same time point. This phenomenon indicated the water is more difficult to diffuse into DCT than ExtT.

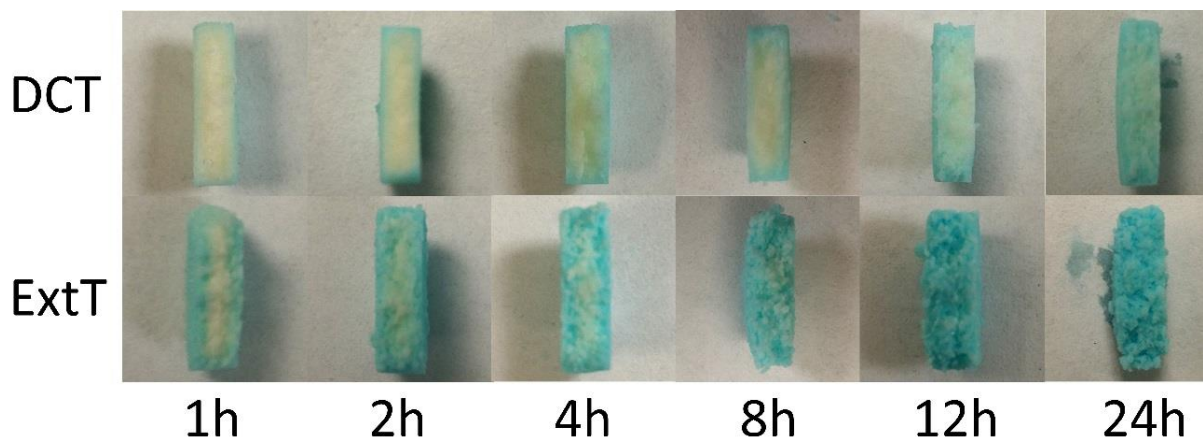


Figure 4-6. Dissolution Medium Sorption Pathway

4.4.5. Tablet Structure Test

To better explain this phenomenon above mentioned, both the surface structure and interior structure of ExtT and DCT were checked with SEM (Figure 4-7). From the surface structure perspective, more amount and bigger size crevices was found on the ExtT. Water could easily enter in the center of the tablets, and absorbed by Kollidon[®] SR in situ. However, the crevice on DCT was less and smaller, which limited the entrance of water directly. Diffusion was the major mechanism for water absorption, which was less efficient. The interior structure was achieved by manually breaking tablets, no knives were used. However, the fracture face of DCT was quite smooth, as cut by knife. This indicated the strength of connection between particles is quite similar to the particle interior strength. Thus, when broken by hand, either the individual

particle could be broken or particles could be departed from each other. In comparison, individual particles could be easily distinguished in ExtT. This indicated the connection between particles is much weaker than the strength of particles itself. In the dissolution scenario, water could easily pass through the particle gap of ExtT, instead of DCT. Thus, the absorption of dissolution medium is much faster in ExtT than DCT.

Thus, it could be concluded that release of theophylline in the formulation mainly depended on water absorbed by the Kollidon[®] SR. The process could be in 4 steps. Firstly, water entered the system either by absorption of Kollidon[®] SR or the crevice of tablet surface. Secondly, water moved inward the tablet through the particle gap, Thirdly, theophylline was solubilized by the water absorbed. Lastly, theophylline diffused out and released.

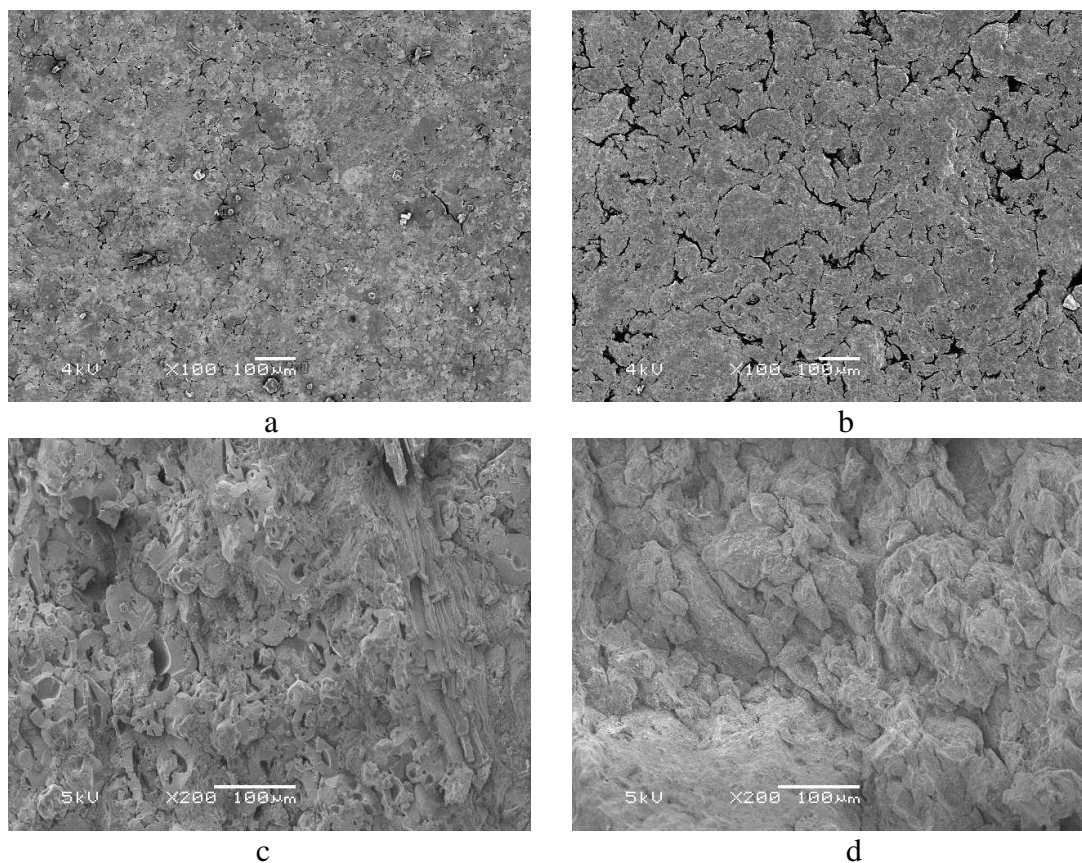


Figure 4-7. Surface structure of a) DCT, b) ExtT and Interior structure of c) DCT, d) ExtT

CHAPTER 5.
SUMMARY AND CONCLUSION

Over the last few decades, twin screw extruder (TSE) has attracted considerable attention in the pharmaceutical industry as an alternative processing instrument due to its advantages compared to other conventional equipment, such as economical processing, small footprint, reduced in-process times, solvent-free and continuous processing. These superiorities have led to the application of twin-screw extruder to produce numerous dosage forms, including pellets, tablets and films. Many other formulations production can also be beneficial from the introduction of twin-screw extruder to the process. In a series of studies, the application of TSE has extended for a further step.

In chapter 2, The use of a novel conjugation of HPH and HME techniques to continuously produce NCSD was investigated. This technique helps to overcome the nanocrystal formulation problems that are associated with the conventional methods. By using this technique, an increase in the dissolution rate was achieved as a result of the decreased particle size and increased surface area, and also owing to the improved wettability. The good stability was attributed to the maintained crystalline state of the drug.

In chapter 3, the previously unreported study of applying twin screw extruder to the dry granulation process was successfully conducted. The effect of various factors on the granule properties was clearly revealed by performing a Resolution V Irregular Fraction Design. Automatic Optimization of processing parameters to achieve the setting goal was achieved by utilizing the obtained model. In general, TSDG was demonstrated to be an alternative method to prepare dry granules. The continuous processing nature, simplicity of operation and easiness of optimization made TSDG quite competitive compared to other conventional dry granulation techniques.

In chapter 4, the different behavior of ExtT and DCT under the same dissolution environment were compared. The mechanism behind this different behavior was further investigated by the water absorption study, dissolution medium absorption tracking study as well as the tablet structure analysis. In general, different structures determined the different water sorption property of tablets, which finally resulted in different dissolution behavior.

BIBLIOGRAPHY

1. Shah, S., et al., *Melt extrusion with poorly soluble drugs*. Int J Pharm, 2013. **453**(1): p. 233-52.
2. Repka, M.A., et al., *Melt extrusion: process to product*. Expert opinion on drug delivery, 2012. **9**(1): p. 105-125.
3. Langley, N., J. DiNunzio, and M.A. Repka, *Melt Extrusion: Materials, Technology and Drug Product Design (AAPS Advances in the Pharmaceutical Sciences Series)*. 2013: Springer.
4. Williams III, R.O., A.B. Watts, and D.A. Miller, *Formulating poorly water soluble drugs*. 2012: Springer.
5. Shah, S. and M.A. Repka, *Melt extrusion in drug delivery: three decades of progress*, in *Melt Extrusion*. 2013, Springer. p. 3-46.
6. McGinity, J.W., et al., *Hot-melt extrusion technology*. Encyclopedia of pharmaceutical technology, 2007. **19**: p. 203-226.
7. Crowley, M.M., et al., *Pharmaceutical applications of hot-melt extrusion: part I*. Drug development and industrial pharmacy, 2007. **33**(9): p. 909-926.
8. Patil, H., R.V. Tiwari, and M.A. Repka, *Hot-melt extrusion: from theory to application in pharmaceutical formulation*. AAPS PharmSciTech, 2016. **17**(1): p. 20-42.
9. Repka, M.A., et al., *Pharmaceutical applications of hot-melt extrusion: Part II*. Drug development and industrial pharmacy, 2007. **33**(10): p. 1043-1057.
10. Saerens, L., et al., *Process monitoring and visualization solutions for hot - melt extrusion: a review*. Journal of Pharmacy and Pharmacology, 2014. **66**(2): p. 180-203.
11. Ghebre-Sellassie, I., et al., *Pharmaceutical extrusion technology*. 2018: CRC Press.

12. Schenck, L., et al., *Achieving a hot melt extrusion design space for the production of solid solutions*. Chemical engineering in the pharmaceutical industry: R&D to manufacturing, 2011: p. 819-836.
13. Follonier, N., E. Doelker, and E.T. Cole, *Evaluation of hot-melt extrusion as a new technique for the production of polymer-based pellets for sustained release capsules containing high loadings of freely soluble drugs*. Drug Development and Industrial Pharmacy, 1994. **20**(8): p. 1323-1339.
14. Crowley, M.M., et al., *Physicochemical properties and mechanism of drug release from ethyl cellulose matrix tablets prepared by direct compression and hot-melt extrusion*. International journal of pharmaceutics, 2004. **269**(2): p. 509-522.
15. Aitken-Nichol, C., F. Zhang, and J.W. McGinity, *Hot melt extrusion of acrylic films*. Pharmaceutical Research, 1996. **13**(5): p. 804-808.
16. Chen, M., et al., *Influence of Processing Parameters and Formulation Factors on the Bioadhesive, Temperature Stability and Drug Release Properties of Hot-Melt Extruded Films Containing Miconazole*. AAPS PharmSciTech, 2014. **15**(3): p. 522-529.
17. Rothen-Weinhold, A., et al., *Formation of peptide impurities in polyester matrices during implant manufacturing*. European Journal of Pharmaceutics and Biopharmaceutics, 2000. **49**(3): p. 253-257.
18. El Hagrasy, A., et al., *Twin screw wet granulation: influence of formulation parameters on granule properties and growth behavior*. Powder technology, 2013. **238**: p. 108-115.
19. Thompson, M. and J. Sun, *Wet granulation in a twin - screw extruder: Implications of screw design*. Journal of pharmaceutical sciences, 2010. **99**(4): p. 2090-2103.

20. Van Melkebeke, B., et al., *Melt granulation using a twin-screw extruder: a case study*. International journal of pharmaceutics, 2006. **326**(1): p. 89-93.
21. Keleb, E., et al., *Continuous twin screw extrusion for the wet granulation of lactose*. International journal of pharmaceutics, 2002. **239**(1): p. 69-80.
22. Patil, H., et al., *Continuous manufacturing of solid lipid nanoparticles by hot melt extrusion*. International journal of pharmaceutics, 2014. **471**(1): p. 153-156.
23. Patil, H., et al., *Continuous Production of Fenofibrate Solid Lipid Nanoparticles by Hot-Melt Extrusion Technology: a Systematic Study Based on a Quality by Design Approach*. The AAPS journal, 2015. **17**(1): p. 194-205.
24. Sekiguchi, K., N. Obi, and Y. Ueda, *Studies on Absorption of Eutectic Mixture. Ii. Absorption of Fused Conglomerates of Chloramphenicol and Urea in Rabbits*. Chem Pharm Bull (Tokyo), 1964. **12**: p. 134-44.
25. Seo, A., et al., *The preparation of agglomerates containing solid dispersions of diazepam by melt agglomeration in a high shear mixer*. Int J Pharm, 2003. **259**(1-2): p. 161-71.
26. Lakshman, J.P., et al., *Application of melt extrusion in the development of a physically and chemically stable high-energy amorphous solid dispersion of a poorly water-soluble drug*. Mol Pharm, 2008. **5**(6): p. 994-1002.
27. Yao, W., et al., *Thermodynamic properties for the system of silybin and poly(ethylene glycol) 6000*. Thermochimica Acta, 2005. **437**(1-2): p. 17-20.
28. Vippagunta, S.R., et al., *Factors affecting the formation of eutectic solid dispersions and their dissolution behavior*. J Pharm Sci, 2007. **96**(2): p. 294-304.

29. Emas, M. and H. Nyqvist, *Methods of studying aging and stabilization of spray-congealed solid dispersions with carnauba wax. 1. Microcalorimetric investigation*. Int J Pharm, 2000. **197**(1-2): p. 117-27.
30. Sarode, A.L., et al., *Hot melt extrusion (HME) for amorphous solid dispersions: Predictive tools for processing and impact of drug-polymer interactions on supersaturation*. Eur J Pharm Sci, 2012. **48**(3): p. 371-384.
31. Janssens, S. and G. Van den Mooter, *Review: physical chemistry of solid dispersions*. J Pharm Pharmacol, 2009. **61**(12): p. 1571-86.
32. Serajuddin, A.T., *Solid dispersion of poorly water-soluble drugs: early promises, subsequent problems, and recent breakthroughs*. J Pharm Sci, 1999. **88**(10): p. 1058-66.
33. Shah, S. and M.A. Repka, *Melt Extrusion in Drug Delivery: Three Decades of Progress*, in *Melt Extrusion Materials, Technology and Drug Product Design*, M.A. Repka, N. Langley, and J. DiNunzio, Editors. 2013, Springer: New York Dordrecht Heidelberg London.
34. Van den Mooter, G., *The use of amorphous solid dispersions: A formulation strategy to overcome poor solubility and dissolution rate*. Drug Discovery Today: Technologies, 2012. **9**(2): p. e79-w85.
35. Vasconcelos, T., B. Sarmiento, and P. Costa, *Solid dispersions as strategy to improve oral bioavailability of poor water soluble drugs*. Drug Discov Today, 2007. **12**(23-24): p. 1068-75.
36. Vo, C.L., C. Park, and B.J. Lee, *Current trends and future perspectives of solid dispersions containing poorly water-soluble drugs*. Eur J Pharm Biopharm, 2013. **85**(3): p. 799-813.

37. Crowley, M.M., et al., *Stability of polyethylene oxide in matrix tablets prepared by hot-melt extrusion*. Biomaterials, 2002. **23**(21): p. 4241-8.
38. Douroumis, D., *Hot-melt extrusion: Pharmaceutical applications*. 2012: John Wiley & Sons.
39. Maniruzzaman, M., et al., *A review of hot-melt extrusion: process technology to pharmaceutical products*. ISRN pharmaceutics, 2012. **2012**.
40. Deng, J., et al., *Energy monitoring and quality control of a single screw extruder*. Applied Energy, 2014. **113**: p. 1775-1785.
41. Andrews, G.P., et al., *Hot-melt extrusion: an emerging drug delivery technology*. Pharmaceutical Technology Europe, 2009. **21**(1): p. 24-27.
42. Speiser, P., *Poorly soluble drugs: a challenge in drug delivery*. Emulsions and nanosuspensions for the formulation of poorly soluble drugs. Medpharm Scientific Publishers, Stuttgart, 1998: p. 15-28.
43. Savjani, K.T., A.K. Gajjar, and J.K. Savjani, *Drug solubility: importance and enhancement techniques*. ISRN pharmaceutics, 2012. **2012**.
44. Gribbon, P. and S. Andreas, *High-throughput drug discovery: what can we expect from HTS?* Drug discovery today, 2005. **10**(1): p. 17-22.
45. Leuner, C. and J. Dressman, *Improving drug solubility for oral delivery using solid dispersions*. European journal of Pharmaceutics and Biopharmaceutics, 2000. **50**(1): p. 47-60.
46. Sweetana, S. and M.J. Akers, *Solubility principles and practices for parenteral drug dosage form development*. PDA journal of pharmaceutical science and technology/PDA, 1995. **50**(5): p. 330-342.

47. Bastin, R.J., M.J. Bowker, and B.J. Slater, *Salt selection and optimisation procedures for pharmaceutical new chemical entities*. Organic Process Research & Development, 2000. **4**(5): p. 427-435.
48. Szejtli, J., *Cyclodextrin technology*. Vol. 1. 1988: Springer Science & Business Media.
49. Del Valle, E.M., *Cyclodextrins and their uses: a review*. Process biochemistry, 2004. **39**(9): p. 1033-1046.
50. Beak, I.-H. and M.-S. Kim, *Improved supersaturation and oral absorption of dutasteride by amorphous solid dispersions*. Chemical and Pharmaceutical Bulletin, 2012. **60**(11): p. 1468-1473.
51. Frank, K.J., et al., *The amorphous solid dispersion of the poorly soluble ABT-102 forms nano/microparticulate structures in aqueous medium: impact on solubility*. International journal of nanomedicine, 2012. **7**: p. 5757.
52. Van den Mooter, G., *The use of amorphous solid dispersions: A formulation strategy to overcome poor solubility and dissolution rate*. Drug Discovery Today: Technologies, 2012. **9**(2): p. e79-e85.
53. Sinha, S., et al., *Solid dispersion as an approach for bioavailability enhancement of poorly water-soluble drug ritonavir*. Aaps Pharmscitech, 2010. **11**(2): p. 518-527.
54. Modi, A. and P. Tayade, *Enhancement of dissolution profile by solid dispersion (kneading) technique*. AAPS pharmscitech, 2006. **7**(3): p. E87.
55. De Brabander, C., et al., *Bioavailability of ibuprofen from hot-melt extruded mini-matrices*. International journal of pharmaceutics, 2004. **271**(1-2): p. 77-84.

56. Kanaze, F., et al., *Dissolution enhancement of flavonoids by solid dispersion in PVP and PEG matrixes: A comparative study*. Journal of applied polymer science, 2006. **102**(1): p. 460-471.
57. Chiou, W.L. and S. Riegelman, *Pharmaceutical applications of solid dispersion systems*. Journal of pharmaceutical sciences, 1971. **60**(9): p. 1281-1302.
58. Alshahrani, S.M., et al., *Stability-enhanced Hot-melt Extruded Amorphous Solid Dispersions via Combinations of Soluplus(R) and HPMCAS-HF*. AAPS PharmSciTech, 2015: p. 1-11.
59. Feng, X., et al., *Evaluation of the recrystallization kinetics of hot-melt extruded polymeric solid dispersions using an improved Avrami equation*. Drug Dev Ind Pharm, 2015. **41**(9): p. 1479-87.
60. Yang, J., K. Grey, and J. Doney, *An improved kinetics approach to describe the physical stability of amorphous solid dispersions*. International journal of pharmaceutics, 2010. **384**(1): p. 24-31.
61. Junghanns, J.-U.A. and R.H. Müller, *Nanocrystal technology, drug delivery and clinical applications*. International journal of nanomedicine, 2008. **3**(3): p. 295.
62. Zhai, X., et al., *Dermal nanocrystals from medium soluble actives - physical stability and stability affecting parameters*. Eur J Pharm Biopharm, 2014. **88**(1): p. 85-91.
63. Kumar, S., et al., *Formulation parameters of crystalline nanosuspensions on spray drying processing: a DoE approach*. Int J Pharm, 2014. **464**(1-2): p. 34-45.
64. Zhai, X., et al., *Nanocrystals of medium soluble actives--novel concept for improved dermal delivery and production strategy*. Int J Pharm, 2014. **470**(1-2): p. 141-50.

65. Sinha, B., R.H. Muller, and J.P. Moschwitzer, *Bottom-up approaches for preparing drug nanocrystals: formulations and factors affecting particle size*. Int J Pharm, 2013. **453**(1): p. 126-41.
66. Moschwitzer, J.P., *Drug nanocrystals in the commercial pharmaceutical development process*. Int J Pharm, 2013. **453**(1): p. 142-56.
67. Moschwitzer, J.P. and R.H. Muller, *Factors influencing the release kinetics of drug nanocrystal-loaded pellet formulations*. Drug Dev Ind Pharm, 2013. **39**(5): p. 762-9.
68. Kesisoglou, F. and A. Mitra, *Crystalline nanosuspensions as potential toxicology and clinical oral formulations for BCS II/IV compounds*. AAPS J, 2012. **14**(4): p. 677-87.
69. Muller, R.H. and C.M. Keck, *Twenty years of drug nanocrystals: where are we, and where do we go?* Eur J Pharm Biopharm, 2012. **80**(1): p. 1-3.
70. Wang, G.D., et al., *Pharmaceutical nanocrystals*. Current Opinion in Chemical Engineering, 2012. **1**(2): p. 102-107.
71. Thommes, M., et al., *Improvement of the dissolution rate of poorly soluble drugs by solid crystal suspensions*. Molecular pharmaceutics, 2011. **8**(3): p. 727-735.
72. Shegokar, R. and R.H. Muller, *Nanocrystals: industrially feasible multifunctional formulation technology for poorly soluble actives*. Int J Pharm, 2010. **399**(1-2): p. 129-39.
73. Van Eerdenbrugh, B., G. Van den Mooter, and P. Augustijns, *Top-down production of drug nanocrystals: nanosuspension stabilization, miniaturization and transformation into solid products*. Int J Pharm, 2008. **364**(1): p. 64-75.
74. Bai, F., et al., *A versatile bottom-up assembly approach to colloidal spheres from nanocrystals*. Angew Chem Int Ed Engl, 2007. **46**(35): p. 6650-3.

75. Scholz, P., et al., *ARTcrystal process for industrial nanocrystal production--optimization of the ART MICCRA pre-milling step*. Int J Pharm, 2014. **465**(1-2): p. 388-95.
76. Noyes, A.A. and W.R. Whitney, *The rate of solution of solid substances in their own solutions*. Journal of the American Chemical Society, 1897. **19**(12): p. 930-934.
77. Müller, R.H., S. Benita, and B. Bohm, *Emulsions and nanosuspensions for the formulation of poorly soluble drugs*. 1998: CRC Press.
78. LLER, R.H.M., J. SCHWITZER, and F.N. Bushrab, *Manufacturing of nanoparticles by milling and homogenization techniques*. A Series of Textbooks and Monographs, 2006: p. 21.
79. Baumgartner, R., et al., *Nano-extrusion: a promising tool for continuous manufacturing of solid nano-formulations*. Int J Pharm, 2014. **477**(1-2): p. 1-11.
80. Perry, R.H. and D.W. Green, *Perry's chemical engineers' handbook*. 1999: McGraw-Hill Professional.
81. Iveson, S.M., et al., *Nucleation, growth and breakage phenomena in agitated wet granulation processes: a review*. Powder technology, 2001. **117**(1-2): p. 3-39.
82. Parikh, D., *Introduction*, in *Handbook of Pharmaceutical Granulation Technology, Second Edition*. 2005, CRC Press. p. 1-6.
83. Vasanthavada, M., et al., *Application of melt granulation technology using twin - screw extruder in development of high - dose modified - release tablet formulation*. Journal of pharmaceutical sciences, 2011. **100**(5): p. 1923-1934.
84. Cantor, S.L., et al., *Pharmaceutical granulation processes, mechanism and the use of binders*. Pharmaceutical dosage forms: tablets, 2008. **1**: p. 261-302.

85. Seem, T.C., et al., *Twin screw granulation—A literature review*. Powder Technology, 2015. **276**: p. 89-102.
86. Tousey, M.D., *The granulation process 101*. Pharm Tech, 2002: p. 8-13.
87. Tousey, M.D., *Optimal Tablet Press Operation: Machine versus Granulation*. Pharmaceutical Technology, 2002(26): p. 52-60.
88. Falzone, A.M., G.E. Peck, and G.P. McCabe, *Effects of changes in roller compactor parameters on granulations produced by compaction*. Drug development and industrial pharmacy, 1992. **18**(4): p. 469-489.
89. Malkowska, S. and K. Khan, *Effect of re-compression on the properties of tablets prepared by dry granulation*. Drug Development and Industrial Pharmacy, 1983. **9**(3): p. 331-347.
90. Shanmugam, S., *Granulation techniques and technologies: recent progresses*. BioImpacts: BI, 2015. **5**(1): p. 55.
91. Ali, S. and N. Langley, *Dry granulation simplifies tableting process*. Pharm Form Quality, 2010. **12**: p. 26-29.
92. Keleb, E., et al., *Twin screw granulation as a simple and efficient tool for continuous wet granulation*. International journal of pharmaceutics, 2004. **273**(1): p. 183-194.
93. Oulahna, D., et al., *Wet granulation: the effect of shear on granule properties*. Powder Technology, 2003. **130**(1): p. 238-246.
94. Mu, B. and M. Thompson, *Examining the mechanics of granulation with a hot melt binder in a twin-screw extruder*. Chemical engineering science, 2012. **81**: p. 46-56.
95. Kleinebudde, P., *Roll compaction/dry granulation: pharmaceutical applications*. European Journal of Pharmaceutics and biopharmaceutics, 2004. **58**(2): p. 317-326.

96. Miller, R., *Roller Compaction Technology*, in *Handbook of Pharmaceutical Granulation Technology, Second Edition*. 2005, CRC Press. p. 159-190.
97. Freitag, F., et al., *How do roll compaction/dry granulation affect the tableting behaviour of inorganic materials?: Microhardness of ribbons and mercury porosimetry measurements of tablets*. *European journal of pharmaceutical sciences*, 2004. **22**(4): p. 325-333.
98. Patel, S., et al., *Understanding size enlargement and hardening of granules on tabletability of unlubricated granules prepared by dry granulation*. *Journal of pharmaceutical sciences*, 2011. **100**(2): p. 758-766.
99. Bacher, C., et al., *Compressibility and compactibility of granules produced by wet and dry granulation*. *International journal of pharmaceutics*, 2008. **358**(1): p. 69-74.
100. Herting, M.G. and P. Kleinebudde, *Roll compaction/dry granulation: effect of raw material particle size on granule and tablet properties*. *International journal of pharmaceutics*, 2007. **338**(1): p. 110-118.
101. Inghelbrecht, S. and J.P. Remon, *Reducing dust and improving granule and tablet quality in the roller compaction process*. *International journal of pharmaceutics*, 1998. **171**(2): p. 195-206.
102. Lakshman, J.P., et al., *Application of melt granulation technology to enhance tableting properties of poorly compactible high - dose drugs*. *Journal of pharmaceutical sciences*, 2011. **100**(4): p. 1553-1565.
103. BASF, A., *Technical information for Kollidon SR*. Ludwigshafen, Germany, 1999.

104. Grund, J., et al., *The effect of polymer properties on direct compression and drug release from water-insoluble controlled release matrix tablets*. International journal of pharmaceutics, 2014. **469**(1): p. 94-101.
105. Sahoo, J., et al., *Comparative study of propranolol hydrochloride release from matrix tablets with Kollidon® SR or hydroxy propyl methyl cellulose*. AAPS PharmSciTech, 2008. **9**(2): p. 577-582.
106. Hauschild, K. and K.M. Picker-Freyer, *Evaluation of tableting and tablet properties of Kollidon SR: the influence of moisture and mixtures with theophylline monohydrate*. Pharmaceutical development and technology, 2006. **11**(1): p. 125-140.
107. Kranz, H. and T. Wagner, *Effects of formulation and process variables on the release of a weakly basic drug from single unit extended release formulations*. European journal of pharmaceutics and biopharmaceutics, 2006. **62**(1): p. 70-76.
108. Saerens, L., et al., *In-line NIR spectroscopy for the understanding of polymer–drug interaction during pharmaceutical hot-melt extrusion*. European Journal of Pharmaceutics and Biopharmaceutics, 2012. **81**(1): p. 230-237.
109. Özgüney, I., D. Shuwisitkul, and R. Bodmeier, *Development and characterization of extended release Kollidon® SR mini-matrices prepared by hot-melt extrusion*. European Journal of Pharmaceutics and Biopharmaceutics, 2009. **73**(1): p. 140-145.
110. Patel, G.V., et al., *Nanosuspension of efavirenz for improved oral bioavailability: formulation optimization, in vitro, in situ and in vivo evaluation*. Drug development and industrial pharmacy, 2013. **40**(1): p. 80-91.
111. Wang, Y., et al., *Stability of nanosuspensions in drug delivery*. Journal of Controlled Release, 2013. **172**(3): p. 1126-1141.

112. Singh, A., et al., *Development and characterization of taste masked Efavirenz pellets utilizing hot melt extrusion*. Journal of Drug Delivery Science and Technology, 2013. **23**(2): p. 157-163.
113. Mohammadi, Z., et al., *Preparation and evaluation of chitosan–DNA–FAP-B nanoparticles as a novel non-viral vector for gene delivery to the lung epithelial cells*. International journal of pharmaceutics, 2011. **409**(1): p. 307-313.
114. Shah, R.M., et al., *Physicochemical characterization of solid lipid nanoparticles (SLNs) prepared by a novel microemulsion technique*. Journal of colloid and interface science, 2014. **428**: p. 286-294.
115. PAGE, N.M.A., C. PAGE, and C. PAGE, *Suitability of Plasticized Polymers for Hot Melt Extrusion*.
116. Meena, A., et al., *Investigation of thermal and viscoelastic properties of polymers relevant to hot melt extrusion, II: Cellulosic polymers*. Journal of Excipients and Food Chemicals, 2014. **5**(1): p. 46-55.
117. Kolter, K. and A. Maschke, *Melt extrusion for pharmaceuticals*. ExAct, 2009. **22**: p. 2-5.
118. Chadha, R., et al., *An insight into thermodynamic relationship between polymorphic forms of efavirenz*. Journal of Pharmacy & Pharmaceutical Sciences, 2012. **15**(2): p. 234-251.
119. Karl, M., et al. *Suitability of pure and plasticized polymers for hot melt extrusion*. in *Poster AAPS Annual Meeting and Exposition, Atlanta*. 2010.
120. Hardung, H., D. Djuric, and S. Ali, *Combining HME & solubilization: Soluplus®—the solid solution*. Drug Deliv Technol, 2010. **10**(3): p. 20-7.
121. Ali, S., et al. *Eye on excipients*.

122. Ostwald, W., *Lehrbuch der allgemeinen Chemie*. Vol. 2. 1886: W. Engelmann.
123. FDA, U.S., *Guidance for Industry Waiver of In Vivo Bioavailability and Bioequivalence Studies for Immediate-Release Solid Oral Dosage Forms Based on a Biopharmaceutics Classification System*, U.S.D.o.H.a.H. Services, F.a.D. Administration, and C.f.D.E.a.R. (CDER), Editors. 2000.
124. Gioia, A., *Intrinsic flowability: a new technology for powder flowability classification*. Pharm Technol, 1980. **2**: p. 65-68.
125. Li, J. and Y. Wu, *Lubricants in pharmaceutical solid dosage forms*. Lubricants, 2014. **2**(1): p. 21-43.
126. Picker-Freyer, K.M. and T. Dürig, *Physical mechanical and tablet formation properties of hydroxypropylcellulose: in pure form and in mixtures*. AAPS PharmSciTech, 2007. **8**(4): p. 82-90.
127. Selmeczi, B., A. Kereszted, and J. Rapo, *Influence of cellulosic derivatives on several parameters of tablets*. Acta Pharm Hung, 1975. **45**: p. 28-36.
128. Alvarez-Lorenzo, C., et al., *Evaluation of low-substituted hydroxypropylcelluloses (L-HPCs) as filler-binders for direct compression*. International journal of pharmaceutics, 2000. **197**(1): p. 107-116.
129. Skinner, G., et al., *The evaluation of fine-particle hydroxypropylcellulose as a roller compaction binder in pharmaceutical applications*. Drug development and industrial pharmacy, 1999. **25**(10): p. 1121-1128.
130. Verhoeven, E., et al., *Influence of formulation and process parameters on the release characteristics of ethylcellulose sustained-release mini-matrices produced by hot-melt*

- extrusion*. European journal of pharmaceutics and biopharmaceutics, 2008. **69**(1): p. 312-319.
131. Verhoeven, E., C. Vervaet, and J.P. Remon, *Xanthan gum to tailor drug release of sustained-release ethylcellulose mini-matrices prepared via hot-melt extrusion: in vitro and in vivo evaluation*. European journal of pharmaceutics and biopharmaceutics, 2006. **63**(3): p. 320-330.
 132. Yamada, T., H. Onishi, and Y. Machida, *Sustained release ketoprofen microparticles with ethylcellulose and carboxymethylethylcellulose*. Journal of controlled Release, 2001. **75**(3): p. 271-282.
 133. Anderson, M.J. and P.J. Whitcomb, *DOE simplified: practical tools for effective experimentation*. 2016: CRC Press.
 134. Ye, X., et al., *Conjugation of hot-melt extrusion with high-pressure homogenization: a novel method of continuously preparing nanocrystal solid dispersions*. AAPS PharmSciTech, 2016. **17**(1): p. 78-88.
 135. Szterner, P., B. Legendre, and M. Sghaier, *Thermodynamic properties of polymorphic forms of theophylline. Part I: DSC, TG, X-ray study*. Journal of thermal analysis and calorimetry, 2010. **99**(1): p. 325-335.
 136. Marsac, P.J., S.L. Shamblin, and L.S. Taylor, *Theoretical and practical approaches for prediction of drug-polymer miscibility and solubility*. Pharmaceutical research, 2006. **23**(10): p. 2417-2426.
 137. Tucker, S.J. and H.M. Hays, *The amount of fines necessary for a tablet granulation*. Journal of the American Pharmaceutical Association, 1959. **48**(6): p. 362-362.

138. Dhenge, R.M., et al., *Twin screw granulation: steps in granule growth*. International journal of pharmaceutics, 2012. **438**(1): p. 20-32.
139. Tu, W.-D., A. Ingram, and J. Seville, *Regime map development for continuous twin screw granulation*. Chemical engineering science, 2013. **87**: p. 315-326.
140. Osborne, J.D., et al., *Investigating the influence of moisture content and pressure on the bonding mechanisms during roller compaction of an amorphous material*. Chemical engineering science, 2013. **86**: p. 61-69.
141. Palzer, S., *Agglomeration of dehydrated consumer foods*. Handbook of Powder Technology, 2007. **11**: p. 591-671.
142. Djuric, D. and P. Kleinebudde, *Continuous granulation with a twin-screw extruder: Impact of material throughput*. Pharmaceutical development and technology, 2010. **15**(5): p. 518-525.
143. Djuric, D., et al., *Comparison of two twin-screw extruders for continuous granulation*. European Journal of Pharmaceutics and Biopharmaceutics, 2009. **71**(1): p. 155-160.
144. Bley, O., J. Siepmann, and R. Bodmeier, *Characterization of moisture - protective polymer coatings using differential scanning calorimetry and dynamic vapor sorption*. Journal of pharmaceutical sciences, 2009. **98**(2): p. 651-664.
145. Feng, X., et al., *The effects of polymer carrier, hot melt extrusion process and downstream processing parameters on the moisture sorption properties of amorphous solid dispersions*. Journal of Pharmacy and Pharmacology, 2016. **68**(5): p. 692-704.

VITA

Xingyou Ye, son of Mr. Zhengqing Ye and Mrs. Yiqing You, was born on October 27, 1987 in Jiangyin, Jiangsu, China. In 2006, he received his high school Diploma from Nanjing High School (Jiangyin, Jiangsu, China). Thereafter, he received his Bachelor's degree in Pharmaceutical Science from Sun Yat-sen University (Guangzhou, Guangdong, China) in 2010.

In 2012, Mr. Ye was accepted into the Ph.D. program of Pharmaceutical Science with an emphasis on Pharmaceutics and Drug Delivery in University of Mississippi. He is a member of American Association of Pharmaceutical Sciences (AAPS). He is also a member of Rho Chi Pharmacy Honor Society. He was the recipient of Dissertation Fellowship for the Spring 2017 semester. He also completed one internship during his Ph.D. in Vertex Pharmaceuticals (Boston, MA, 2016).